Response to Referee 1

Overview:

This paper presents trace metal data from the Mauritanian shelf and places the observed distributions of redox elements in the context of O_2 control. The trace metal data look to be excellent, though the flux calculations need some further explaining so the reader can follow them through every step that was made. Overall the arguments presented for O_2 as a control in this dynamic environment are very weak and instead the data points more to the role of scavenging, aerosol deposition, resuspension and cross shelf transport. Just because it is in an oxygen minimum zone does not mean that oxygen controls the distribution of redox elements, as the data looks very similar to that from most coastal shelf regions. The paper at present is overly long and should have been edited down before submission to a more concise set of sections concentrating on the main processes as there are several sections (e.g. 3.4.2) that could summarize most of the relevant information to a simple paragraph with inclusion of a summary table. A substantially revised manuscript focusing on the key findings for which there is evidence would likely have significant impact in this field.

We thank the reviewer for the detailed constructive comments on our manuscript and address each comment in the following. The responses to the reviewer are given in bold font. Changes we made to the manuscript are highlighted in blue. Page and line numbers refer to the position in the original manuscript.

General Comments:

Contradictory vertical flux information: The main problem with the paper at present is with the vertical flux calculations as the repeat station data is analysed in an Eulerian framework with the concept that it is the same water mass that is being sampled at the same site several days later and horizontal advection is ignored. Yet the paper clearly states that the changes seen between repeat samplings was from an advective inflow (Thomsen et al., 2018) and that this regions is known for its high current velocities in summer (Klenz et al., 2018). While I understand what the authors are trying to link their data with changes in O_2, in the absence of a Lagrangian framework this makes no sense as we are left with comparing two snap shots of completely different scenes that just happened to be at the same spot.

The vertical flux calculation used here is independent of lateral (advective and diffusive) processes. The misunderstanding may be due to an ill-worded sentence in which we tried to explain the deviation of the vertical advective and diffusive fluxes.
Certainly, there are no advective terms in a Lagrangian framework, only diffusive terms remain. However, it is unclear to us why one would like to interpret our data in a Lagrangian framework. Thomsen et al. (2019) have shown that the O_2 variability is caused by alongshore advection and to a somewhat smaller extent by enhanced local consumption. Here, we look at average vertical processes and have the advantage of sampling during two rather different situations. Close to the shelf at the location of our repeated stations however, the variability in oxygen was explained by changes in local oxygen respiration rates and not by a change in water mass composition (Thomsen et al. 2019). We concur that the description of the oxygen variability on Page 11, Line 17 may have been unclear and have clarified the following part accordingly:
Variability in oxygen concentrations observed further offshore was attributed to physical transport of SACW into the region (Thomsen et al., 2019). In contrast, closer to the coast, enhanced pelagic

oxygen consumption rates were determined that significantly contribute to the variability in observed oxygen concentrations (Thomsen et al., 2019).

The description of the flux calculations is also not easy to follow and it is unclear exactly what depth ranges are being considered, is it just into the mixed layer or is it over the entire depth range. The strong point is the combination of microstructure profiles and trace metal concentrations to estimate robust values for the diffusive flux. The advective fluxes however are not well constrained at all as the methodology clearly has some problems; firstly close to the coast, scatterometer winds are not reliable due to the masking that takes place close to the coast in the data analysis, so some explanation of how this was taken into account needs to be provided, secondly the

In the revised version, we have substantially improved the description of the flux calculation based on the reviewer's specific remarks (detailed in the reply to the specific remarks below). We also included a discussion of the uncertainties inherent to determining vertical advective fluxes. The quality of the scatterometer winds close to the coast have been found to be almost as good as for the open sea winds (e.g. Verhoef et al., 2012). Mauritania–Senegalese upwelling region comparisons between scatterometer winds and near coastal land stations have shown differences of up to 20% in meridional and zonal wind component (Ndoye et al., 2014). However, Steinfeldt et al. (2015) validated the parameterized vertical velocities (Gill, 1982) used here against scatterometer winds (see Figure 4a in their paper). The agreement between cruise average vertical velocities (obtained from the helium disequilibrium and turbulence data) and the upwelling velocities derived via Gill's parameterization using satellite winds was very encouraging and motivated us to apply this formalism here. The revised description of the flux calculations in section 2.7 reads as follows:

2.7 Turbulence measurements and vertical flux calculations

In order to advance understanding of the role of benthic Fe supply to the productive surface waters of the upwelling region, vertical diffusive fluxes (eq 1: left term, right hand side) and wind induced vertical advective fluxes (eq 1: right term, right hand side) were estimated. On the continental margin below the surface mixed layer, solutes are transferred vertically toward the near-surface layers by turbulent mixing processes and by vertical advection forced by Ekman divergence (e.g. Kock et al., 2012; Milne et al., 2017; Rhein et al., 2010; Steinfeldt et al., 2015, Tanhua and Liu, 2015):

$$J_Z = K_z \frac{\partial [TM]}{\partial z} + w \cdot \Delta [TM] \qquad (1)$$

Here, K_z is the turbulent eddy diffusivity in $m^2\ s^{-1}$, ∂[TM]/ ∂z the vertical gradient with depth (z) of the TM concentration [TM] in µmol m^{-4}, Δ[TM] a TM concentration difference in µmol m^{-3} and w represents vertical velocity in m s^{-1}. Average advective and diffusive TM fluxes were calculated for a depth interval from the shallow O_2-depleted waters to surface waters. The exact depth interval varied for each station (see Table S2) due to differences in the depths where TM samples were collected. The upper depth (8–29 m) was always in layers with enhanced chlorophyll *a* fluorescence, although for some stations the upper depth was below the surface mixed layer.

Diffusive Fe fluxes were determined by combining TM concentration measurements from the TM-CTD stations with nearby measured microstructure profiles. The microstructure measurements were performed with an MSS90-D profiler (S/N 32, Sea & Sun Technology). The loosely-tethered profiler was optimized to sink at a rate of 0.55 m s^{-1} and equipped with three shear sensors, a fast-response temperature sensor, and an acceleration sensor, two tilt sensors and conductivity, temperature, depth sensors sampling with a lower response time. At TM-CTD stations with bottom depths less than 400 m, 18 to 65 microstructure profiles were available at each station. At deeper stations, 5 to 12 profiles were used. Standard processing procedures were used to determine the rate of kinetic

energy dissipation (ε) of turbulence in the water column (see Schafstall et al. (2010) for detailed description). Subsequently, K_z values were determined from $K_\rho = \Gamma \varepsilon N^{-2}$ (Osborn, 1980), where N is stratification and Γ is the mixing efficiency for which a value of 0.2 was used. The use of this value has recently been shown to yield good agreement between turbulent eddy diffusivities determined from microstructure measurements and from tracer release experiments performed in our study region (Köllner et al., 2016). The 95% confidence intervals for station-averaged K_ρ values were determined from Gaussian error propagation following Schafstall et al. (2010). Finally, diffusive fluxes were estimated by multiplying station-averaged $K_\square$ with the vertical gradient of the respective TM solute, implicitly assuming $K_z=K_\rho$.

The vertical advective flux by Ekman divergence requires determination of vertical velocity in the water column that varies with depth and distance from the coast line. Convincing agreement between vertical velocities derived from Ekman divergence following Gill (1982) determined from scatterometer winds and from helium isotope disequilibrium within the Mauritanian and Peruvian coastal upwelling regions was found by Steinfeldt et al. (2015) (see their Fig. 4). In their study, vertical velocities were parameterized as (Gill, 1982):

$$w = \frac{\tau_y}{\rho f L_r} e^{-x/L_r} \qquad (2)$$

where τ_y represents the alongshore wind stress, ρ the density of sea water, x the distance from maximum Ekman divergence taken here as the position at 50 m bottom depth on the shelf and L_r the first baroclinic Rossby radius. The parameterization results from considering the baroclinic response of winds parallel to a coastline in a two-layer ocean (Gill, 1982). The baroclinic Rossby radius $L_r = f^{-1}\sqrt{g\frac{\rho_2-\rho_1}{\rho}\frac{H_1H_2}{H_1+H_2}}$ ($\rho_{1/2}$ and $H_{1/2}$ are density and thickness of the surface and lower layer, respectively) was found to be 15 km from hydrographical data collected during the cruise. Similar values were determined by Steinfeld et al. (2015) in the same region. Using average alongshore wind stress from satellite data (0.057 Nm^{-2}, determined from daily winds from Remote Sensing Systems ASCAT C-2015, version v02.1 (Ricciardulli and Wentz, 2016) at 18°22.5'N, 016°7.5°W using $\tau_y = \rho_{air} C_d v^2$, where v represents alongshore wind, C_d is drag coefficient for which 1.15×10^{-3} was used (e.g. Fairall et al., 2003) and ρ_{air} is density of air) for June 2014, maximum vertical velocities of 3.7×10^{-5} m s^{-1} were determined for the shelf region (50 m water depth), which decayed offshore to 1.7×10^{-6} m s^{-1} at the position of the 1000 m isobath at 18°N. As these vertical velocities describe the magnitude of upwelling at the base of the mixed-layer, additional corrections need to be considered for deeper depths. Here, we approximated the vertical decay of w as a linear function which diminishes at the ocean floor.

The calculation of the vertical advective flux supplying solutes from the shallow O_2-depleted waters to surface waters requires knowledge of a concentration difference Δ[TM] associated with the upwelling flux. Ideally, the vertical length scale over which the concentration difference is determined can be diagnosed as the TM concentration variance divided by its mean vertical gradient (e.g. Hayes et al., 1991). However, in our study TM concentration time series data are not available. Previous studies have used a vertical length scale of 20 m to calculate the concentration differences between the target depth and the water below (e.g. Hayes et al., 1991; Steinfeldt et al., 2015; Tanhua and Liu, 2015). For our calculations, we chose to use a smaller length scale of 10 m following Hayes et al. (1991) which results in vertical advective TM flux presumably on the lower side of possible values.

The value of the alongshore wind stress utilized here changed from the original version. This is due to a change in location where the wind stress was calculated for, which is 12 km further inshore. This however has little impact on our calculated dFe fluxes, as the vertical velocity is calculated

separately for each station location using a term decreasing vertical velocities with distance from the location where the wind stress was calculated (equation 3).

To adequately describe uncertainties inherent to the vertical advective flux calculation we added the following text to section 3.4.3:

It should be noted that there are considerable uncertainties in the flux estimates presented above. While uncertainties in the diffusive flux originate predominately from the elevated variability of turbulence (see Schafstall et al., 2010 for details), uncertainties in the vertical advective flux originate from unaccounted for contributions from e.g. the spatial structure of the wind, particularly in the offshore direction, its temporal variability (e.g. Capet et al., 2004; Desbiolles et al. 2014, 2016; Ndoye et al., 2014), and uncertainties in the satellite wind product near the coast (e.g. Verhoef et al, 2012). Furthermore, the distribution of vertical velocities with depth is assumed to be linear here.

At the time this work was performed along the Mauritanian coast the area that was sampled has typically little or no upwelling present (Cropper et al., 2014; Tanhua and Liu, 2015; Varela et al., 2015). In the present work the authors chose to use the same wind based approach as that used earlier by Steinfeldt et al. (2015) in as study based predominantly on He isotopes. In that study they found upwelling during the summer months (M68-3) though the error bars are quite large 2.4 ± 1.5 x 10-5 m s^{-1}. Steinfeldt commented on the differences between their work and Tanhua and Liu, noting that the latter's data set only contains a few stations along 18 N, while their coastal stations along that line also have low vertical velocities (between 0 and 2x10-5 ms^{-1}), with much higher upwelling velocities to the north. It is not to say that there wasn't upwelling at this time, just that it needs to be better explained and put into context, indeed support for upwelling at this time comes from comparison to a companion paper also in BGD at present (Thomsen et al., 2018) but the authors don't make mention of that work except for the low oxygen resuspension events. The present paper would clearly benefit from linking more to the Thomsen et al. (2018) work and also to Yücel et al. (2015) work carried out along the same transect as both of those papers show the inherent variability in dissolved parameters in the bottom waters of this region.

Maps of SST and alongshore winds measured by the research vessel during the measurement program are shown Figure 1 by Thomsen et al. (2019). As stated above, cold surface waters were still present near the Mauritanian coast and moderate equatorward alongshore wind were encountered during the cruise, ensuring offshore Ekman transport. The work by Thomsen et al. (2019) is now referenced in several places of the manuscript. We also compare our results to Yücel et al. (2015).

The physical oceanography presented in the manuscript would also benefit from consideration of recent modelling studies on upwelling from other EBUS (Jacox and Edwards, 2011, 2012; Lentz, 1992; Lentz and Chapman, 2004; Lentz and Fewings, 2012; Messié and Chavez, 2015). The studies listed here show how the Burger number (Lentz and Chapman, 2004) with its dependence on the shelf slope and buoyancy frequency were important in understanding upwelling in such regions. Inclusion of this information would then also give the current paper more impact as it would be applicable to other EBUS as well. There are also a number of recent papers on the role of filaments and particle fluxes in this region (Bory et al., 2001; Fischer et al., 2009; Iversen et al., 2010; Rees et al., 2011) which also could be useful for interpreting the results found in the current work.

We thank the reviewer for this comment and the additional references provided. However, we feel that for the current study, such additional details of the physical oceanography are not essential for interpreting our measured trace element concentrations, which is the overall objective of this paper. Particle transport along filaments may indeed be an important transport mechanisms of trace metals in this region, which we mention in the manuscript. However, we cannot further discuss this using our data, as we ourselves didn't analyse particles and their distribution and composition likely shows a large temporal and spatial variability (as also pointed out in the

mentioned papers) and we therefor can only refer to the general possible role, but don't see the possibility in further interpreting our results using their data.

O_2 as a sole control on metal abundance: This work tries to suggest that changes in metal concentrations in the water column are due to changes in O_2 concentrations but the O_2 values observed are not low enough to cause significant changes in Fe, Mn or Al redox speciation so it is more likely that the observed changes are related to resuspension events in this very dynamic mixing environment (Schafstall et al., 2010). Resuspension has been known to be a major control on dissolved iron and other metals in shelf regions for some time now (Croot and Hunter, 1998; de Jong et al., 2012; Elrod et al., 2004; Johnson et al., 1999) and this would also impact other hydroxide dominated elements (e.g. Al, Th and to a lesser extent Mn). Colloidal species are also likely important here (Moran and Moore, 1988, 1989; Schlosser and Croot, 2008; Schlosser et al., 2013).

We are not trying to argue that oxygen is the only control on trace metal distribution and sediment release in this area. In the sections on remineralization and atmospheric deposition, we also highlight the additional influence of these processes. However, the temporal variation in trace metal concentrations observed here seems to be majorly driven by the change in oxygen concentrations despite the large concomitant change in turbidity. In section '3.6.2', we discuss the respective role of sediment resuspension but our dAl and LpAl data do not support a large change in sediment resuspension between the two deployments. Dissolved Al concentrations are very similar between the two deployments, while LpAl is lower at station 8 when dFe and LpFe are higher and slightly higher at station 3 when dFe and LpFe are larger. As pointed out by the reviewer, sediment resuspension (and also dust deposition) would, in addition to Fe, impact Al concentrations.

Why is O_2 unlikely to be a control on trace metals in the Mauritanian shelf? Simple - the shelf region here is typically described as being well oxygenated in the sediments (Gier et al., 2016) with the exception of the extremely shallow parts of the Banc d'Arguin (Duineveld et al., 1993; Kock et al., 2008; Schafstall et al., 2010). The only real sediment work I am aware of is that from Nolting et al. (1999) and Gier et al. (2016) and these took place mostly in oxygenated sediments it appears. That O_2 plays a role in the release of such metals is well known (Homoky et al., 2012; Severmann et al., 2010), but iron is only released reductively when O_2 is completely depleted (Sundby et al., 1986). The Severmann et a. (2010) work shows a nice relationship between Fe fluxes and O_2, with the large caveat that the landers used there likely consume all the O_2 in the sediment (though not all of the oxygen in the water in the chamber) before the Fe efflux begins, but then even at the O_2 concentrations found on the Mauritanian shelf the flux they predict is not lot large compared to what could be generated by resuspension – additionally intense mixing tends to keep oxygen levels higher lowering the flux of reduced iron but increasing that from resuspension. Interestingly similar iron fluxes to the Mauritanian are seen in the well-oxygenated waters of the Ross Sea (Marsay et al., 2014) indicating the role of resuspension dominates and not oxygen.

In a study of sediment composition and benthic fluxes during the same cruise (Schroller-Lomnitz et al., 2018), enhanced Fe(II) concentrations of up to 30 µM are observed within a few cm sediment depth, indicating reductive dissolution does occur in these sediments. These Fe(II) concentrations are not as high as observed in some other regions (Severmann et al. 2010), but are for example also similar to Fe(II) concentrations in sediment underlying the entirely anoxic Peruvian OMZ (Scholz et al. 2014). We acknowledge that oxygen concentrations are not the only factor influencing benthic Fe fluxes. Other factors are for example organic matter content, sediment type, sediment grain size and shelf topography influencing sediment resuspension (Homoky et al., 2016). Such factors can result in different benthic Fe fluxes from different regions despite similar bottom water oxygen concentrations. In order to provide this information to the reader, we modified the following sentence at Page 4 Line 5:

Differences in benthic TM supply in field studies however suggest other factors such as sediment type, shelf topography and organic matter supply also influence the benthic release of TMs (Homoky et al., 2016)

However, these are all factors that do not vary for the same location within a few days. Sediment resuspension is indeed another factor that might have changed fluxes in our study regions, however as mentioned above, our Al data from the repeated stations do not support this. While oxygen concentrations in the water column are not low enough to reduce Fe in situ (although reduction of Fe might be argued to occur in anoxic micro-environments within particles (Bianchi et al. 2018)), a change in water column oxygen might reduce the oxic-anoxic transition zone within the sediments facilitating Fe(II) efflux and slowing down oxidation kinetics (Homoky et al., 2012, Millero et al., 1987). Dissolved Fe released from reducing sediments might be prevented from immediate precipitation once in contact with oxygen by stabilizing processes such as ligand-complexation and a large fraction of the dFe might be present as colloids. Benthic Fe fluxes in the Ross Sea appear to be around an order of magnitude smaller than the fluxes observed during our cruise in the Mauritanian OMZ (Schroller-Lomnitz et al. 2018). Also dFe concentrations near the seafloor in the Ross Sea are much lower than our observed near bottom dFe concentrations (Marsay et al. 2014).

A previous study in the Mauritanian upwelling along almost the same transect (Schlosser and Croot, 2009) indicated that iron solubility was apparently controlled by remineralization as it varied with O_2, pH and phosphate concentrations. While no measurements of Fe solubility were made in the present work it does raise the question of whether pH may also be a control on the distribution of metals seen in this study but which has not been considered here. Although the PCA analysis made in this work would suggest that the resuspended elements (Fe, Al, Mn) were not related to the remineralization indicators.

Indeed, pH might have an influence on the solubility of trace metals. Unfortunately, no pH data are available from our cruise. As pointed out by the reviewer, the PCA analysis does not indicate a nutrient-like remineralization-driven distribution of Fe, Co and Mn. Therefore, remineralisation processes do not seem to be a major driver for these elements here.

The importance of scavenging on dissolved metals is mentioned in the introduction but after page 3 it does not come back into the text. Given that there is high particle numbers across this transect , either from the high productivity in surface waters, dust deposition, or from benthic resuspension events it is amazing that this process is not invoked as a control on dissolved metal concentrations in the discussion. The turbidity data indicates that particles are likely important, but this is not discussed in any context in the manuscript. If O_2 is the control that the authors say it is then they should at least follow through from their introduction and examine the role of scavenging on the scavenged elements.

While we indirectly mention this process at a few places throughout the manuscript, we didn't explicitly use the term scavenging very often. We changed a few paragraphs to use the term scavenging for a better linkage between the processes described in the introduction and our data discussion, and have further extended the discussion in respect to scavenging processes.

List of changes:

Paragraph Page 21, Line 6: Particles in the water column can either comprise a source or a sink of dissolved TMs. In the top 50 m of the water column a large part of the LpTMs may be part of living biological cells (e.g. phytoplankton) or organic detritus, and can enter the dissolved TM pool by remineralization (Bruland and Lohan, 2006) Additionally, LpTMs may be part of lithogenic phases from Saharan dust and sediment particles, or authigenic phases. Authigenic phases are formed in-situ by TM adsorption onto particle surfaces or by the formation of amorphous TM oxides and hydroxides

(e.g. FeO(OH) in the mineral structure of goethite) (Sherrell and Boyle, 1992), processes referred to as scavenging.The extent of scavenging processes is largely influenced by the amount and type of particles present (Balistrieri et al., 1981; Honeyman et al., 1988).

Sentence Page 21, Line 23: Furthermore, offshore transport of acid-labile Fe particles formed by scavenging (oxidation/adsorption) of dissolved Fe originating from a benthic source was observed in the North Pacific (Lam and Bishop, 2008) and may contribute to the bioavailable Fe pool.

Sentence Page 22 , Line 2: The large additional LpFe source at depths is likely associated with benthic dFe inputs, with a subsequent transfer to the particulate phase by scavenging.

Atmospheric flux estimates: Using dissolved Al concentrations to estimate the aerosol flux of the other elements is complicated as while there is good data on the elemental composition of the Saharan aerosols (Fomba et al., 2013; Kandler et al., 2011; Müller et al., 2010) what is missing is reliable fractional solubility data (Baker and Croot, 2010) for all of the elements that represent dissolution in seawater and residence times for all of these elements in the surface ocean. The residence time section in the manuscript is very interesting and could be highlighted and compared more to other works from the same region (Croot et al., 2004; Dammshäuser et al., 2013; Jickells, 1995; Jickells, 1999) as presently this aspect of the work is under developed. In the present work the residence time for Al is most likely on the order of 3-6 months given the large inputs of Al from the Saharan dust or indeed it may be much shorter given work on iron in the same region (Croot et al., 2004).

We agree with the reviewer. The estimation of atmospheric fluxes using dAl concentrations in the mixed layer is difficult to constrain. Especially in this region where seasonality plays a major role in controlling dAl concentrations in surface waters as observed from numerous north to south transects which display a large range in dAl concentrations (Menzel Barraqueta et al., 2019). Indeed, the residence time appears to be lower in this region as suggested for iron by Croot et al., 2004. In Menzel Barraqueta et al., 2019 they used an Al residence time of 1.25 years (extracted from Han et al., 2008) for the tropical Atlantic and calculated an atmospheric deposition flux well below modeling studies. However, assuming a residence time of 3 months did yield deposition fluxes that were equal, within uncertainty, to modeling studies. First, we shortened this section as suggested in the reviewer's overview and then added some more detailed discussion about the residence time and solubility. The modified section reads as follows:

1.4.1 Atmospheric deposition

Aluminum is present as a relatively constant fraction of ~8.15 wt% in the continental crust (Rudnick and Gao, 2006), is supplied to open ocean surface waters mainly by atmospheric deposition (Orians and Bruland, 1986) and is not considered to be taken up by phytoplankton (apart from a small amount being incorporated into siliceous diatom frustules; Gehlen et al., 2002). Therefore, dAl in the surface mixed layer is used as a tracer for atmospheric deposition to the surface ocean (Measures and Brown, 1996; Measures and Vink, 2000). The atmospheric input in the study region is mainly influenced by North African/Saharan mineral dust with only a small contribution of anthropogenic sources which differ greatly in TM composition and solubilities from mineral dust (Baker et al., 2013; Patey et al., 2015; Shelley et al., 2015). Close to continental shelves, Al can also be supplied by sediment resuspension in addition to atmospheric input (Menzel Barraqueta et al., 2018; Middag et al., 2012; Moran and Moore, 1991). Enhanced aerosol optical depth above our study region (Supplementary Fig. S3&4) indicates high dust loading at the time of our cruise.

Our dAl concentrations in surface water ranged between 30 and 49 nmol L^{-1} and LpAl between 3.4 and 18.2 nmol L^{-1}. Dissolved Al concentrations decreased with depth (Fig. 8), indicating that Al was released by aeolian dust deposition to surface waters and removed through scavenging at depth (Orians and Bruland, 1985).

Dissolved atmospheric deposition fluxes can vary largely depending on the aerosol solubility, which is dependent on aerosol source, atmospheric aerosol processing during transport and dissolution in surface waters (Jickells, 1999). Here, atmospheric dFe fluxes were calculated using the dAl inventory in the surface mixed layer, a residence time of dAl of 0.65 ± 0.45 years as reported for the Canary Current System (Dammshäuser et al., 2011), and a ratio of 0.31 for dust derived dissolved Fe/Al (Buck et al., 2010). This approach is independent of the fractional solubility of Al, as we do not account for total atmospheric deposition fluxes, and only use the already dissolved fraction of Al. However, this approach is dependent on the ratio of Fe/Al from dissolution of aerosols. This ratio, however, is not clearly defined and can vary between different dust sources and deposition pathways, such as wet or dry deposition (e.g. Shelley et al., 2018). In our study region, dry deposition is the dominant deposition pathway, as it is located north of the Intertropical Convergence Zone and precipitation is minimal < 0.001 g/cm^{-3} (NASA). Here, we utilized a ratio observed for total aerosol samples in the remote North Atlantic from a Saharan dust source (Buck et al. 2010). Soluble ratios under the Saharan dust plume were however lower for all leach media (Fe/Al: 0.051–0.25; Shelley et al. 2018), indicating that the ratio of 0.31 utilized here, might result in an overestimation of the dFe flux estimates. This approach also assumes that dAl is only supplied to the surface ocean via atmospheric deposition. Vertical fluxes of Al from sediment resuspension are unlikely to contribute significantly to concentrations of dAl in surface waters here as dAl concentrations decreased with depth, indicating removal of dAl via scavenging.

Mean atmospheric dFe fluxes of the individual stations were 0.63–1.4 µmol m^{-2} d^{-1} (Fig. 5, Supplementary Table S2), values similar to reported fluxes close to our study region of 2.12 µmol m^{-2} d^{-1} further north between 22.5–25°N and 26.5–27.5°W (Rijkenberg et al., 2012) and 0.120 µmol m^{-2} d^{-1} around 20°N close to the African coast (Ussher et al., 2013). The uncertainty in the residence time of dAl, however, creates a large uncertainty in calculated fluxes resulting in a lowest flux of 0.37 µmol m^{-2} d^{-1} when using the largest estimated residence time of 1.1 years and a highest flux of 4.65 µmol m^{-2} d^{-1} when using the shortest estimated residence time of 0.2 years. In fact, a residence time of 3 months has been shown to give similar results for total Al atmospheric deposition fluxes as modeling studies (Menzel Barraquetta et al., 2019). Low residence times of a few months have also been suggested for Al and Fe in areas with a large dust deposition including our study region (e.g. Croot et al. 2004, Dammshäuser et al., 2011). Therefore, we suggest that the atmospheric dFe flux is more likely to be closer to the upper range of our flux estimates. However, the atmospheric deposition fluxes using a short residence time may be larger than the annual average since the dust load is highest between June and August in our study area (Supplementary Fig. S4).

In the present work the atmospheric deposition is not well presented as it does not discuss the role of aerosol solubility in the flux calculations and does not distinguish categorically between the total aerosol flux and what it terms is the dissolved flux – which as the deposition is predominantly dry means that it is metals that are solubilized post deposition. It would help to include at the very least satellite data on the atmospheric aerosol loading to pinpoint if there was dust deposition immediately before or during the occupation of these stations.

The definition of dFe flux is not very clear in the manuscript at the moment and we added a few changes to clarify this (see changes above). Indeed, fractional solubilities of Al and Fe after deposition are key to the calculations. The calculation using seawater dAl concentrations doesn't require the absolute fractional solubility value, but the ratio of Fe/Al from dust dissolution, which can vary dependant on e.g. dust source, atmospheric processing, and between wet and dry deposition. We added some more detail on this uncertainty to the flux description in order to clarify this. We also added a plot showing satellite data related to dust loading, averaged for the month of our cruise (June 2014) and a plot showing monthly averaged dust loading for the cruise region over 24 months, both in Supplementary Information.

Added plots:

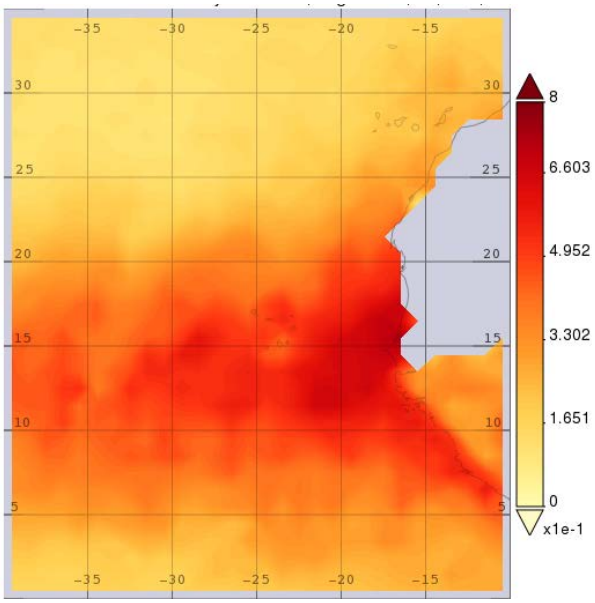

Figure S3. Time averaged map of aerosol optical depth 550 nm (dark target), monthly 1 deg (MODIS-Terra MOD08_M3 v6.1) for the month of June 2014.

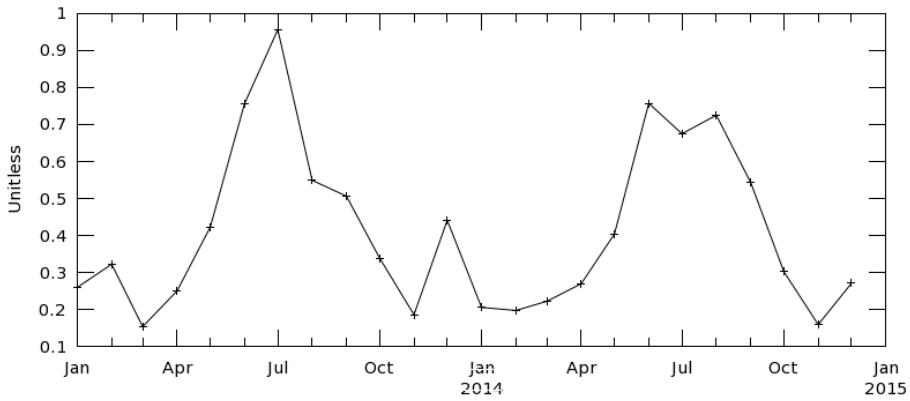

Figure S4. Area-averaged time series of aerosol optical depth 550 nm (dark target), monthly 1 deg (MODIS-Terra MOD08_M3 v6.1). Time series for January 2013 to December 2014 for the region between 19.5W, 17.5N, 16.5W and 18.5N.

Sections 3.5 and 3.6: These sections are long and don't add that much to the paper at present, as they read like an earlier draft of a PhD thesis and they should be shortened and tightly focused on the main points that are supported by the data. The central problem with these sections is that two repeat stations are interpreted mostly in the context of O_2 and not simply resuspension.

We acknowledge the reviewers opinion on the length of these sections, but we think that these two sections are very important for the manuscripts findings as they evaluate the role of scavenging and the influence of oxygen and sediment resuspension or dust deposition on the temporal variability of the trace metal concentrations. Additionally, the section "3.6.2 Atmospheric dust deposition and sediment resuspension" discusses the possibility of sediment resuspension by comparing Al data from the repeated stations.

Geochemical data from the NW African sediments: I was a little surprised that there was little discussion of the geochemistry of the sediments and then the relationship between the dust and water column compositions. A further paper that could be included is that of Itambi et al. (2010) who examined the magnetic mineral inventory of the sediments off Senegal.

We added a brief description of the geochemistry of the sediments in our study region at Page 11, after Line 23:

The sediments in the study area contain a large amount of carbonate, biogenic silica and quartz (Hartman et al. 1976). The fraction of sand and mud varies largely depending on bottom depth, with sand comprising between 7 and 70% of the dry weight (Dale et al., 2014). The particulate organic carbon (POC) content varies between 0.55 wt% at shallow depth (66 and 90 m) and increases to 3.3 wt% at 1108 m depth (Schroller-Lomnitz et al., 2019). A more detailed description of the sediments underlying our study region and sediment parameters collected on the same cruise, including Fe(II) concentrations and Fe/Al ratios, are given in Schroller-Lomnitz et al. (2019).

We also thank the reviewer for providing the additional reference. However, as this reference relates to much longer time scales, which might not be relevant for our study, and as it is in a different location at a much greater water depth (Depths 3500 m), we feel this is probably not a necessary addition.

Other particle data for the North Atlantic: I was surprised not to see any comparison to the particle data of Kuss and coworkers (Kuss and Kremling, 1999a, b; Kuss et al., 2010; Scholten et al., 2001; Waniek et al., 2005) as while it is only near surface data it does cover a similar transect and include time series data from sediment traps. There is also other recent trap data from close to the Canaries which gives more seasonal data (Brust et al., 2011; Brust and Waniek, 2010).

The particle data in the listed references were all quite far from our study region and were likely to receive atmospheric inputs in different magnitudes and from different sources. Our location was much closer to the coast, which has a likely influence on the particle composition. We only have the leachable particulate fraction in our study here and no total particulate data and therefore we do not see a benefit from including such a comparison.

Specific Comments:

P1 Line 20: What evidence is provided here that dust deposition did not play a role?

The assumption that dust deposition 'only played a minor role' on the differences between the two deployments was based on the determination of dissolved and leachable particulate Al concentrations at the repeated stations, which do not show much difference between the two deployments (see section 3.6.2.). This does not mean that trace metals are not also supplied by atmospheric deposition, but didn't seem to be the driver of the variability at repeated stations.

The sentence in the Abstract was modified as follows:

Variations in organic matter remineralization and lithogenic inputs (atmospheric deposition or sediment resuspension; assessed using Al as indicator for lithogenic inputs) only played a minor role in redox-sensitive TM variability.

P1 Line 23: How were the DFe atmospheric fluxes estimated? As it is most likely dry deposition so how was the dissolution assessed?

See response to general comments above. We used dAl inventories, which comprises the already dissolved fraction and applied a conversion by using a ratio of Fe/Al from atmospheric deposition which was previously obtained for aerosol samples in a nearby region (Buck et al. 2010).

We added the following information to the sentence:

Vertical dFe fluxes from O_2-depleted subsurface to surface waters (0.08–13.5 µmol m^{-2} d^{-1}) driven by turbulent mixing and vertical advection were an order of magnitude larger than atmospheric

deposition fluxes (0.63–1.43 µmol m^{-2} d^{-1}; estimated using dAl inventories in the surface mixed layer) in the continental slope and shelf region.

Also see changes to made to the discussion section for atmospheric deposition fluxes above.

P5 Line 19: What was the purpose of the 2nd Mn cartridge if it was not analysed? (P6, Line 24)

Both Mn cartidges were used for studies on Th-234. The $^{224}Ra/^{223}Ra$ ratios shown here, are only determined from one cartridge. We added the following information:

In this work, $^{224}Ra/^{223}Ra$ ratios are shown, which were analyzed from the first Mn cartridge.

P5 Line 20: Please include information on the flow rate through the pumps.

We added the following information to the sentence:

The pumped water volumes varied between 1000 L and 1700 L and flow rates were 10–15 L min^{-1}.

P6 Line 19: The reagent is Lumogallion not Lumogallium.

Thank you. We corrected this in the text.

P6 Line 20: Lumogallion

Corrected in text.

P6 Line 24: Please include information about the methodology that was used for these measurements and the basic operating conditions.

We extended the methods description accordingly, which now reads as follows:

2.3 Aluminum measurements

Aluminum concentrations were determined in surface water samples for all stations along the transect and at two stations (3 and 8) for the entire water column. Samples were analyzed for Al using the batch lumogallion method (Hydes and Liss, 1976). Acidified samples were buffered manually with a 2 M ammonium acetate buffer (Romil, UpA) to a pH between 5.1 and 5.2. The buffer was prepared using ammonium hydroxide (Romil, UpA) and acetic acid (Romil, UpA) in de-ionized water (MilliQ, Millipore). Buffered samples were spiked with a 2 mg L^{-1} lumogallion (TCI) solution allowing the complexing agent to be in excess. The lumogallion solution was prepared in 2 M ammonium acetate buffer (Romil, UpA). After spiking, samples were heated up for 1.5 h at 80°C in an oven (Heratherm, Thermo Scientific) and left to cool down overnight at room temperature to allow the formation of a fluorescent Al complex. Samples were measured using a fluorescence spectrophotometer (Cary Eclipse, Agilent). The samples were measured with an excitation and emission wavelength of 465 and 555 nm, respectively. The excitation and emission slits were set to 10. The plastic cuvettes used for the measurements were pre-cleaned in a 2 M HCl (Trace metal grade, Fisher) for at least 24 h. In between samples, the cuvette was thoroughly rinsed with de-ionized water followed by actual sample. The same cuvette was used during an analytical session. All samples were analyzed in duplicate and the concentrations calculated from the peak heights via standard addition. Samples and reagent natural fluorescence was monitored by analyzing their content in the absence of the complexing agent. The standards were prepared in low trace metal seawater from a 500 nmol L^{-1} stock standard solution prepared from a 1000 ppm Al standard solution (Merck Millipore). A typical calibration had the following standard concentrations: 0, 10, 20, 40, and 60 nmol L^{-1}. GEOTRACES reference seaweater (GS) was run with a mean average Al value of 27.76 ± 0.17 nmol L^{-1} (n=4; consensus value 28.2 ± 0.2 nmol L^{-1}).

P6 Line 30: The iodide data is not presented so the reader can not assess what the relevance of this parameter is. For instance, was the iodide concentration ever more than what might be expected for total iodine at the salinity of the seawater as this would be a good indicator of excess iodine from a benthic source.

Iodide concentrations were enhanced within the oxygen minimum zone but not to high values as observed in the Peruvian OMZ and they were not higher than would be expected for total iodine. Therefore we do not see evidence for a benthic source. However, we acknowledge that it would be of interest to show the spatial distribution and added the following figure of the Iodide distribution in Supplementary Material:

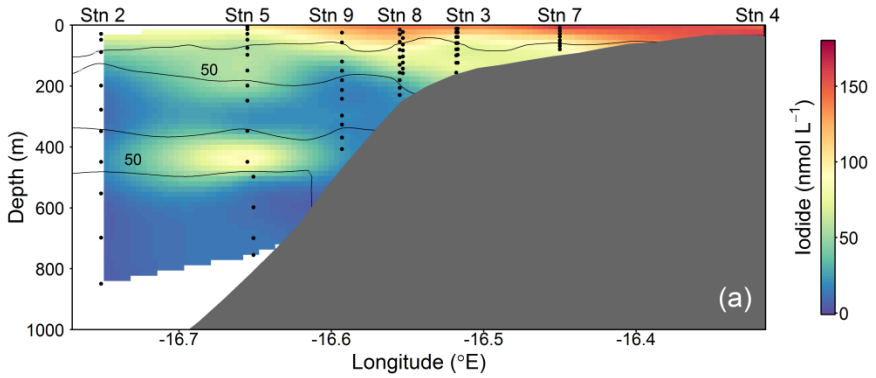

Figure S1. Spatial distributions of Iodide across the Mauritanian shelf at 18°20'N in June 2014. Each sample location is indicated as black dot and oxygen contours at 50 µmol kg^{-1} enclosing the upper and lower OMZ are displayed as black contour lines.

P7 Line 4: Were the Turbidity and Chlorophyll sensors calibrated during this expedition? Was the Turbidity sensor zeroed between CTD casts?

For the turbidity data used in the manuscript, we used the Wetlab sensor output corrected by the calibration coefficients provided by the manufacturer. No further calibration was applied. Further, the turbidity sensor was not zeroed between individual CTD casts. However, we did not observe a drift of the turbidity readings. Instead, a constant offset of 0.12 NTU (nephelometric turbidity unit) was distinct in the data throughout the cruise. To make the calibration procedure more clear, we added:
Turbidity and chlorophyll *a* were measured with a combined Wetlabs turbidity and fluorescence sensor that was attached to the CTD. The output of both sensors was corrected using the calibration provided by the manufacturer.
See also comment below.

P7 line 9: So the decay was assumed linear for all stations, no matter the depth?

We assume the reviewer is referring to the oxygen sensor calibration here. The sentence in the manuscript (page 7 line 7-8) stated: "The O_2 calibration was undertaken using a linear fit with respect to O_2 concentration, temperature, and pressure."
For calibration of the Seabird oxygen sensor, we first use standard Seabird processing during which the sensor calibration coefficients provided by the manufacturer are applied. The output of the Seabird processing is oxygen concentration in µmol/kg. In a second processing step, we fit the oxygen sensor data to the oxygen concentration measured from water samples on board the cruise via Winkler titration. This is done by minimize the differences between the Winkler titration samples from the bottle data and the respective oxygen sensor data using linear functions for pressure (i.e. depth), temperature and oxygen concentrations itself. For some oxygen sensors, a quadratic fit in pressure (i.e. depth) works better than a linear fit. This, however, was not the case

for the oxygen sensors (dual Seabird CTD system) used during the M107 cruise. The uncertainty of this calibration is provided by the standard deviation between the samples and the sensor readings after applying the calibration. We mention this uncertainty in the text. The oxygen sensors are typically calibrated at Seabird laboratories annually or every second year, depending on the duration the sensor was used during cruises.
These details above are given in the cruise report of the M107 cruise. To keep this manuscript concise, we replaced the sentence (page 7 line7-8) by the following text:

Oxygen sensor data was initially processed using calibration coefficients provided by the manufacturer. Subsequently, O_2 sensor data were fitted to the O_2 concentrations determined by the Winkler titration method using linear functions for temperature, O_2 and pressure (i.e. depth).

P7 Line 17: How was the tap-water assessed to be Ra free? Was it provided from the ship's system as they can be notorious for Ra contamination. More details need to be provided here.

The following changes were made to the manuscript (Page 7, Line 17) to clarify this:

On-board the ship the Mn-cartridges and Mn-fibers were washed with Ra-free tap water to remove any residual sea salt and particles. Ra was removed from the tap water by passing it through a Mn-fiber filled cartridge. Afterwards, both cartridges and fibers were partially dried with filtered compressed air to remove excess water.

P7 Line 24: How was the ^{228}Th assessed? Was it only from the background counts after 3 weeks when the initial ^{224}Ra had decayed?

Yes. Th-228 was measured 3 weeks after the first measurement of ^{224}Ra. The following sentence was added at Page 7 Line 24 to make this clear to the reader:

The ^{228}Th activity was measured three weeks after the first measurement of ^{224}Ra, when the initial ^{224}Ra had decayed.

P8 Line 2: Concentration difference between which levels? At times it seems it is between 8-29 m (P 8, Line 8) and at other times it seems it is over multiple levels (P9, Line 15)? This section of the methodology needs to be better explained.

Indeed, the text was unclear, thank you. We changed the lines formerly on page 8, line 8 to: Average advective and diffusive TM fluxes were calculated for a depth interval from the shallow O_2-depleted waters to surface waters. The exact depth interval varied for each station (see Table S2) due to differences in the depths where TM samples were collected. The upper depth (8–29 m) was always in layers with enhanced chlorophyll *a* fluorescence, although for some stations the upper depth was below the surface mixed layer.
The discussion on former page 9, line 15 was changed to:
Ideally, the vertical length scale over which the concentration difference is determined can be diagnosed as the TM concentration variance divided by its mean vertical gradient (e.g. Hayes et al., 1991). However, in our study TM concentration time series data are not available. Previous studies have used a vertical length scale of 20 m to calculate the concentration differences between the target depth and the water below (e.g. Hayes et al., 1991; Steinfeldt et al., 2015; Tanhua and Liu, 2015). For our calculations, we chose to use a smaller length scale of 10 m following Hayes et al. (1991) which results in vertical advective TM flux presumably on the lower side of possible values.

P8 Line 4: How valid is it to ignore lateral fluxes in a region where there are strong filaments and cross shelf transport (Fischer et al., 2009; Gabric et al., 1993; Klenz et al., 2018; Rees et al., 2011; Schafstall et al., 2010)? Indeed the recent paper by Klenz et al. (2018) shows that at this time there are very high current velocities along the 18 ° N line.

Thank you for this comment. Apparently, our description here is unclear. In fact, the vertical fluxes determined in the manuscript do not depend on lateral fluxes. With the sentence in question "The equation is solved by vertically integrating the tracer transport budget equation between two vertical layers while ignoring lateral fluxes, changes of w with depth and assuming steady state." (page 8 lines 3-5) we wanted to express how the two vertical fluxes, vertical advection and vertical diffusion, can be derived from the transport budget equation which is fundamental to the analysis (e.g. Brandt et al., 2010). Transport budget equations balance advective and diffusive flux divergences. As many studies determine transport budgets for the mixed-layer, fluxes instead of flux divergences are used in the vertical component (e.g. Schafstall et al., 2010; Rhein et al., 2010; Kock et al., 2012; Steinfeldt et al., 2015; Tanhua and Liu, 2015). However, fundamentally all these studies solve

$$\frac{\partial C}{\partial t} = -u\frac{\partial C}{\partial x} - v\frac{\partial C}{\partial y} - w\frac{\partial C}{\partial z} + \frac{\partial}{\partial x}K_x\frac{\partial C}{\partial x} + \frac{\partial}{\partial y}K_y\frac{\partial C}{\partial y} + \frac{\partial}{\partial z}K_z\frac{\partial C}{\partial z} - S^- + S^+$$

Where S^- are sinks and S^+ are sources of solute concentration C. Expressions for the vertical advective flux and the vertical diffusive flux as used in the manuscript (and the other studies mentioned above) can be derived by: "The equation is solved by vertically integrating the tracer transport budget equation between two vertical layers while ignoring lateral fluxes, changes of w with depth and assuming steady state." as we had stated in the text in the earlier version. However, judging from the reviewer's remark, the sentence does not advance understanding of the nature of the fluxes determined in our manuscript and elsewhere, but is unclear instead. We thus decided to delete the sentence.

P8 Line 14: How close to the bottom did the microstructure profiles get to? Typically they do not go into the benthic boundary layer for fear of doing damage to the probes if they hit the sediment. Information on how close to the bottom the sensors got would be extremely helpful in assessing whether or not the fluxes from the sediment were well constrained. Similar information for the trace metal sampling should also be supplied.

We run the microstructure probe all the way to bottom and thus obtain full depth profiles of the dissipation rate of turbulent kinetic energy. The profiler is not damaged when impinging on the bottom. However, we are calculating fluxes in the upper water column between 20 m and 50 m depth. Neither near-bottom turbulence data nor TM data are needed for determining the diffusive and advective fluxes presented here.

P9 Line 5: I am missing a step here as this website seems to provide only wind speed data, so how was the alongshore wind stress calculated? The number seems reasonable given global compilations (Varela et al., 2015) but what are the uncertainties? There is a NOAA site that calculates everything https://www.pfeg.noaa.gov/products/PFEL/modeled/indices/upwelling/NA/how_computed.html

The wind stress was calculated from daily ASCAT wind measurements from 18°22.5'N, 016°22.5°W using $\tau_y = \rho_{air} C_d v^2$ where v represents alongshore wind, C_d is drag coefficient for which 1.15x10^{-3} was used (e.g. Fairall et al., 2003) and ρ_{air} is density of air. The value of 0.057Nm^{-2} represents an average of all wind stress values that were determined from individual ASCAT wind velocities available for June 2014. To provide this information to the reader, we added: (0.057 Nm^{-2}, determined from daily winds from Remote Sensing Systems ASCAT C-2015, version v02.1 (Ricciardulli and Wentz, 2016) at 18°22.5'N, 016°7.5°W using $\tau_y = \rho_{air} C_d v^2$, where v represents alongshore wind, C_d is drag coefficient for which 1.15x10^{-3} was used (e.g. Fairall et al., 2003) and ρ_{air} is density of air)

As stated above, differences between land stations and ASCAT winds in the order of 20% were found by Ndoye et al. (2014). However, as further detailed above, other uncertainties dominate the errors in our flux calculations.

P9 line 5: How was the wind close to the coast assessed? For ASCAT wind velocities closer than ~70 km (25-km products) or ~35 km (12.5-km products) from the coast are flagged because of land contamination. This is due to the fact that - in the case of the 12.5-km product - backscatter measurements (σ0) of up to 35 km away from each WVC centre are used in the spatial averaging. It would appear that station 4 would be too close to the coast to use an ASCAT wind product, so some explanation needs to be provided here.

The wind product used in this study is described above. The used product "Remote Sensing Systems ASCAT C-2015, version v02.1" includes the 12.5 Km ASCAT L1B backscatter data from EUMETSAT. We use the wind values from the position 18°22.5'N, 016°22.5°W which are not flagged. The position is located about 35km away from shore. Our methodology to determine vertical velocities follows Steinfeldt et al. (2015), who used the first available ASCAT satellite wind value along with the Gill parameterization. We could have also used wind data measured by the research vessel (that compared quite well to the satellite derived winds) but refrained from doing so because the Gill paramerization was validated using satellite winds. As stated before, we now include a discussion of the uncertainties of our flux determinations.

P9 Line 6: These estimates of the upwelling velocity contradict the findings of Tanhua and Liu (2015) and others (Cropper et al., 2014), who reported that there was no upwelling over the summer, the same season when this expedition took place. The upwelling flux estimates listed here are also close to the maximum rates estimated using tracers by those authors for periods when the upwelling is active so some explanation is required here – see the general comment above regarding this.

Cropper et al. (2014) discuss upwelling indices and SST gradients averaged between 12° and 19°N. Our analysis is located at the northern boundary of their box. Differences between their and our analysis most likely originates from regional differences is thus not mentioned here. Further, Tanhua and Liu (2015) used data collected in between July 12 and August 6, 2006, one month later than the data reported here. Again, we refrain from a discussion because we believe it would leave the reader more confused. We added some reference to the Tanhua and Liu study and the seasonality of upwelling to section 3.1.

P9 Line 12-17: The explanation for the flux estimate being made here needs to be better described, as for most readers usually the vertical advective flux would be the velocity times the concentration and would not involve the gradient in the concentration as shown on line 17 here. It needs to be explained then why you use the gradient approach and which way around the gradient is (e.g. based on the equation as it stands you could have upwelling but still have a net negative flux from the surface waters if the metal concentration gradient is negative, this would happen when there was a higher metal concentration in the surface waters than below).

We eliminated the gradient expression equation in the revised version of the manuscript and instead simply refer to concentration differences. We also simplified the description of the approach and now state:

Ideally, the vertical length scale over which the concentration difference is determined can be diagnosed as the TM concentration variance divided by its mean vertical gradient (e.g. Hayes et al., 1991). However, in our study TM concentration time series data are not available. Previous studies have used a vertical length scale of 20 m to calculate the concentration differences between the target depth and the water below (e.g. Hayes et al., 1991; Steinfeldt et al., 2015; Tanhua and Liu,

2015). For our calculations, we chose to use a smaller length scale of 10 m following Hayes et al. (1991) which results in vertical advective TM flux presumably on the lower side of possible values.

P10 Line 8: So horizontal advection is at its greatest in summer, but horizontal fluxes are not considered in interpreting the trace metal and O_2 data?

In the manuscript, we discuss the potential origin of elevated trace metal concentrations from the shelf at the transect and from the shelf further south. We also mention a potential influence of changes in the residence time of the water masses on the shelf as a factor which influences trace metal concentrations. In order to highlight this further we added some discussion about a change in source waters and local oxygen respiration for the repeated stations based on observations by Thomsen et al. (2018). See answer to comment below.

P11 Line 2: Though it should be noted they are an order of magnitude or more lower than the Celtic Sea and the St Lawrence seaway.

For clarification, we added this information to the sentence:

Vertical fluxes of nutrients driven by mixing processes are amongst the largest reported in literature, however lower than in the Celtic Sea (Tweddle et al., 2013) and the lower St. Lawrence Estuary (Cyr et al., 2015).

P11 Line 21: Other studies in the same region have pointed to the role of CDOM and reactive oxygen species in potentially controlling metal distributions (Heller et al., 2016; Wuttig et al., 2013). Indeed Heller et al. (2016) observed changes in FDOM consistent that could be consistent with microbial respiration of resuspended sediment material, a process also invoked by Thomsen et al. (2018) to explain low oxygen patches in these waters.

Reactive oxygen species and CDOM might in fact have an influence on trace metal concentrations in surface waters and maybe also in the deep ocean. But this field is not well understood yet and we don't feel like we can add anything that helps to better understand this interaction or helps interpreting our data. The influence of CDOM is particularly unclear as it is involved in the production of superoxide in the surface ocean during photoreduction (Micinski et al. 1993), but CDOM may also be a sink of superoxide (Heller et al., 2016). Furthermore, in the ETNA Fe appeared to be relative inert to the reaction with superoxide (O_2^-) even though this element showed the most pronounced changes coinciding with O_2 changes, (Wuttig et al., 2013).

P11 Line 17: If Thomsen et al. (2018) indicate this was from horizontal advection then this would invalidate the approach for estimating the vertical fluxes – see the general comment on this above.

See answer to general comment.

P12 Line 4: The Hawco et al. (2016) paper is for the Pacific and a much more O_2 depleted water column with sulfidic sediments so a very different environment.

We removed the Hawco et al. (2016) reference in this sentence.

P12 Line 8: The values are also similar to values found by Wuttig et al. (2013) for the Tropical North Atlantic and near to coastal West Africa.

We appreciate pointing out this important reference for trace metal data in this region. We added the Wuttig et al. (2013) reference to this sentence. The sampled locations have a greater distance from the coast and bottom depth than our coastal stations and are more comparable with our stations further offshore where we observe a similar concentration range.

P12 Line 14: Of direct relevance to this work is the result that oxygen has also been shown to have a strong impact on Co speciation in the Tropical North Atlantic (Baars and Croot, 2015). This work should therefore be included in the discussion of the present data set.

Thanks for pointing out this important reference here. We have added the reference to the sentence on P12 Line 4 and also used it in section 3.6.1 in order to discuss the dCo variability between repeated stations. The following was added to the paragraph starting at Page 23 Line 17:

This is in accordance with previously observed correlation of dCo with PO_4^{3-} in addition to O_2 (Baars and Croot, 2015; Saito et al., 2017). However, we observed a very low Pearson correlation of dCo with PO_4 of only 0.15 compared to oxygen (-0.58) (Supplementary Table S1) below 50 m water depth, suggesting a stronger influence of oxygen than remineralization on the overall distribution of dCo for our study area.

P12 Line 26: Mn data is also found in the work of Wuttig et al. (2013) and this work is again of direct relevance to the current paper with regard to the relevance of reactions with oxygen.

We also added this reference to this paragraph.

P12 Line 35: Please define LOQ here and what its value is.

We added the definition of LOQ the first time used in this section, which is on Page 11 Line 30, as follows:

In contrast, LpCo concentrations varied between below limit of quantification (LOQ) and 0.179 nmol L^{-1} and were generally highest in surface waters and close to the coast (Fig. 3d).

The Limit of Quantification is also defined in the methods section including how it was calculated. It is not possible to state a single value here, as we quantified the LOQ individually for each station and depth using the percentage uncertainty of the dissolved and total dissolvable concentration, as both are used to quantify the leachable particulate concentration.

P13 Line 24: Is there any evidence for sulfide release from the sediments in this region (see the general comment on this above also)?

Sulfide was present at around 10 cm sediment depth for water depth of 47 and 90 m, whereas sulfate reduction was observed close to the sediment surface down to 236 m water depth (Gier et al. 2017). Also see answer to general comment above.

P13 Line 36: Did you encounter MOW in this work?

No, we did not encounter MOW here.

P14 Line 27: It is worth noting here that dilution does not impact the ratio of the two radium isotopes. Though the assumption is that there is only a single uniform benthic source.

We added this explanation to the description of the use of $^{224}Ra/^{223}Ra$ ratios in the paragraph above at Page 14 Line 23:

The ratio $^{224}Ra/^{223}Ra$ is not affected by dilution assuming there is no mixing with waters having significantly different $^{224}Ra/^{223}Ra$ ratios.

P14 Line 29: Radium is conservative the other elements are not – resuspension and scavenging are the most likely controls as the O_2 concentration is not low enough to impact iron or manganese.

See answer to general comment on the influence of oxygen concentrations. Scavenging processes may be influenced by oxygen concentrations and sediment release may be enhanced under lower O_2.

P15 Line 7: This location is not on the 18° N transect so is it a source region to the south which is then advected north as you suggest so again the horizontal fluxes seem to dominant here.

Yes, there are horizontal fluxes, but unfortunately we are unable to quantify them in the present study.

P15 Line 15: How was the PCA performed? Were the data all normalized to have a mean of 0 and a standard deviation of 1 before analysis? P15 Line 18: O_2 and AOU are linearly related so they would be expected to be orthogonal to each other in the PCA – this is ok though as only the PCA components need to be independent.

The PCA data are scaled to unit variance. In the original figure legend we state: Loadings/scores have been scaled symmetrically by square root of the eigenvalue. For full details we refer the reviewer and readers to the R documentation for the PCA calculation function used (as described in the original manuscript).

P16 Line 7: What evidence is there that the sediments are anoxic? Sediment work performed along the same transect line shows no evidence for this (Gier et al., 2016). See the general comment on this above.

See response to general comment: High Fe(II) values (~20–30 µM) were observed within a few cm of sediment indicating reductive dissolution is occurring (Gier et al., 2017; Schroller-Lomnitz et al., 2018).

P16 Line 24: This assumes that all of the dissolved iron is from remineralization and not from dust dissolution (Baker et al., 2013; Baker and Croot, 2010; Baker et al., 2006a; Baker and Jickells, 2006; Baker and Jickells, 2017; Baker et al., 2006b), given the proximity to the Sahara and the impact it is on Aluminum concentrations this seems a contradiction. There is also the potential for direct remineralization of Saharan dust by zooplankton (Barbeau et al., 2001; Barbeau and Moffett, 2000; Barbeau et al., 1996; Laglera et al., 2017; Schmidt et al., 2016).

Yes, this assumes that the utilized offshore reference values from previous publication are mainly influenced by remineralization. There is a large uncertainty in the calculation and therefore we are using the full range of lowest and highest dFe/C ratios. This is just a crude estimate. We already emphasize this in the text though: "These offshore ratios may still be influenced by an atmospheric source of dFe, which would result in an overestimation of dFe/C ratios from remineralization and thereby an overestimation of the fraction of remineralized dFe"

P17 Section 3.4.2 – See the general comment about the atmospheric fluxes.

Answered above

P19 Line 6: See the general comment above regarding residence times.

Answered above

P19 Line 32: This would indicate it is being scavenged. There is no discussion of the role of scavenging in this manuscript after the introduction. Surely this deserves some attention given it is likely a major control on dissolved metal concentrations.

We modified the sentence accordingly to highlight the influence of scavenging as follows:

Vertical fluxes of Al from sediment resuspension are unlikely to contribute significantly to concentrations of dAl in surface waters here as dAl concentrations decreased with depth, indicating removal of dAl via scavenging.

Also see response to general comments above.

P20 Line 11: Closest to the shelf is also likely to be the most impacted by the ASCAT limitation near the coast so it will have to be explained if this value is far enough away from the coast. The station 4 advective flux is also an order of magnitude more than any of the other stations so some indication of why this is needs to be supplied as the reader does not see the distribution at station 4.

The parameterization from Gill uses a single wind stress value close to the coast. No offshore wind data is used. The vertical velocities away from the coast are determined by the x-dependence (exponential decay). We refer the reviewer to equation (2).

P20 Line 16: Has anyone checked the sea surface height data? Were there any mesoscale eddies around at this time (Karstensen et al., 2015)?

SSH, SST and shipboard velocity data did not show mesoscale eddies in the study area. In addition the analyses of Schütte et al. (2016) showed that they are mainly generated at the eastern boundary during boreal summer, whereas our cruise was in June.

P20 Line 32: Though most of the sediment is derived from Saharan dust and biogenic material, so you can't escape the dust entirely as a source.

Yes, Saharan dust can indirectly be a source of trace metal after being deposited to the seafloor and then undergoing reductive and non-reductive dissolution. In this section we only compare the direct atmospheric fluxes to the vertical fluxes from below, not discussing where the trace metals supplied by vertical fluxes originated from, which could be from a benthic source potentially influenced by dust deposition to the seafloor. We agree that it is important to mention the influence of dust derived trace metals on sediment release somewhere in the manuscript.

Therefore, we added the following statement to the Conclusion part of the manuscript (P25 Line9):

However, deposition of atmospheric dust is a source of Fe to sediments in our study region and consequently indirectly contributes to benthic released TMs.

P21 Line 15: What does an NTU represent here? It has not been defined in the paper anywhere. This could simply be background noise of an uncalibrated instrument as figure 7 seems to show 0.2 NTU most of the time.

Thank you for pointing out that we did not properly introduce NTU. The values in NTU (nephelometric turbidity unit) refers to the unit of data output of the Wetlab turbidity sensor. It represents the proportion of white light scattered back to a transceiver by the particulate load in a body of water, represented on an arbitrary scale and referenced against measurements made in the laboratory by the manufacturer on aqueous suspensions of formazin beads. For the turbidity data used in the manuscript, we used the Wetlab sensor output corrected by the calibration coefficients provided by the manufacturer. No further calibration was applied. The most frequent small turbidity value measured in the deep ocean and in large distance to the seafloor was 0.12 NTU. Standard deviation in this oceanic region was 0.01 NTU, suggesting that a value larger than 0.14 NTU reliably measure elevated turbidity in the water column.
To make this more clear to the reader, we added following sentences to the manuscript at Page 7, line 4 : "Turbidity ..." to the following:

Turbidity and chlorophyll *a* were measured with a combined Wetlabs turbidity and fluorescence sensor that was attached to the CTD. The output of both sensors was corrected using the calibration provided by the manufacturer. Throughout this manuscript, turbidity data are presented in nephelometric turbidity units (NTU). The noise level of the sensor in our data set was found to be lower than 0.14 NTU.

P21 Line 19: Reductive dissolution is occurring in the oxygenated waters here?

Thanks for pointing out the potential for misunderstanding this sentence. We meant from reductive dissolution occurring in the sediments representing the TM source. We changed the sentence to the following:

Furthermore, offshore transport of acid-labile Fe particles formed by scavenging (oxidation/adsorption) of dissolved Fe originating from a benthic source was observed in the North Pacific (Lam and Bishop, 2008) and may contribute to the bioavailable Fe pool.

P22 Line 17: This is assuming that it is the same water mass being sampled, but early we are told that this is water that came from the south, so it clearly isn't and thus trying to argue that this is a temporal trend in the same water is flawed. At the very least you could at least show the data on the same density surfaces. See the general comment on this above.

For the repeated stations below 50 m - where we observe the shift in trace metals - temperature vs salinity plots indicate that the water masses didn't change. The exact source of the water and the velocity of water mass transport may still be different even though the water mass properties seem to be the same. The change in oxygen at these locations discussed in Thomsen et al. (2019), were also described as not being caused by a change in water masses. These author argued that the percentage of South Atlantic Central Waters bringing in oxygen were not a reason for the shift in O_2, and it was likely that the change in oxygen concentrations could be explained by in-situ oxygen consumption/respiration processes. The temporal variability at this location is not attributed with a change in water masses although it may come from the south. Further offshore low oxygen anomalies were associated with locally increased SACW fractions (Thomsen et al., 2019). The SACW fraction was observed to stay relatively constant near the seabed. As stated above, we think the description in the original manuscript was misleading and adjusted the paragraph on Page 11, Line 17.

We also added these data plotted against density to the Supplementary Information.

P25 Line 14: You have shown the variability in a shelf system but no evidence that this is controlled by O_2 at this location. The recent paper by Schlosser et al. (2018) did however show the impact of a sulfidic event on trace metal concentrations in the water column so that is an example already.

See response to general comment. The influence of sulfidic event in an anoxic water column on trace metal distribution is a very important finding, but the influencing processes are very different from the influence of different levels of oxygen concentrations and therefore not directly comparable to our findings. In the study by Schlosser et al. (2018), no short-term variability in oxygen concentrations was observed and H_2S concentrations were also only determined for one deployment at one station.

P26 Line 4: FW are not the initials of one of the authors, so we don't know who this is until we read later in the acknowledgements.

Thanks for pointing this out. We added the full name of that person here.

Figure 3: There is no iodide data shown, yet it was used in the PCA and Radium was not.

We added a figure showing the spatial distribution of iodide to the Supplementary Material. See answer to comment on iodide above.

Figure 3: The radium data shows considerable 'young waters' in the near surface offshore, some more explanation is needed for where this might have contacted the sediments last. Or is it an artefact of the contouring in R as it is hard to see the data points.

The Radium data at this place shows indeed 'younger waters' and is not an artefact of the contouring. We describe in the original manuscript that this water has a likely origin from the shelf further south. We added a sentence referring to Thomsen at el. (2019), describing the contribution of SACW in this area. We are unable to provide more information about the origin of this water.

Figure 6: suggest you use a different symbol for the leachable as when they overlap it is hard to tell which is which when they are all the same symbol.

Thanks for this comment, to avoid confusion, we turned the symbol for all data points above 50 m into diamonds.

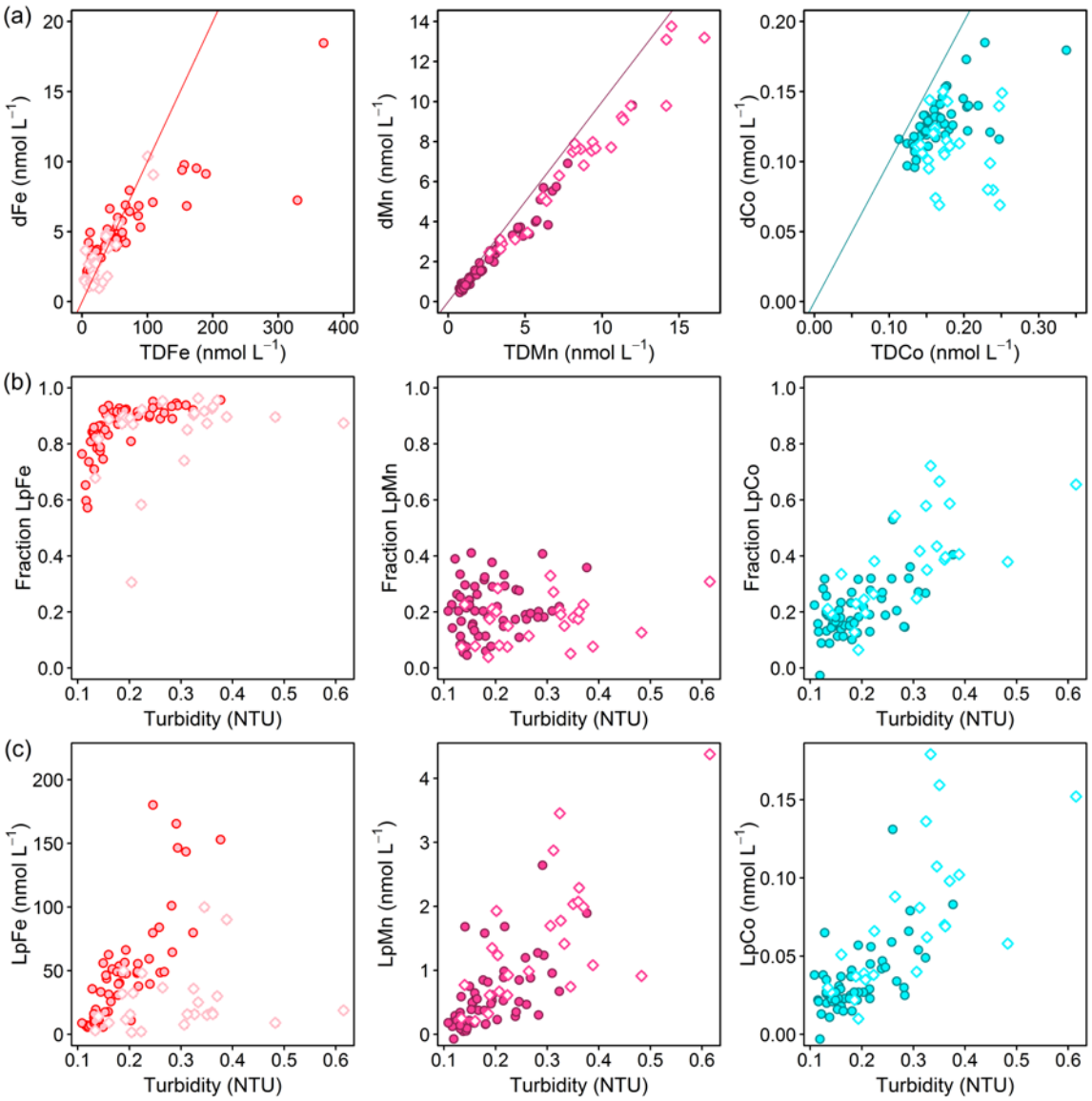

Figure 1. (a) Dissolved against total dissolvable trace metal concentrations for Fe (left; red line: TDFe = 10*dFe), Mn (middle; purple line: TDMn = dMn) and Co (right; turquoise line: TDCo = dCo). (b) Fraction of leachable particulate trace metals (Lp/TD) against turbidity and (c) Leachable particulate

concentrations against turbidity for Fe (left), Mn (middle) and Co (right). Filled circles display all data points below 50 m depth, open diamonds at depths shallower than 50 m.

Figure 7: As above it would be easier to read if different symbols were used.

Thanks again. We converted changed the symbols for the second deployment into triangles.

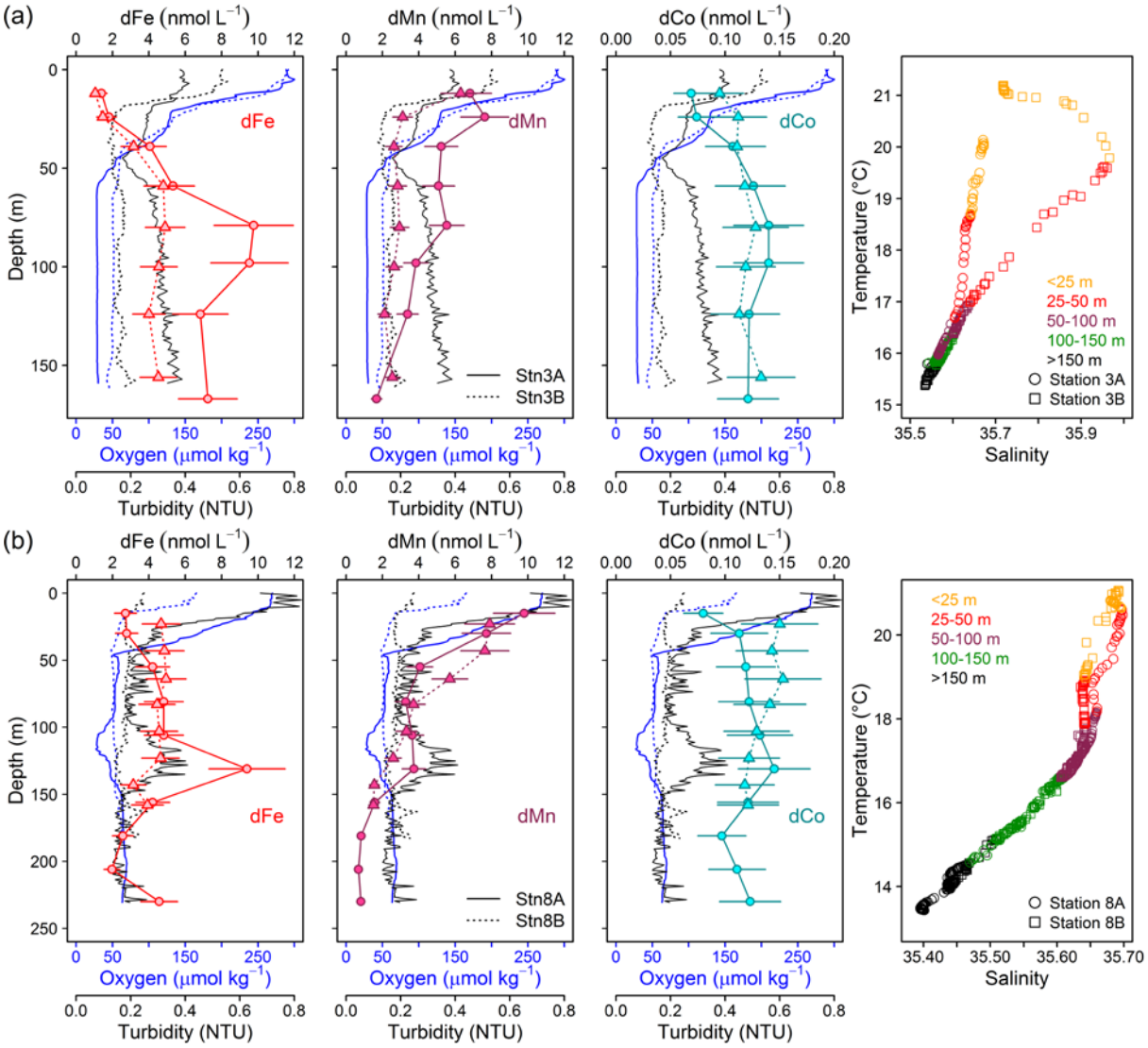

Figure 2. Repeat stations: oxygen concentration, turbidity and dissolved trace metals (Fe, Mn and Co) and temperature vs salinity plots. First deployment displayed as solid line and circles and second deployment displayed as dashed line and triangles. (a) Station 3 (18.23°N, 16.52°W, 170 m water depth, 9 days between deployments). (b) Station 8 (18.22°N, 16.55°N, 189–238 m water depth, 2 days between deployments).

Figure 7: The oxygen and turbidity anomalies mentioned seem to be related as mentioned in the text but the turbidity is more gaussian shaped while the oxygen has a bimodal distribution. It would have been more useful to have plotted all of this in density space so that we could see if the water masses were similar as the T/S properties look quite different but the symbols are so large that this information is lost.

We added a plot showing the density distribution of the different deployments to the Supplementary Material:

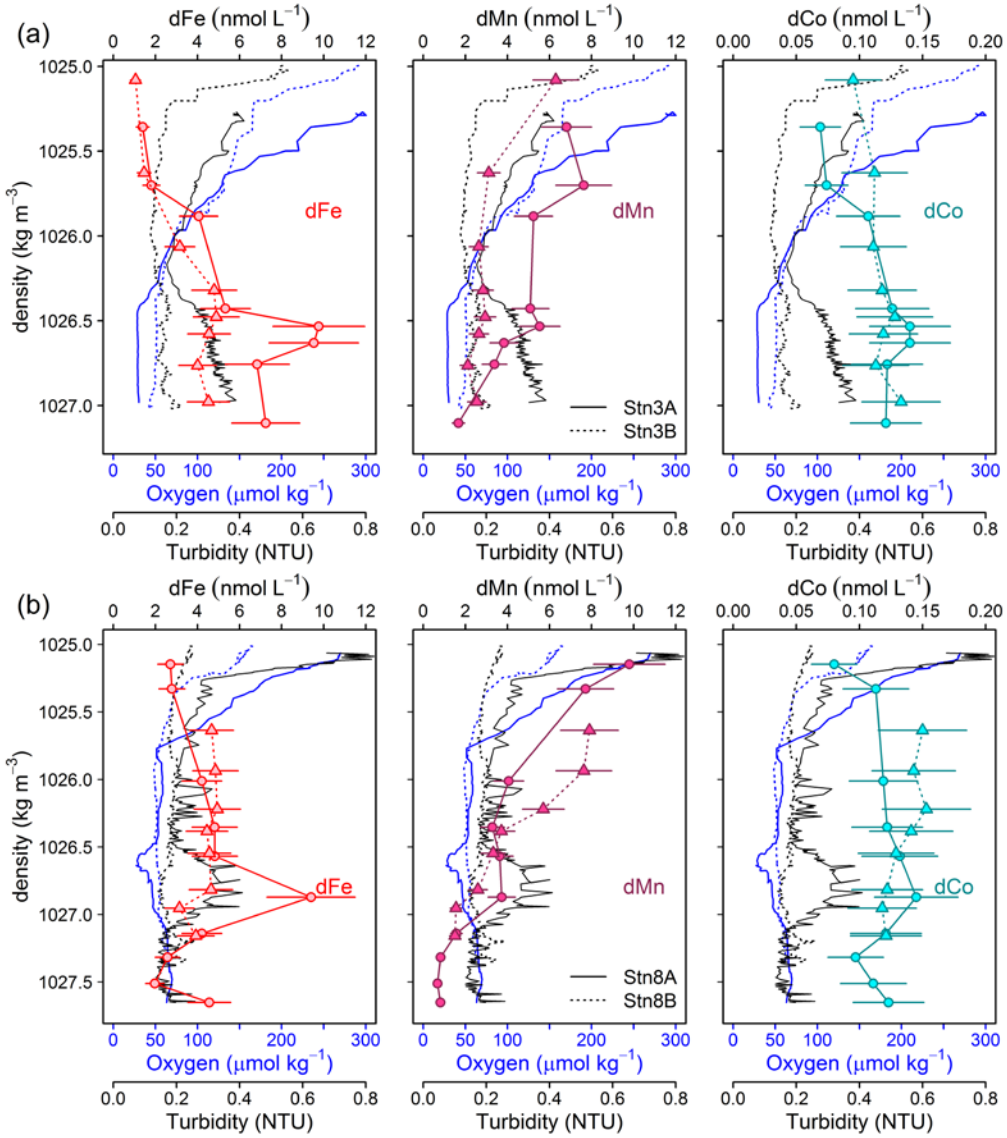

Figure S5. Density plots for oxygen concentration, turbidity and dissolved trace metals (Fe, Mn and Co) for repeated profiles. First deployment displayed as solid line and second deployment displayed as dashed line. (a) Station 3 (18.23°N, 16.52°W, 170 m water depth, 9 days between deployments). (b) Station 8 (18.22°N, 16.55°N, 189–238 m water depth, 2 days between deployments).

Figure 8: Different symbols between deployments would help. For station 8 and the dissolved Cd it is impossible to see if the data in the deep is the same or there was only 1 time that you sampled the deep waters.

We have also changed the symbols here accordingly.

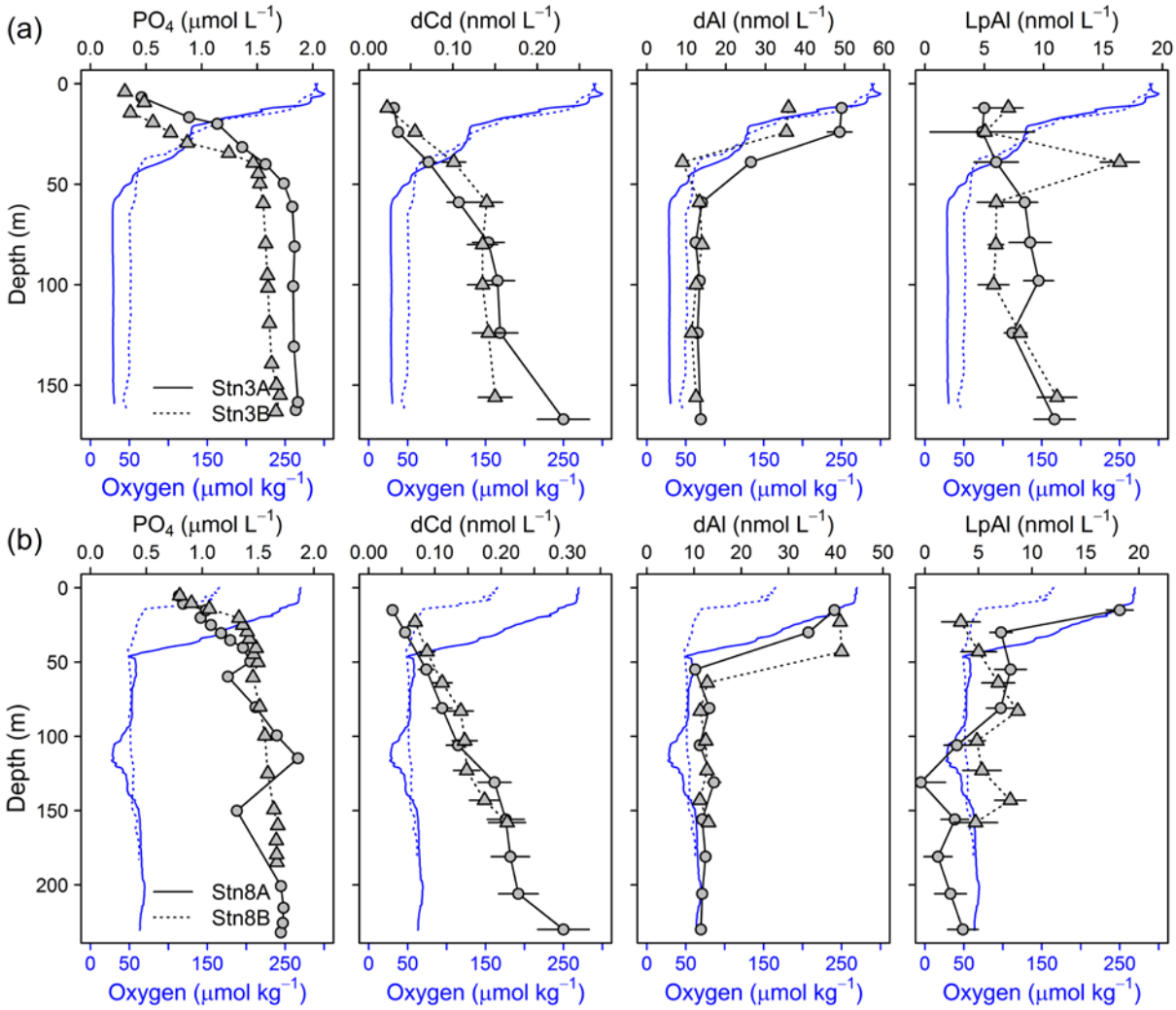

Figure 3. Depth profiles of dCd, PO_4, dAl and LpAl of repeat stations. First deployment displayed as solid black line and circles and second deployment displayed as dashed black line and triangles. Oxygen concentrations are indicated as blue solid line for the first deployment and dashed blue line for the second deployment. (a) Station 3 (18.23°N, 16.52°W, 170 m water depth, 9 days between deployments and (b) Station 8 (18.22°N, 16.55°N, 189–238 m water depth, 2 days between deployments).

Figure 8: Why the phosphate depletion at 150 m at station 8? It seems there is also data missing from above and below that point – any explanation why? Is this data point anomalous then as it is does not appear to be oceanographically consistent?

We agree that it appears to outlie from the other data, but we have no explanation for this. There are no phosphate data missing from this profile, but agree this is unfortunate as this would allow a better evaluation of the reliability of this point.

We thank the reviewer again for their detailed treatment of our manuscript.

References:

Baars, O., and Croot, P. L.: Dissolved cobalt speciation and reactivity in the eastern tropical North Atlantic, Mar Chem, 173, 310-319, https://doi.org/10.1016/j.marchem.2014.10.006, 2015.

Baker, A. R., Adams, C., Bell, T. G., Jickells, T. D., and Ganzeveld, L.: Estimation of atmospheric nutrient inputs to the Atlantic Ocean from 50°N to 50°S based on large-scale field sampling: Iron and other dust-associated elements, Global Biogeochem Cy, 27, 755-767, https://doi.org/10.1002/gbc.20062, 2013.

Balistrieri, L., Brewer, P. G., and Murray, J. W.: Scavenging residence times of trace metals and surface chemistry of sinking particles in the deep ocean, Deep Sea Res Part A. Oceanogr Res Pap, 28(2), 101-121, https://doi.org/10.1016/0198-0149(81)90085-6, 1981.

Bianchi, D., Weber, T. S., Kiko, R., and Deutsch, C.: Global niche of marine anaerobic metabolisms expanded by particle microenvironments, Nature Geoscience, 11(4), 263, 2018.

Brandt, P., V. Hormann, A. Körtzinger, M. Visbeck, G. Krahmann, L. Stramma, R. Lumpkin and C. Schmid: Changes in the ventilation of the oxygen minimum zone of the tropical North Atlantic, J Phys Oceanogr, 40, 1784–1801, https://doi.org/10.1175/2010JPO4301.1, 2010.

Buck, C. S., Landing, W. M., Resing, J. A., and Measures, C. I.: The solubility and deposition of aerosol Fe and other trace elements in the North Atlantic Ocean: Observations from the A16N CLIVAR/CO2 repeat hydrography section, Mar Chem, 120, 57-70, https://doi.org/10.1016/j.marchem.2008.08.003, 2010.

Capet, X. J., Marchesiello, P., and McWilliams, J. C.: Upwelling response to coastal wind profiles, Geophys Res Lett, 31, L13311, https://doi.org/10.1029/2004GL020123, 2004.

Croot, P. L., Streu, P., and Baker, A. R.: Short residence time for iron in surface seawater impacted by atmospheric dry deposition from Saharan dust events, Geophys Res Lett, 31(23), https://doi.org/10.1029/2004GL020153, 2004.

Cropper, T. E., Hanna, E., and Bigg, G. R.: Spatial and temporal seasonal trends in coastal upwelling off Northwest Africa, 1981–2012. Deep Sea Research Part I: Oceanographic Research Papers, 86, 94-111, https://doi.org/10.1016/j.dsr.2014.01.007, 2014.

Cyr, F., Bourgault, D., Galbraith, P. S., and Gosselin, M.: Turbulent nitrate fluxes in the Lower St. Lawrence Estuary, Canada, J Geophys Res-Oceans, 120, 2308-2330, https://doi.org/10.1002/2014jc010272, 2015.

Dammshäuser, A., Wagener, T., and Croot, P. L.: Surface water dissolved aluminum and titanium: Tracers for specific time scales of dust deposition to the Atlantic?, Geophys Res Lett, 38, L24601, https://doi.org/10.1029/2011gl049847, 2011.

Desbiolles, F., Blanke, B., and Bentamy, A.: Short-term upwelling events at the western African coast related to synoptic atmospheric structures as derived from satellite observations, J Geophys Res-Oceans, 119, 461-483, https://doi.org/10.1002/2013JC009278, 2014.

Desbiolles, F., B. Blanke, A. Bentamy and C. Roy (2016), Response of the Southern Benguela upwelling system to fine-scale modifications of the coastal wind. Journal of Marine Systems, 156, 46-55.

Fairall, C.W., Bradley, E.F., Hare, J.E., Grachev, A.A., and Edson, J.B.: Bulk Parameterization of Air–Sea Fluxes: Updates and Verification for the COARE Algorithm. J Climate, 16, 571–591, https://doi.org/10.1175/1520-0442(2003)016<0571:BPOASF>2.0.CO;2, 2003.

Gehlen, M., Beck, L., Calas, G., Flank, A. M., Van Bennekom, A. J., and Van Beusekom, J. E. E.: Unraveling the atomic structure of biogenic silica: Evidence of the structural association of Al and Si in diatom frustules, Geochim Cosmochim Ac, 66, 1601-1609, https://doi.org/10.1016/S0016-7037(01)00877-8, 2002.

Gier, J., Löscher, C. R., Dale, A. W., Sommer, S., Lomnitz, U., and Treude, T.: Benthic dinitrogen fixation traversing the oxygen minimum zone off Mauritania (NW Africa), Frontiers in Marine Science, 4, 390, https://doi.org/10.3389/fmars.2017.00390, 2017.

Gill, A.: Atmosphere-Ocean Dynamics, Academic Press, California, 1982.

Han, Q., Moore, J. K., Zender, C., Measures, C., and Hydes, D.: Constraining oceanic dust 760 deposition using surface ocean dissolved Al, Global Biogeochemical Cycles, 22(2), 2008.

Hayes, S. P., Chang, P., and McPhaden, M. J.: Variability of the sea surface temperature in the eastern equatorial Pacific during 1986–1988, J Geophys Res, 96, 10553-10566, https://doi.org/10.1029/91JC00942, 1991.

Heller, M. I., Wuttig, K., & Croot, P. L.: Identifying the sources and sinks of CDOM/FDOM across the Mauritanian Shelf and their potential role in the decomposition of superoxide (O2-), Frontiers in Marine Science, 3, 132, https://doi.org/10.3389/fmars.2016.00132, 2016.

Homoky, W. B., Severmann, S., McManus, J., Berelson, W. M., Riedel, T. E., Statham, P. J., and Mills, R. A.: Dissolved oxygen and suspended particles regulate the benthic flux of iron from continental margins, Marine Chemistry, 134, 59-70, https://doi.org/10.1016/j.marchem.2012.03.003, 2012.

Homoky, W. B., Weber, T., Berelson, W. M., Conway, T. M., Henderson, G. M., van Hulten, M., Jeandel, C., Severmann, S., and Tagliabue, A.: Quantifying trace element and isotope fluxes at the ocean-sediment boundary: a review, Philos T R Soc A, 374, 20160246, https://doi.org/10.1098/rsta.2016.0246, 2016.

Honeyman, B. D., Balistrieri, L. S., and Murray, J. W.: Oceanic trace metal scavenging: the importance of particle concentration, Deep Sea Res Part A. Oceanogr Res Pap, 35(2), 227-246, https://doi.org/10.1016/0198-0149(88)90038-6, 1988.

Hydes, D. J. and Liss, P. S.: Fluorimetric method for determination of low concentrations of dissolved aluminum in natural waters, Analyst, 101, 922-931, https://doi.org/10.1039/an9760100922, 1976.

Jickells, T. D.: The inputs of dust derived elements to the Sargasso Sea; a synthesis, Mar Chem, 68(1-2), 5-14, https://doi.org/10.1016/S0304-4203(99)00061-4, 1999.

Kock, A., Schafstall, J., Dengler, M., Brandt, P., and Bange, H. W.: Sea-to-air and diapycnal nitrous oxide fluxes in the eastern tropical North Atlantic Ocean, Biogeosciences, 9, 957-964, https://doi.org/10.5194/bg-9-957-2012, 2012.

Lam, P. J. and Bishop, J. K. B.: The continental margin is a key source of iron to the HNLC North Pacific Ocean, Geophys Res Lett, 35, L07608, https://doi.org/10.1029/2008gl033294, 2008.

Marsay, C. M., Sedwick, P. N., Dinniman, M. S., Barrett, P. M., Mack, S. L., & McGillicuddy, D. J.: Estimating the benthic efflux of dissolved iron on the Ross Sea continental shelf, Geophysical Research Letters, 41(21), 7576-7583, https://doi.org/10.1002/2014GL061684, 2014.

Measures, C. I. and Brown, E. T.: Estimating dust input to the Atlantic Ocean using surface water aluminium concentrations. In: The impact of desert dust across the Mediterranean, Guerzoni, S. and Chester, R. (Eds.), Environmental Science and Technology Library, Springer, Dordrecht, 1996.

Measures, C. I. and Vink, S.: On the use of dissolved aluminum in surface waters to estimate dust deposition to the ocean, Global Biogeochem Cy, 14, 317-327, https://doi.org/10.1029/1999gb001188, 2000.

Menzel Barraqueta, J.-L., Schlosser, C., Planquette, H., Gourain, A., Cheize, M., Boutorh, J., Shelley, R., Pereira, L. C., Gledhill, M., Hopwood, M. J., Lacan, F., Lherminier, P., Sarthou, G., and Achterberg, E. P.: Aluminium in the North Atlantic Ocean and the Labrador Sea (GEOTRACES GA01 section): roles of continental inputs and biogenic particle removal, Biogeosciences, 15, 5271-5286, https://doi.org/10.5194/bg-15-5271-2018, 2018.

Menzel Barraqueta, J.-L., Klar, J. K., Gledhill, M., Schlosser, C., Shelley, R., Planquette, H. F., Wenzel, B., Sarthou, G., and Achterberg, E. P.: Atmospheric deposition fluxes over the Atlantic Ocean: a GEOTRACES case study, Biogeosciences, 16, 1525-1542, https://doi.org/10.5194/bg-16-1525-2019, 2019.

Micinski, E., Ball, L. A., and Zafiriou, O. C.: Photochemical oxygen activation - superoxide radical detection and production-rates in the Eastern Caribbean, *J Geophys Res Oceans* 98, 2299–2306. https://doi.org/10.1029/92JC02766, 1993.

Middag, R., de Baar, H. J. W., Laan, P., and Huhn, O.: The effects of continental margins and water mass circulation on the distribution of dissolved aluminum and manganese in Drake Passage, J Geophys Res-Oceans, 117, C01019, https://doi.org/10.1029/2011jc007434, 2012.

Millero, F. J., Sotolongo, S., & Izaguirre, M.: The oxidation kinetics of Fe (II) in seawater, Geochimica et Cosmochimica Acta, 51(4), 793-801, https://doi.org/10.1016/0016-7037(87)90093-7, 1987.

Milne, A., Schlosser, C., Wake, B. D., Achterberg, E. P., Chance, R., Baker, A. R., Forryan, A., and Lohan, M. C.: Particulate phases are key in controlling dissolved iron concentrations in the (sub)tropical North Atlantic, Geophys Res Lett, 44, 2377-2387, https://doi.org/10.1002/2016gl072314, 2017.

Moran, S. B. and Moore, R. M.: The potential source of dissolved aluminum from resuspended sediments to the North Atlantic Deep Water, Geochim Cosmochim Ac, 55, 2745-2751, https://doi.org/10.1016/0016-7037(91)90441-7, 1991.

Ndoye, S., Capet, X., Estrade, P., Sow, B., Dagorne, D., Lazar, A., Gaye, A. and Brehmer, P.: SST patterns and dynamics of the southern Senegal-Gambia upwelling center, J Geophys Res Oceans, 119, 8315–8335, https://doi.org/10.1002/2014JC010242, 2014.

Orians, K. J. and Bruland, K. W.: Dissolved aluminum in the Central North Pacific, Nature, 316, 427-429, https://doi.org/10.1038/316427a0, 1985.

Orians, K. J. and Bruland, K. W.: The biogeochemistry of aluminum in the Pacific Ocean, Earth Planet Sc Lett, 78, 397-410, https://doi.org/10.1016/0012-821x(86)90006-3, 1986.

Osborn, T. R.: Estimates of the local rate of vertical diffusion from dissipation measurements, J Phys Oceanogr, 10, 83-89, https://doi.org/10.1175/15200485(1980)010<0083:Eotlro>2.0.Co;2, 1980.

Patey, M. D., Achterberg, E. P., Rijkenberg, M. J., and Pearce, R.: Aerosol time-series measurements over the tropical Northeast Atlantic Ocean: Dust sources, elemental composition and mineralogy, Mar Chem, 174, 103-119, https://doi.org/10.1016/j.marchem.2015.06.004, 2015.

Rhein, M., Dengler, M., Sültenfuß, J., Hummels, R., Hüttl-Kabus, S., and Bourles, B.: Upwelling and associated heat flux in the equatorial Atlantic inferred from helium isotope disequilibrium, J Geophys Res, 115, C08021, https://doi.org/10.1029/2009JC005772, 2010.

Ricciardulli, L., and Wentz, F. J.: Remote Sensing Systems ASCAT C-2015 Daily Ocean Vector Winds on 0.25 deg grid, Version 02.1. Santa Rosa, CA: Remote Sensing Systems. Available at www.remss.com/missions/ascat, 2016.

Rijkenberg, M. J. A., Steigenberger, S., Powell, C. F., van Haren, H., Patey, M. D., Baker, A. R., and Achterberg, E. P.: Fluxes and distribution of dissolved iron in the eastern (sub-) tropical North Atlantic Ocean, Global Biogeochem Cy, 26, GB3004, https://doi.org/10.1029/2011gb004264, 2012.

Rudnick, R. L., and Gao, S.: Composition of the continental crust. In: Treatise on geochemistry, Holland, H. D. and Turekian, K. K. (Eds.), Pergamon, Oxford, UK, 2006.

Saito, M. A., Noble, A. E., Hawco, N., Twining, B. S., Ohnemus, D. C., John, S. G., Lam, P., Conway, T. M., Johnson, R., Moran, D., and McIlvin, M.: The acceleration of dissolved cobalt's ecological stoichiometry due to biological uptake, remineralization, and scavenging in the Atlantic Ocean, Biogeosciences, 14, 4637-4662, https://doi.org/10.5194/bg-14-4637-2017, 2017.

Schafstall, J., Dengler, M., Brandt, P., and Bange, H.: Tidal-induced mixing and diapycnal nutrient fluxes in the Mauritanian upwelling region, J Geophys Res-Oceans, 115, C10014, https://doi.org/10.1029/2009jc005940, 2010.

Schlosser, C., Streu, P., Frank, M., Lavik, G., Croot, P. L., Dengler, M., and Achterberg, E. P.: H_2S events in the Peruvian oxygen minimum zone facilitate enhanced dissolved Fe concentrations, Sci Rep, 8, https://doi.org/10.1038/s41598-018-30580-w, 2018.

Scholz, F., Severmann, S., McManus, J., Noffke, A., Lomnitz, U., and Hensen, C.: On the isotope composition of reactive iron in marine sediments: Redox shuttle versus early diagenesis. Chemical Geology, 389, 48-59, https://doi.org/10.1016/j.chemgeo.2014.09.009, 2014.

Schroller-Lomnitz, U., Hensen, C., Dale, A. W., Scholz, F., Clemens, D., Sommer, S., Noffke, A., and Wallmann, K.: Dissolved benthic phosphate, iron and carbon fluxes in the Mauritanian upwelling system and implications for ongoing deoxygenation, Deep-Sea Res Pt I, 143, 70-84, https://doi.org/10.1016/j.dsr.2018.11.008, 2019.

Schütte, F., Brandt, P., and Karstensen, J.: Occurrence and characteristics of mesoscale eddies in the tropical north-east Atlantic Ocean, Ocean Sci., 12, 663-685, doi:10.5194/os-12-663-2016, 2016.

Severmann, S., McManus, J., Berelson, W. M., and Hammond, D. E.: The continental shelf benthic iron flux and its isotope composition, Geochim Cosmochim Ac, 74, 3984-4004, https://doi.org/10.1016/j.gca.2010.04.022, 2010.

Shelley, R. U., Morton, P. L., and Landing, W. M.: Elemental ratios and enrichment factors in aerosols from the US-GEOTRACES North Atlantic transects, Deep-Sea Res Pt II, 116, 262-272, https://doi.org/10.1016/j.dsr2.2014.12.005, 2015.

Shelley, R. U., Landing, W. M., Ussher, S. J., Planquette, H., and Sarthou, G.: Regional trends in the fractional solubility of Fe and other metals from North Atlantic aerosols (GEOTRACES cruises GA01 and GA03) following a two-stage leach, Biogeosciences, 15, 2271-2288, https://doi.org/10.5194/bg-15-2271-2018, 2018.

Sherrell, R. M., and Boyle, E. A.: The trace metal composition of suspended particles in the oceanic water column near Bermuda, Earth Planet Sc Lett, 111, 155-174, https://doi.org/10.1016/0012-821x(92)90176-V, 1992.

Sommer, S., Dengler, M., and Treude, T.: Benthic element cycling, fluxes and transport of solutes across the benthic boundary layer in the Mauritanian oxygen minimum zone, (SFB754) – Cruise No. M107 – May 30 – July 03, 2014 – Fortaleza (Brazil) – Las Palmas (Spain), METEOR-Berichte, M107, 54 pp., DFG-Senatskommission für Ozeanographie, https://doi.org/10.2312/cr_m107, 2015.

Steinfeldt, R., Sultenfuss, J., Dengler, M., Fischer, T., and Rhein, M.: Coastal upwelling off Peru and Mauritania inferred from helium isotope disequilibrium, Biogeosciences, 12, 7519-7533, https://doi.org/10.5194/bg-12-7519-2015, 2015.

Tanhua, T., and Liu, M.: Upwelling velocity and ventilation in the Mauritanian upwelling system estimated by CFC-12 and SF6 observations, J Mar Sys, 151, 57-70, https://doi.org/10.1016/j.jmarsys.2015.07.002, 2015.

Thomsen, S., Karstensen, J., Kiko, R., Krahmann, G., Dengler, M., and Engel, A.: Remote and local drivers of oxygen and nitrate variability in the shallow oxygen minimum zone off Mauritania in June 2014, Biogeosciences, 16, 979-998, https://doi.org/10.5194/bg-16-979-2019, 2019.

Tweddle, J. F., Sharples, J., Palmer, M. R., Davidson K., and McNeill, S.: Enhanced nutrient fluxes at the shelf sea seasonal thermoclinecaused by stratified flow over a bank, Prog Oceanogr, 117, 37–47, https://doi.org/10.1016/j.pocean.2013.06.018, 2013.

Ussher, S. J., Achterberg, E. P., Powell, C., Baker, A. R., Jickells, T. D., Torres, R., and Worsfold, P. J.: Impact of atmospheric deposition on the contrasting iron biogeochemistry of the North and South Atlantic Ocean, Global Biogeochem Cy, 27, 1096-1107, https://doi.org/10.1002/gbc.20056, 2013.

Verhoef, A., Portabella, M., and Stoffelen, A.: High resolution ASCAT scatterometer winds near the coast, IEEE, Trans Geosci Remote Sens, 50, 2481-248, https://doi.org/10.1109/TGRS.2011.2175001, 2012.

Wuttig, K., Heller, M. I., and Croot, P. L.: Pathways of Superoxide (O_2^-) Decay in the Eastern Tropical North Atlantic, Environ Sci Technol, 47(18), 10249-10256, https://doi.org/10.1021/es401658t, 2013.

Yücel, M., Beaton, A. D., Dengler, M., Mowlem, M. C., Sohl, F., and Sommer, S.: Nitrate and Nitrite Variability at the Seafloor of an Oxygen Minimum Zone Revealed by a Novel Microfluidic In-Situ Chemical Sensor, PLoS ONE 10(7), e0132785, https://doi.org/10.1371/journal.pone.0132785, 2015.

Response to Referee 2

This is an important paper that illustrates the potential importance of benthic shelf sediments as a source of Fe to the oceans interior, and linking spatial and temporal variability to oxygen concentrations. While I think the authors make a good case for the role of oxygen, the paper is flawed by three serious omissions that must be corrected before publication.

We thank the reviewer for the constructive comments and address each of them below.

1. Iodide is reported as a critical parameter in the principal component analysis and there are detailed protocols for iodide analysis, yet no data are reported in the paper or in the supplement. These data are of great interest in their own right. While iodide has been reported in truly anaerobic, denitrifying water columns, it has not been well studied in these low oxygen regimes. One presumes that these data will appear in Pangaea eventually, but why not here?

Thanks for pointing out the importance of our iodide data. We have now added a plot showing the spatial distribution of iodide in the Supplementary Material. The data will also be uploaded in Pangea.

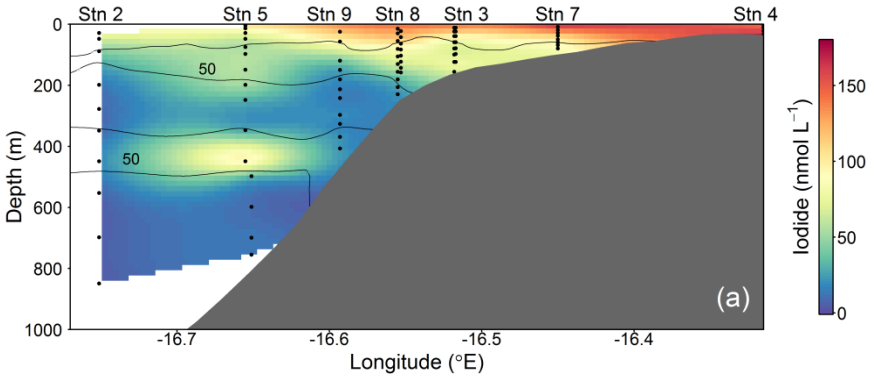

Figure S1. Spatial distributions of Iodide across the Mauritanian shelf at 18°20'N in June 2014. Each sample location is indicated as black dot and oxygen contours at 50 µmol kg^{-1} enclosing the upper and lower OMZ are displayed as black contour lines.

2. Similarly, Ra-228 data are not reported, nor is there any quantitative assessment of Ra-228 correlations with Fe to support their conclusions about lateral transport.

Unfortunately Ra-228 was not determined along our transect. Therefore, we can't provide such information. Due to the long half-life of ^{228}Ra of 5.7 years, this isotope would show sediment-water interaction on longer time scales. In our study close to the source, shorter timescales are of larger interest. Additionally, there doesn't necessarily need to be a correlation between Fe and ^{228}Ra when Fe is released from sediments, because ^{228}Ra behaves conservative, whereas iron is removed by scavenging.

3. The authors imply that the approach used to determine vertical eddy diffusivity will appear in the Supplementary materials, but it does not.

The approach used to determine vertical eddy diffusivity is explained in detail in the method section of the main manuscript in the paragraph starting at Page 8, Line 9. For a more detailed description, we refer to Schafstall et al. (2010).

Controls on redox-sensitive trace metals in the Mauritanian oxygen minimum zone

Insa Rapp[1*], Christian Schlosser[1], Jan-Lukas Menzel Barraqueta[1, 2], Bernhard Wenzel[1], Jan Lüdke[1], Jan Scholten[3], Beat Gasser[4], Patrick Reichert[1], Martha Gledhill[1], Marcus Dengler[1], and Eric P. Achterberg[1]

[1]Helmholtz Centre for Ocean Research Kiel (GEOMAR), Wischhofstr. 1-3, 24148 Kiel, Germany

[2]Department of Earth Sciences, Stellenbosch University, Stellenbosch, 7600, South Africa

[3]Institute of Geosciences, Christian-Albrecht University Kiel (CAU), Otto-Hahn-Platz 1, 24118 Kiel, Germany

[4]International Atomic Energy Agency (IAEA), Environment Laboratories, 4 Quai Antoine 1er, 98012 Monaco

*Corresponding author. irapp@geomar.de

ABSTRACT

The availability of the micronutrient iron (Fe) in surface waters determines primary production, N_2 fixation and microbial community structure in large parts of the world´s ocean, and thus plays an important role in ocean carbon and nitrogen cycles. Eastern boundary upwelling systems and the connected oxygen minimum zones (OMZs) are typically associated with elevated concentrations of redox-sensitive trace metals (e.g. Fe, manganese (Mn) and cobalt (Co)), with shelf sediments typically forming a key source. Over the last five decades, an expansion and intensification of OMZs has been observed and this trend is likely to proceed. However, it is unclear how trace metal (TM) distributions and transport are influenced by decreasing oxygen (O_2) concentrations. Here we present dissolved (d; <0.2 µm) and leachable particulate (Lp; >0.2 µm) TM data collected at 7 stations along a 50 km transect in the Mauritanian shelf region. We observed enhanced concentrations of Fe, Co and Mn corresponding with low O_2 concentrations (<50 µmol kg^{-1}), which were decoupled from major nutrients and nutrient-like and scavenged TMs (cadmium (Cd), lead (Pb), nickel (Ni) and copper (Cu)). Additionally, data from repeated station occupations indicated a direct link between dissolved and leachable particulate Fe, Co, Mn, and O_2. An observed dFe decrease from 10 to 5 nmol L^{-1} coincided with an O_2 increase from 30 to 50 µmol kg^{-1} and with a concomitant decrease in turbidity. The changes in Fe (Co and Mn) were likely driven by variations in their release from sediment pore water, facilitated by lower O_2 concentrations and longer residence time of the water mass on the shelf. Variations in organic matter remineralization and lithogenic inputs (atmospheric deposition or sediment resuspension; assessed using Al as indicator for lithogenic inputs) only played a minor role in redox-sensitive TM variability. Vertical dFe fluxes from O_2-depleted subsurface to surface waters (0.08–13.5 µmol m^{-2} d^{-1}) ~~were~~ driven by turbulent mixing and vertical advection~~, and~~ were an order of magnitude larger than atmospheric deposition fluxes (0.63–1.43 µmol m^{-2} d^{-1}; estimated using dAl inventories in the surface mixed layer) in the continental slope and shelf region. Benthic fluxes are therefore the dominant dFe supply to surface waters on the continental margins of the Mauritanian upwelling region. Overall, our results indicated that the projected future decrease in O_2 concentrations in OMZs may result in increases in Fe, Mn and Co concentrations.

1. INTRODUCTION

The micronutrient iron (Fe) is essential for phytoplankton growth, but due to biological uptake coupled with a low solubility and low supply rates, the availability of Fe is typically low in open ocean surface waters (Bruland and Lohan, 2006). As a result, Fe limits primary production in high nitrate low chlorophyll regions (Boyd, 2007) and regulates dinitrogen (N_2) fixation in (sub)-tropical waters (Moore et al., 2009). Alongside Fe, other trace metals (TMs) such as cobalt (Co), manganese (Mn), zinc (Zn)~~, cadmium (Cd)~~ and copper (Cu) may (co-)limit phytoplankton growth and influence community composition (Browning et al., 2017; Moore et al., 2013; Morel and Price, 2003; Saito et al., 2008).

Oxygen minimum zones (OMZs) are characterized by stable subsurface oxygen (O_2) minima, which are maintained by a combination of enhanced O_2 consumption in the thermocline and a limited supply of O_2 rich water masses (e.g. Brandt et al., 2015; Karstensen et al., 2008; Wyrtki, 1962). Enhanced O_2 consumption is a result of elevated surface productivity caused by upwelling of nutrient-rich subsurface waters in eastern boundary regions of the oceans through Ekman divergence, and intense remineralization of sinking particles (e.g. Helly and Levin, 2004). Elevated organic matter supply and water column O_2 depletion lead to enhanced benthic release of redox-sensitive elements by influencing sediment diagenetic processes (Noffke et al., 2012; Severmann et al., 2010). Elevated concentrations of sediment derived dissolved Fe, Co and Mn have been associated with lateral offshore advection in O_2 depleted waters in the Arabian Sea, Pacific and Atlantic Ocean (Biller and Bruland, 2013; Hatta et al., 2015; Hawco et al., 2016; Milne et al., 2017; Moffett et al., 2015; Noble et al., 2012).

Oxygen concentrations affect the distribution of redox-sensitive TMs by controlling oxidation rates and influencing microbially mediated redox transformations. The reduced form of redox-sensitive TMs, such as iron (Fe(II)), cobalt (Co(II)) and manganese (Mn(II)), have a higher solubility in aqueous solutions than their oxidized forms (Fe(III), Co(III), Mn(III/IV)) (Liu and Millero, 2002; Stumm and Morgan, 1995). Reduction of these metals occurs to a large extent in anoxic sediment pore waters by microbial induced dissolution of particulate Fe(III) and Mn(III/IV) oxyhydroxides (Burdige, 1993; Chaillou et al., 2002; Froelich et al., 1979). Sediment pore waters are released to overlying bottom waters by diffusion and bio-irrigation and during submarine groundwater discharge (Beck et al., 2007; Elrod et al., 2004; Green et al., 2002). In contact with O_2 and other oxidants (e.g. nitrate (Schlosser et al., 2018) and hydrogen peroxide (Moffett and Zika, 1987)), Fe(II) oxidizes to the poorly soluble Fe(III) species, that are rapidly transformed into amorphous Fe oxyhydroxides or scavenged onto particle surfaces (Moffett and Zika, 1987; Scholz et al., 2016; Wu and Luther, 1994). Mn(II) also oxidizes to insoluble Mn(III/IV) oxides, but due to the slow abiotic oxidation kinetics, especially under low O_2 conditions (e.g. von Langen et al., 1997), biotic oxidation by manganese oxidizing bacteria is the main oxidation mechanism for Mn (Moffett, 1994; Sunda and Huntsman, 1988; Tebo and Emerson, 1986). Co(II) removal is mainly associated with incorporation of Co into Mn oxides by Co co-oxidation (Moffett and Ho, 1996).

Stabilizing mechanisms that prevent removal by scavenging and precipitation of Fe, Co and Mn are organic ligand complexation (Elrod et al., 2004; Liu and Millero, 2002; Oldham et al., 2017; Parker et al., 2007) and adsorption onto small slow sinking or neutrally buoyant particles (Lam et al., 2012). Recent studies suggest a potentially important role for dynamic exchange processes between dissolved and particulate phases of Fe, thereby influencing cycling and transport (Achterberg et al., 2018; Fitzsimmons et al., 2017; Labatut et al., 2014; Milne et al., 2017). This was further indicated by Fe isotope studies suggesting an equilibrium isotopic fractionation between the dissolved and particulate

phase in deep waters (Labatut et al., 2014) and the concomitant deepening of the dissolved and particulate Fe plume that originated from a hydrothermal vent (Fitzsimmons et al., 2017).

Spatial and seasonal variations in TMs that are released from sediments, as well as ex-situ sediment incubation experiments suggest a direct influence of bottom water and water column O_2 concentrations on the distribution of Fe, Co and Mn (e.g. Biller and Bruland, 2013; Homoky et al., 2012). Differences in benthic TM supply in field studies however suggest other factors such as sediment type, shelf topography and organic matter supply also~~are also influenced~~ influence the benthic release of TMs~~by a range of other processes as for example sediment type and organic matter supply~~ (Homoky et al., 2016). Ex-situ sediment incubation experiments offer a potential means to disentangle the influence of O_2 concentrations relative to these controls (Homoky et al., 2012). These experiments, however, need to be interpreted within the context of the confined conditions that eliminate potentially important interactions in open systems, such as seawater exchange and mixing. Furthermore, they offer no means to confidently evaluate controls on TM distributions in the pelagic water column.

In an attempt to resolve the controls on TM release and stabilization in OMZs we measured the concentration of a suite of TMs along a 50 km long transect on the Mauritanian shelf in the Eastern Tropical North Atlantic (ETNA). The Mauritanian shelf is associated with a major OMZ (minimum O_2 concentrations below 40 µmol kg^{-1}; Brandt et al., 2015) and is an important Fe source to the North Atlantic Ocean (Milne et al., 2017). Furthermore, atmospheric dust deposition from the Saharan desert can markedly elevate surface water Fe concentrations in the ETNA (Conway and John, 2014; Rijkenberg et al., 2012). Recent observations suggest a decline in O_2 content of the oceans, particularly in the northern and southern eastern Atlantic, and an expansion of OMZs, modulated by the variability of our climate system (Hahn et al., 2017; Schmidtko et al., 2017; Stramma et al., 2008b). These changes may result in changes in TM supply, and a mechanistic understanding of the factors regulating TM release and stabilization in OMZs is therefore urgently needed. The aim of this study was to evaluate the direct influence of variability in water column O_2 concentrations on the distribution of redox-sensitive TMs and to identify responsible control mechanisms. Firstly, we assess the fluxes of dFe in the OMZ to surface waters by vertical advection and diffusive mixing and compared those to the atmospheric deposition flux of dFe. Secondly, we evaluate the importance of redox and non-redox controls on Fe, Co and Mn by focusing on the influence of O_2 and particles on the distribution of dissolved and leachable particulate TMs, including redox-sensitive (Fe, Co and Mn) and nutrient-type and scavenged trace metals (aluminum (Al), lead (Pb), nickel (Ni), Cd and Cu). Thirdly, we determine the influence of variability of the eastern boundary circulation and O_2 concentrations in regulating TM concentrations.

2. METHODS

2.1 Sampling

Samples were collected on RV Meteor cruise M107 in June 2014 during nine deployments at seven locations (two stations were occupied twice) along a cross-shelf transect at 18°20'N on the Mauritanian shelf in the ETNA (Figure 1). The bottom depths of stations varied between 50 m on the shelf to 1136 m furthest off shore. Seawater sampling was carried out using a trace metal clean CTD (TM-CTD, Sea-Bird SBE25) rosette frame equipped with 24 trace metal clean samplers (12 L, Ocean Test Equipment (OTE)). The CTD frame was attached to plastic coated nonconductive steel cable and deployed using a carousel auto-fire module (AFM, Sea-Bird) that closed the bottles at predefined depths. After recovery, the bottles were transferred to a clean-laboratory container and pressurized to 0.2 bar overpressure using filtered N_2 gas. Samples were collected unfiltered for total dissolvable (TD) TM measurements, and filtered using a 0.2 µm cartridge filter (Acropack 500, Pall) for dissolved (d) TMs and iodide. Trace metal samples were collected in acid clean 125 mL low density polyethylene (LDPE) bottles (Nalgene), and iodide samples in opaque 60 mL high density polyethylene (HDPE) bottles (Nalgene). Trace metal samples were acidified to pH 1.9 using ultra clean HCl (UpA, Romil) and stored double-bagged for >6 months before preconcentration and analysis. Samples for iodide measurements were stored frozen at -20°C until analysis.

Samples for the determination of radium isotopes (^{223}Ra; $t_{½}$ = 11.4 d; ^{224}Ra $t_{½}$ = 3.7 d) were obtained using in-situ filtration pumps (Challenger Oceanic) following the procedures described in Charette et al. (2015) and Henderson et al. (2013). Briefly, each in-situ filtration pump was equipped with two particle filters (70 µm; 1 µm) and two Mn dioxide (MnO_2) impregnated cartridges (CUNO Micro Klean III acrylic) on which dissolved Ra adsorbs. In this work, ^{224}Ra/^{223}Ra ratios are shown, which were analyzed from the first cartridge. The pumped water volumes varied between 1000 L and 1700 L and flow rates were 10–15 L min^{-1}. For the determination of Ra in surface waters (~5 m water depth) about 200–300 L of seawater was pumped into several ~~500~~ 120 L plastic barrels followed by filtration over MnO_2 coated acrylic fibers (Mn-fibers).

2.2 Trace metal analysis

Determination of Co, Mn, Fe, Cd, Pb, Ni and Cu was carried out as described in Rapp et al. (2017). Briefly, samples were preconcentrated using an automated preconcentration device (Sea*FAST*, Elemental Scientific Inc.) equipped with a cation chelating resin (WAKO; Kagaya et al., 2009). Samples were UV-digested prior to preconcentration to breakdown metal-organic complexes, which would cause an underestimation of the determined TM concentrations. Samples were buffered in-line to pH 6.4 ± 0.2 using 1.5 M ammonium acetate buffer, before loading onto the resin. The pH buffer was prepared using an ammonium hydroxide solution (22%, OPTIMA grade, Fisher) and acetic acid (glacial, OPTIMA grade, Fisher) in de-ionized water (MilliQ, Millipore), adjusted to pH 8.5. Retained TMs were eluted from the resin using 1 M distilled HNO_3 and collected in 4 mL polypropylene scintillation vials (Wheaton). The acid was distilled from supra-pure HNO_3 (SpA grade, Romil) using a sub-boiling PFA distillation system (DST-1000, Savillex). Preconcentration was performed within a

clean laboratory (ISO 5) and all sample and reagent handling was performed within the same laboratory in an ISO 3 laminar flow bench with a HEPA filter unit. Preconcentrated samples were analyzed by high resolution inductively coupled plasma-mass spectrometry (HR-ICP-MS, ELEMENT XR, ThermoFisher Scientific) using isotope dilution for Fe, Cd, Pb, Cu and Ni and standard additions for Co and Mn. SAFe reference seawater S and D2 were analyzed with each analytical run and concentrations produced were in good agreement with consensus values (Table 1).

Leachable particulate (Lp) concentrations were calculated as the difference between total dissolvable and dissolved concentrations. The limit of quantification (LOQ) for the Lp concentrations was determined as the sum of the analytical standard deviations of TD and dissolved concentrations. Extended uncertainty calculations were performed using the Nordtest approach (Naykki et al., 2015) accounting for random as well as systematic errors (Rapp et al., 2017). The Lp fraction represents the particulate fraction which is readily dissolvable in the acidified samples during storage at pH 1.9 for 6 months and therefore does not contain any refractory particle components. This more labile fraction of particulate TMs mainly includes TMs in organic/biogenic particles, adsorbed to particle surfaces and TM oxides/oxyhydroxides (Hurst et al., 2010).

2.3 Aluminum measurements

Aluminum concentrations were determined in surface water samples for all stations along the transect and at two stations (3 and 8) for the entire water column. Samples were analyzed for Al ~~according to~~using the batch lumogallion method (Hydes and Liss ~~(~~, 1976). Acidified samples were buffered manually with a 2 M ammonium acetate buffer (Romil, UpA) to a pH between 5.1 and 5.2. The buffer was prepared using ammonium hydroxide (Romil, UpA) and acetic acid (Romil, UpA) in de-ionized water (MilliQ, Millipore). Buffered samples were spiked with a 2 mg L^{-1} ~~lumogallium~~ lumogallion (TCI) solution allowing the complexing agent to be in excess. The ~~lumogallium~~ lumogallion solution was prepared in 2 M ammonium acetate buffer (Romil, UpA). After spiking, samples were heated up for 1.5 h at 80°C in an oven (Heratherm, Thermo Scientific) and left to cool down overnight at room temperature to allow the formation of a ~~fluorescence~~ fluorescent Al complex. Samples were measured using a fluorescence spectrophotometer (Cary Eclipse, Agilent). The samples were measured with an excitation and emission wavelength of 465 and 555 nm, respectively. The excitation and emission slits were set to 10. The plastic cuvettes used for the measurements were pre-cleaned in a 2 M HCl (Trace metal grade, Fisher) for at least 24 h. In between samples, the cuvette was thoroughly rinsed with de-ionized water followed by actual sample. The same cuvette was used during an analytical session. All samples were analyzed in duplicate and the concentrations calculated from the peak heights via standard addition. Samples and reagent natural fluorescence was monitored by analyzing their content in the absence of the complexing agent. The standards were prepared in low trace metal seawater from a 500 nmol L^{-1} stock standard solution prepared from a 1000 ppm Al standard solution (Merck Millipore). A typical calibration had the following standard concentrations: 0, 10, 20, 40, and 60 nmol

L^{-1}. GEOTRACES reference seawater (GS) was run with a mean average Al value of 27.76 ± 0.17 nmol L^{-1} (n=4; consensus value 28.2 ± 0.2 nmol L^{-1}).

2.4 Iodide measurements

Frozen samples were defrosted overnight at room temperature prior to analysis for iodide by cathodic stripping square wave voltammetry after Luther et al. (1988). The voltammetry unit consisted of a voltammeter stand (663 VA, Metrohm), an autosampler (863 Compact Autosampler, Metrohm) and an automatic burette (843 Pump Station, Metrohm) for automated spike addition. The system was controlled by Computrace software (797 VA; Metrohm).

2.5 Oxygen, salinity, nutrient, turbidity and chlorophyll fluorescence analysis

Oxygen, salinity, nutrients, turbidity and chlorophyll fluorescence was measured during 62 CTD deployments (including some repeated deployments at the same location) along the 18°20`N transect using a Sea-Bird SBE 9 CTD rosette system equipped with double sensor packages for O_2, salinity and temperature and 24 ~~niskin~~ Niskin samplers (10 L; OTE). Turbidity and chlorophyll *a* were measured with a combined Wetlabs turbidity and fluorescence sensor that was attached to the CTD. The output of both sensors was corrected using the calibration provided by the manufacturer. Throughout this manuscript, turbidity data are presented in nephelometric turbidity units (NTU). The noise level of the sensor in our data set was found to be lower than 0.14 NTU.~~Turbidity and chlorophyll a fluorescence were measured with single sensor units on the CTD.~~ Oxygen sensor data were calibrated by Winkler titration (Hansen, 2007; Winkler, ~~1988~~1888; Sommer et al., 2015) on 348 discrete water samples that were collected from the OTE samplers. Oxygen sensor data was initially processed using calibration coefficients provided by the manufacturer. Subsequently, O_2 sensor data were fitted to the O_2 concentrations determined by the Winkler titration method using linear functions for temperature, O_2 and pressure (i.e. depth). ~~The O_2 calibration was undertaken using a linear fit with respect to O_2 concentration, temperature, and pressure.~~ An uncertainty of 1.5 µmol kg^{-1} was determined for O_2 concentrations. On-board nutrient measurements of nitrite (NO_2^-), nitrate (NO_3^-), phosphate (PO_4^{3-}) and silicic acid ($Si(OH)_4$) of the discrete water samples were conducted using a QuAAtro autoanalyzer (Seal Analytical) according to Grasshoff et al. (1983).

Apparent Oxygen Utilization (AOU) was calculated as the difference between saturation concentrations of O_2 and measured O_2 concentrations. The saturation concentration of O_2 was calculated after the Weiss methods (Weiss, 1970) using the R package marelac (Soataert et al., 2016), taking into account salinity and temperature.

2.6 Radium analysis

On-board the ship the Mn-cartridges and Mn-fibers were washed with Ra-free tap water ~~and afterwards~~to remove any residual sea salt and particles. Ra was removed from the tap water by slowly (<1 L min^{-1}) passing it through a Mn-fiber filled cartridge. Afterwards, both cartridges and fibers were partially dried with filtered compressed air to remove excess water. The samples were analyzed for ^{223}Ra, ^{224}Ra and ^{228}Th using a Radium Delayed Coincidence Counting System (RaDeCC) (Moore and Arnold, 1996). For the efficiency calibration of the RaDeCC, ^{227}Ac and ^{232}Th standard solutions were used, and the calibration followed the procedure described in Scholten et al. (2010) and Moore and Cai (2013). Counting errors were propagated following Garcia-Solsona et al. (2008). Excess ^{224}Ra ($^{224}Ra_{ex}$), i.e. the ^{224}Ra activity corrected for ^{228}Th-supported ^{224}Ra was calculated by subtracting the ^{228}Th activity from the ^{224}Ra activity. The ^{228}Th activity was measured three weeks after the first measurement of ^{224}Ra, when the initial ^{224}Ra had decayed. As we measured only the first Mn cartridge and the Mn cartridges do not adsorb radium quantitatively, we report here only $^{224}Ra_{ex}/^{223}Ra$ ratios.

2.7 Turbulence measurements and vertical flux calculations

In order to advance understanding of the role of benthic Fe supply to the ~~high~~ productive surface waters of the upwelling region, vertical diffusive fluxes (eq 1: left term, right hand side) and ~~upwelling~~ wind induced vertical advective fluxes (eq 1: right term, right hand side) were estimated. On the continental margin~~At depth~~ below the surface mixed layer ~~in the water on a continental margin~~, solutes are transferred vertically toward the near-surface ~~waters~~ layers by turbulent mixing processes and by vertical advection forced by Ekman divergence (e.g. Kock et al., 2012; Milne et al., 2017; Rhein et al., 2010; Steinfeldt et al., 2015, Tanhua and Liu, 2015):

$$J_Z = K_z \frac{\partial [TM]}{\partial z} + w \cdot \Delta [TM] \qquad (1)$$

Here, K_z is the turbulent eddy diffusivity in $m^2\ s^{-1}$, ∂[TM]/ ∂z the vertical gradient with depth (z) of the TM concentration [TM] in µmol m^{-4}, Δ[TM] a TM concentration difference in µmol m^{-3} and *w* represents vertical velocity in m s^{-1}. ~~The equation is solved by vertically integrating the tracer transport budget equation between two vertical layers while ignoring lateral fluxes, changes of *w* with depth and assuming steady state. Vertical advective fluxes resulting from meso- and submesoscale processes along sloping isopycnals were not considered. The TM fluxes were evaluated for the depth interval from the upper boundary of the shallow O_2-depleted waters to a depth of increased chlorophyll a fluorescence (8–29 m depth).~~ Average advective and diffusive TM fluxes were calculated for a depth interval from the shallow O_2-depleted waters to surface waters. The exact depth interval varied for each station (see Table S2) due to differences in the depths where TM samples were collected. The upper depth (8–29 m) was always in layers with enhanced chlorophyll *a* fluorescence, although for some stations the upper depth was below the surface mixed layer.

Diffusive Fe fluxes were determined by combining TM concentration measurements from the TM-CTD stations with nearby measured microstructure profiles. The microstructure measurements were performed with an MSS90-D profiler (S/N 32, Sea & Sun Technology). The loosely-tethered profiler was optimized to sink at a rate of 0.55 m s^{-1} and equipped with three shear sensors, a fast-response temperature sensor, and an acceleration sensor, two tilt sensors and conductivity, temperature, depth sensors sampling with a lower response time. At TM-CTD stations with bottom depths less than 400 m, 18 to 65 microstructure profiles were available at each station. At deeper stations, ~~the number reduced to~~ 5 to 12 profiles were used. Standard processing procedures were used to determine the rate of kinetic energy dissipation (ε) of turbulence in the water column (see Schafstall et al. (2010) for detailed description). Subsequently, K_Z values were determined from $K_{\rho} = \Gamma \varepsilon N^{-2}$ (Osborn, 1980), where N is stratification and Γ is the mixing efficiency for which a value of 0.2 was used. The use of this value has recently been shown to yield good agreement between turbulent eddy diffusivities determined from microstructure measurements and from tracer release experiments performed in our study region (Köllner et al., 2016). The 95% confidence intervals for station-averaged K_ρ values were determined from Gaussian error propagation following Schafstall et al. (2010). Finally, diffusive fluxes were estimated by multiplying station-averaged K_ρ with the vertical gradient of the respective TM solute, implicitly assuming K_Z=K_ρ.

The vertical advective flux by Ekman divergence requires determination of vertical velocity in the water column that varies with depth and distance from the coast line. Convincing agreement between vertical velocities derived from Ekman divergence following Gill (1982) determined from scatterometer winds and from helium isotope disequilibrium within the Mauritanian and Peruvian coastal upwelling regions was found by Steinfeldt et al. (2015) (see their Fig. 4). In their study, vertical velocities were parameterized as (Gill, 1982):~~Recent studies found good agreement between vertical velocities derived from Ekman divergence and from helium isotope equilibrium within the Mauritanian and Peruvian coastal upwelling regions (Steinfeldt et al., 2015) when parameterizing vertical velocities as (Gill, 1982):~~

$$w = \frac{\tau_y}{\rho f L_r} e^{-x/L_r} \qquad (2)$$

where τ_y represents the alongshore wind stress, ρ the density of sea water, x the distance from maximum Ekman divergence taken here as the position at 50 m bottom depth on the shelf and L_r the first baroclinic Rossby radius. The parameterization results from considering the baroclinic response of winds parallel to a coastline in a two-layer ocean (Gill, 1982). The baroclinic Rossby radius $L_r = f^{-1}\sqrt{g\frac{\rho_2-\rho_1}{\rho}\frac{H_1 H_2}{H_1+H_2}}$ ($\rho_{1/2}$ and $H_{1/2}$ ~~is~~ are density and thickness of the surface and lower layer, respectively) was found to be 15 km from ~~hydrography~~ hydrographical data collected during the cruise~~, . similar~~ Similar ~~to the~~ values were determined by Steinfeld et al. (2015) in the same region.

Using average alongshore wind stress from satellite data (0.057 Nm^{-2}, determined from daily winds from Remote Sensing Systems ASCAT C-2015, version v02.1 (Ricciardulli and Wentz, 2016) at 18°22.5'N, 016°7.5°W using $\tau_y = \rho_{air} C_d v^2$, where v represents alongshore wind, C_d is drag coefficient for which 1.15×10^{-3} was used (e.g. Fairall et al., 2003) and ρ_{air} is density of air) for June 2014, maximum vertical velocities of 3.7×10^{-5} m s^{-1} were determined for the shelf region (50 m water depth), which decayed offshore to 1.7×10^{-6} m s^{-1} at the position of the 1000 m isobath at 18°N. As these vertical velocities describe the magnitude of upwelling at the base of the mixed-layer, additional corrections need to be considered for deeper depths. Here, we approximated the vertical decay of *w* as a linear function which diminishes at the ocean floor.

The calculation of the vertical advective flux supplying solutes from the shallow O_2-depleted waters to the surface waterschlorophyll *a* maximum requires knowledge of a concentration difference Δ[TM] associated with the upwelling flux. Ideally, the vertical length scale over which of the concentration difference is determined can be diagnosed as the by TM concentration variance divided by its mean vertical gradient (e.g. Hayes et al., 1991). However, in our study TM concentration time series data are not available. Previous studies have used a vertical length scale of 20 m to calculate the concentration differences between the target depth and the water below (e.g. Hayes et al., 1991; Steinfeldt et al., 2015; Tanhua and Liu, 2015). For our calculations, we chose to use a smaller length scale of 10 m following Hayes et al. (1991) which results in vertical advective TM flux presumably on the lower side of possible values. correlation analysis of vertical velocity fluctuations and concentration variability at different depths (w':[TM]'). As these data are not available, we chose to use the mean vertical concentration differences over a vertical distance of 10 m. Thus, the vertical advective flux F_{az} at each station was estimated from $F_{az} = w(x,z) \cdot \frac{\partial [TM]}{\partial z} 10\ m$.

2.8 Figures

All figures were produced in R (version 3.4.3). Data gridding in figures 2 and 3 was performed using the Tps function within the fields package in R (Nychka et al., 2016).

3. RESULTS & DISCUSSION

3.1 Oceanographic settings of the study area

The cruise was conducted in June 2014 along a transect crossing a narrow shelf off the Mauritanian coast at 18°20'N. The vertical structure of the OMZ in this region is characterized by a deep OMZ at about 400 m depth, and a shallow OMZ at about 100 m depth (Brandt et al., 2015). Coastal upwelling of nutrient-rich deep water occurs as a result of offshore transport of surface waters caused by a Northeast Trade wind component parallel to the coast. While north of 20°N upwelling persists throughout the year, upwelling south of 20°N, including the Mauritanian upwelling region, undergoes

seasonal changes in upwelling strength (Barton et al., 1998), with strongest upwelling occurring between December and April. The seasonal variability is mainly driven by changes in wind forcing associated with the migration of the Intertropical Convergence Zone (~~Schafstall et al., 2010~~Lathuilère et al. 2008). During the cruise period, cold upwelled waters with temperature less than 20°C were still present on shelf and upper continental slope (Thomsen et al., 2019, their Fig. 1) indicating active upwelling.

The eastern boundary circulation consists of the Mauritania Current (MC, Fig. 1) flowing poleward at the surface against the equatorward winds and of the Poleward Undercurrent (PUC) flowing in the same direction at depths between 50 and 300 m (Barton, 1989; Klenz et al., 2018; Mittelstaedt, 1983; Peña-Izquierdo et al., 2015). Both currents supply cold, O_2 and nutrient-rich waters of predominantly South Atlantic origin (South Atlantic Central Water, SACW) to the coastal upwelling region (e.g. Mittelstaedt, 1991; Mittelstaedt, 1983; Peña-Izquierdo et al., 2015). In response to the changing winds, the eastern boundary circulation likewise exhibits a pronounced seasonal variability (Klenz et al., 2018; Stramma et al., 2008a). The strongest poleward flow is observed during the relaxation period between May and July when alongshore, upwelling-favorable winds weaken but wind stress curl is at its maximum (Klenz et al., 2018). During the upwelling season in boreal winter, the circulation more closely resembles the classical eastern boundary circulation regime, with a weak poleward undercurrent flowing beneath an equatorward coastal jet (Klenz et al., 2018; Kounta et al., 2018). At deeper levels (300–500 m depth), flow was found to be equatorward during both seasons. The shallow (<300 m depth) boundary circulations turn offshore at the southern flank of the Cape Verde frontal zone (CVFZ) (e.g. Tomczak, 1981; Zenk et al., 1991) at about 20°N, separating SACW from more saline and O_2-rich Central Waters formed in the North Atlantic (NACW). The circulation in June 2014 was typical for a relaxation period characterized by ~~little upwelling and a~~ strong poleward flow over the ~~entire~~ shelf and the upper continental slope between the surface and 250 m depth (Klenz et al., 2018; Thomsen et al., 2019). During the later parts of the cruise, the core of the MC moved offshore and reduced poleward flow was observed near the shelf break. Periods of elevated northward flow on the Mauritanian shelf inhibits the onshore near-bottom supply of low oxygen but nitrate-rich waters onto the shelf with consequences for benthic nitrogen cycling (Yücel et al., 2015).

Meridional sections of water mass properties and O_2 concentrations from around 18°N showed that waters with an enhanced SACW proportion advected from the south as well as NACW coming from the north, have higher O_2 concentrations than the ambient waters (Klenz et al., 2018). The mixture of SACW and NACW waters found in the thermocline particularly during boreal winter, previously identified as a regional water mass and termed the Cape Verde SACW (SACWcv) by Peña-Izquierdo et al. (2015), is a signature of an older water mass with lower O_2 concentrations than those of SACW or NACW due to a longer residence time and O_2 consumption through remineralization. Elevated pelagic oxygen consumption levels at the Mauritanian continental margin were recently determined by

Thomsen et al. (~~2018~~2019). During the transition period in May through July upper Central Waters (50–300 m depth) are dominated by SACW accounting for 80–90 % of the water masses in the boundary current region (Klenz et al., 2018).

The SACW transported poleward within the boundary circulation is supplied by the zonal North Equatorial Counter Current (NECC) and North Equatorial Under Current (NEUC), which flow eastward at about 5°N (Brandt et al., 2015) before diverging into a northward and a southward flowing branch in front of the African coast.

As a result of interactions between tidal currents, topography and critically sloping upper continental slope topography (e.g. Eriksen, 1982), the Mauritanian upwelling region is known for elevated nonlinear internal wave activity resulting in enhanced mixing in the water column of the upper slope and shelf region (Schafstall et al., 2010). Vertical fluxes of nutrients driven by mixing processes are amongst the largest reported in literature, however lower than in the Celtic Sea (Tweddle et al., 2013) and the lower St. Lawrence Estuary (Cyr et al., 2015).

The CTD and microstructure deployments were performed along the east-west transect in the period June 8 to June 27 (2014) (Fig. 1). Oxygen concentrations reached a deep minimum of 40–50 µmol kg^{-1} at about 400 m and a shallow minimum of 30–50 µmol kg^{-1} at about 50–100 m (Fig. 2), which is in agreement with previous studies (Brandt et al., 2015; Thomsen et al., ~~2018~~2019). Mixed layer depths ranged between 10 and 22 m during the cruise. Salinity was highest at the surface (ca. 36.02) and generally decreased with depth to a minimum of 34.71 at around 1000 m. Nitrate (NO_3^-) concentrations in the surface mixed layer varied between 0.1 and 11.3 µmol L^{-1} and phosphate (PO_4^{2-}) between 0.15 and 0.91 µmol L^{-1}. NO_3^- and PO_4^{2-} concentrations increased with depth to a maximum of 47.6 and 3.2 µmol L^{-1}, respectively (Fig. 2).

Over a time period of 19 days, two trace metal stations along the transect~~were reoccupied along the transect~~ at water depths of 170 m (18.23 °N, 16.52 °W, 1st deployment: June 12, 2nd deployment: June 21) and 189–238 m (18.22°N, 16.55°N, 1st deployment: June 24, 2nd deployment: June 26) were reoccupied. Minimum O_2 concentrations of 30 µmol kg^{-1} observed before June 15~~, which~~ increased to 50 µmol kg^{-1} after June 19 or June 24, depending on the location. This oxygenation event~~, that was also~~ captured in ocean glider measurements is discussed in detail by Thomsen et al. (~~2018~~2019). Variability in oxygen concentrations observed further offshore was attributed to physical transport of SACW into the region (Thomsen et al. 2019). In contrast, closer to the coast, enhanced pelagic oxygen consumption rates were determined that significantly contribute to the variability in observed oxygen concentrations (Thomsen et al., 2019). ~~They attributed the change to physical transport of SACW into the region (Thomsen et al., 2018), most likely associated with the observed increase in current speed of the MC flowing northward parallel to the coast line and transporting relatively O_2 rich water while decreasing the residence time of the SACW along the continental margin. Additionally,~~

~~pelagic oxygen consumption was found to contribute to the variability in oxygen concentrations close to the seafloor (Thomsen et al., 2018).~~

The sediments in the study area contain a large amount of carbonate, biogenic silica and quartz (Hartman et al. 1976). The fraction of sand and mud varies largely depending on bottom depth, with sand comprising between 7 and 70% of the dry weight (Dale et al., 2014). The particulate organic carbon (POC) content varies between 0.55 wt% at shallow depth (66 and 90 m) and increases to 3.3 wt% at 1108 m depth (Schroller-Lomnitz et al., 2019). A more detailed description of the sediments underlying our study region and sediment parameters collected on the same cruise, including Fe(II) concentrations and Fe/Al ratios, are given in Schroller-Lomnitz et al. (2019).

3.2 Spatial distributions of dissolved and leachable particulate trace metals

Dissolved Fe and LpFe concentrations ranged between 0.97–18.5 nmol L^{-1} and 1.6–351 nmol L^{-1}, respectively (Fig. 3a, b). Surface waters (5–29 m) had lowest dFe (0.97–4.7 nmol L^{-1}) and LpFe (1.6–35.9 nmol L^{-1}) concentrations, whereas highest concentrations were present on the shelf close to the seafloor (up to 18.5 nmol L^{-1} dFe and 351 nmol L^{-1} LpFe). Enhanced concentrations of both Fe fractions at any given station were observed at depths with low O_2 concentrations (30–60 µmol O_2 kg^{-1}). A similar distribution pattern was observed for dCo, with concentrations between 0.069 and 0.185 nmol L^{-1} (Fig. 3c). In contrast, LpCo concentrations varied ~~between~~ from below the limit of quantification (LOQ) ~~and~~ up to 0.179 nmol L^{-1} and were generally highest in surface waters and close to the coast (Fig. 3d). Compared to dFe, the concentration range of dCo was much narrower and enhanced concentrations were observed over a broader depth range and further offshore.

Surface dFe and dCo concentrations were low, presumably due to enhanced biological uptake. No clear increasing trend in dFe and dCo with depth was observed, indicating that processes other than, or in addition to, remineralization influenced their distributions. Elevated concentrations were found close to the sediments and within low O_2 waters. This suggested a benthic source of Fe and Co under O_2-depleted conditions, and offshore transport along O_2-depleted water filaments, which is in agreement with previous studies (e.g. Baars and Croot, 2015; Hatta et al., 2015; ~~Hawco et al., 2016~~; Noble et al., 2012). Our sharper onshore-offshore gradient of dFe concentrations compared to dCo in O_2-depleted waters shows that oxidation and removal mechanisms/scavenging rates were faster for Fe than Co (Noble et al., 2012). Previously reported dFe concentrations in coastal regions of the tropical North Atlantic were lower than we observed, between 0.5–6.3 nmol L^{-1} (Hatta et al., 2015; Milne et al., 2017; Wuttig et al., 2013). However, all these samples were collected at a greater distance from the coast. In the near-coastal Oregon and Washington shelf bottom water dFe concentrations were similar to our study under equivalent O_2 concentrations (18.7–42.4 nmol L^{-1} dFe, 42–61 µmol kg^{-1} O_2; Lohan and Bruland, 2008), whereas in the euxinic waters from the Peruvian shelf region, dFe concentrations were more than an order of magnitude higher, exceeding 200 to 300 nmol L^{-1} (Schlosser et al., 2018;

Scholz et al., 2016). Similar dCo concentrations to our study were observed in the North and South Atlantic, with highest concentrations of ~0.16 nmol L^{-1} present within O_2-depleted waters (Noble et al., 2012; Noble et al., 2017).

Dissolved Mn concentrations ranged between 0.46–13.8 nmol L^{-1} and LpMn between below LOQ–4.4 nmol L^{-1} (Fig. 3e, f). Highest dMn and LpMn concentrations were observed in surface waters, generally decreasing with depth. Additionally, concentrations were highest on the shelf and decreased offshore. The dMn concentrations were generally elevated within and below the deeper O_2-depleted waters with 0.70–1.34 nmol L^{-1} compared to 0.46–0.91 nmol L^{-1} just above. The increased dMn concentrations within the deeper O_2-depleted waters (~350–500 m depth) indicate a benthic source, similar to Fe and Co, which is in accordance with previous studies (Noble et al., 2012). However, in the shallow O_2-depleted waters (~50–200 m depth), this effect is not resolvable due to high surface concentrations, which were maintained by photo-reduction of Mn oxides to soluble Mn(II) that prevents loss of Mn from solution (Sunda and Huntsman, 1994). Reported dMn concentrations in the North and South Atlantic were lower than in our study, with concentrations <3.5 nmol L^{-1} in surface waters and around 0.5–1 nmol L^{-1} dMn within the OMZ (Hatta et al., 2015; Noble et al., 2012; Wuttig et al. 2013). As for dFe, these lower reported values can also be explained by sampling stations positioned at further distance from the coast and removal of dMn via biological oxidation processes with distance from the source (Moffett and Ho, 1996).

Dissolved Cd and Ni concentrations were lowest in surface waters with 0.022–0.032 nmol Cd L^{-1} and 2.6–2.8 nmol Ni L^{-1}, and showed an increasing trend with depth to maximum values of 0.60 nmol L^{-1} and 5.8 nmol L^{-1}, respectively (Fig. 3g, m). Leachable particulate Cd concentrations were between below LOQ and 0.20 nmol L^{-1}, and LpNi concentrations between below LOQ and 1.7 nmol L^{-1}. A large fraction of Ni (72–100%) was present in the dissolved form. The majority of LpNi samples were below the LOQ (>70% of the data) and LpNi is therefore not included in Fig. 3. LpCd concentrations were highest close to the coast and decreased offshore (Fig. 3h). In surface waters close to the coast the LpCd fraction was dominant with up to 84.3% of the entire Cd pool (d + Lp). The fraction of LpCd in surface water beyond the shelf break (including stations 2, 1 and 9) contributed still up to 54.3% of the Cd pool, whereas below 50 m only 0–12.8% of TDCd was in the Lp phase beyond the shelf break. In contrast to Fe, Co and Mn, no increases in Cd and Ni were observed near the seafloor and within the O_2-depleted waters indicating that Cd and Ni concentrations are mainly controlled by remineralization of sinking organic matter, which is typical for these two nutrient-like TMs (Biller and Bruland, 2013). Similar distributions with concentrations between 0 and 1000 m water depth ranging from ~2–5.5 and ~0–0.55 nmol L^{-1} for dNi and dCd, respectively, were observed during the GEOTRACES transect GA03_w in the tropical North Atlantic (Mawji et al., 2015; Schlitzer et al., 2018).

Dissolved Cu concentrations in surface waters ranged between 0.63–0.81 nmol L^{-1} (Fig. 3i). Concentrations increased with depth to around 1.37 nmol L^{-1} at 700 m depth close to the seafloor, whereas highest observed concentrations further offshore were 0.95 nmol L^{-1} at the greatest sampled depth of 850 m. These results indicate that in addition to remineralization processes of sinking biogenic particles, the distribution of Cu is influenced by inputs from the seafloor. This is in accordance with previous studies, suggesting that Cu is released from continental shelf sediments under oxic and moderately reducing conditions (Biller and Bruland, 2013; Heggie, 1982), whereas no increase in Cu concentrations near the seafloor was observed at low bottom water O_2 concentrations (O_2 <10 ~~µM~~µmol L^{-1}; Johnson et al., 1988). A decrease in Cu concentrations in the bottom boundary layer was also reported with a seasonal decrease in O_2 in summer from a minimum of 70 ~~µM~~ µmol L^{-1} O_2 in May to 40 ~~µM~~ µmol L^{-1} O_2 in August, suggesting a decrease in sedimentary release of Cu (Biller and Bruland, 2013). In strongly reducing sediments and the presence of H_2S, Cu forms inorganic sulfides and precipitates, which may explain reduced sedimentary Cu release under low bottom water O_2 concentrations (Biller and Bruland, 2013). Therefore, the sediment source of dCu might show a different dependency on bottom water O_2 concentrations than dFe, dCo and dMn explaining the distinct distribution of dCu. Concentrations of LpCu were between below the LOQ to 0.61 nmol L^{-1} with enhanced levels at station 4 close to the coast and at mid depths of the three stations furthest offshore (9, 5 and 2) (Fig. 3j).

Observed dPb concentrations were lowest in the surface waters at 9–14 pmol L^{-1} and increased with depth to 29–86 pmol L^{-1} below 600 m depth (Fig. 3k). Lead is not considered a nutrient-like TM (e.g. Boyle et al., 2014), but our observations indicate a release of Pb from sinking particles following remineralization. The concentration range and depth distribution is similar to reported distributions further offshore at about 21°W (Noble et al., 2015). These authors suggested that increased concentrations of up to 70 pmol L^{-1} between 600 and 800 m depth were related to the influence of Mediterranean Outflow Waters (MOW). Additionally, increased Pb concentrations in proximity to sediments have been attributed to the benthic release of historic Pb through reversible scavenging from particles and the release of dPb associated with Fe/Mn oxyhydroxides during reductive dissolution of those oxides in anoxic sediments (Rusiecka et al., 2018). The major source of Pb to the ocean is atmospheric dust deposition from anthropogenic emissions (Bridgestock et al., 2016; Nriagu and Pacyna, 1988; Veron et al., 1994) with a recent indication of reduced anthropogenic Pb inputs to surface waters in the eastern tropical Atlantic under the North African dust plume (Bridgestock et al., 2016). Low surface water concentrations on the Mauritanian shelf indicate low atmospheric inputs of Pb to this region. LpPb was below the LOQ–27 pmol L^{-1}, and the distribution of LpPb was similar to that of LpFe, with subsurface maxima within O_2-depleted waters (Fig. 3l) and may indicate increased scavenging of dPb in these layers which might be associated with Fe containing particles.

In general, sediment derived TM concentrations decrease with distance from the shelf and with time that passed since the water mass has been in contact with the sediments due to water mass mixing and removal processes such as precipitation and scavenging (Bruland and Lohan, 2006). Radium isotopes can be used as a tracer for benthic sources. The major source of Ra to the ocean is input from sediments through the efflux of pore water, sediment resuspension, and submarine groundwater discharge (Moore, 1987; Moore and Arnold, 1996; Rama and Moore, 1996). Due to the distinctive half-lives of the different Ra isotopes (e.g. ^{224}Ra ($t_{1/2}$ = 3.66 d) and ^{223}Ra ($t_{1/2}$ = 11.4 d)) and their conservative behaviour in seawater, it is possible to quantify the time that has passed since a parcel of water was in contact with the sediments using the following equation by Moore (2000):

$$\left(\frac{A_{224}}{A_{223}}\right)_{obs} = \left(\frac{A_{224}}{A_{223}}\right)_{i} \frac{e^{-\lambda_{224}\tau}}{e^{-\lambda_{223}\tau}} \quad (23)$$

solved for water mass age (τ):

$$\tau = \frac{\ln\left(\frac{A_{224}}{A_{223}}\right)_{obs} - \ln\left(\frac{A_{224}}{A_{223}}\right)_{i}}{\lambda_{223} - \lambda_{224}} \quad (34)$$

where A_{224}/A_{223} is the activity ratio of ^{223}Ra and ^{224}Ra, with the subscript *obs* for the observed seawater ratio and the subscript *i* for the initial groundwater endmember ratio, and λ_{223} and λ_{224} are the decay constants in d^{-1} for ^{223}Ra and ^{224}Ra. The ratio ^{224}Ra/^{223}Ra is not affected by dilution assuming there is no mixing with waters having significantly different ^{224}Ra/^{223}Ra ratios.

Highest $^{224}Ra_{ex}/^{223}$Ra activity ratios were observed close to the seafloor (Fig. 3n). The average $^{224}Ra_{ex}/^{223}$Ra ratio in proximity to the sediment source (< 20 m above seafloor) was 4.1 ± 0.7 and was similar to reported ratios for shelf waters off South Carolina ($^{224}Ra_{ex}/^{223}$Ra = 4.1 ± 0.7; Moore, 2000). The $^{224}Ra_{ex}/^{223}$Ra ratios decreased away from their benthic source due to decay ($^{224}Ra_{ex}/^{223}$Ra = 0–0.5 in surface waters). Ratios close to the seafloor were relatively constant along the transect at bottom depths <600 m, whereas dFe, dCo and dMn concentrations varied largely in the bottom samples. This suggests that factors, which are not influencing the Ra distribution, impacted the distributions of dFe, dCo and dMn, with a likely influence of enhanced O_2 concentrations reducing sediment release or increasing removal rates of these metals at water depths between 200 and 400 m. At around 800 m bottom depth, $^{224}Ra_{ex}/^{223}$Ra ratios were slightly elevated and coincided with increased dCo, dFe, dMn and dCu concentrations despite O_2 concentrations >70 µmol kg^{-1}. This suggests that the enhanced TM concentrations at this location were influenced by a strong sediment source which may be related to the presence of a benthic nepheloid layer as indicated by an increase in turbidity in proximity to the seafloor. An elevated $^{224}Ra_{ex}/^{223}$Ra ratio of 3.5 ± 0.6 was observed at about 16.65°N and 80 m water depth (bottom depth 782 m) and coincided with a local maximum of dFe, dMn and dCo and reduced O_2 concentrations. These observations indicate that the waters with the local maximum of dFe, dMn

and dCo have been in relatively recent contact (12–20 days assuming initial pore water $^{224}Ra_{ex}/^{223}Ra$ ratios between 18–38; Moore, 2007) with sediments, likely originated from south of our transect as a result of a strong poleward flow (Klenz et al., 2018), and that the dynamic current system in this region can cause local and short-term variability in the transport of sediment derived TMs.

3.3 Classification of different groups of trace metals based on principal component analysis

Principal Component Analysis (PCA) was performed (using the RDA function within the vegan package in R; Oksanen et al., 2017) to investigate different groups and correlations in the data set. Dissolved TMs (Fe, Mn, Co, Ni, Pb, Cu and Cd), nutrients (silicic acid, nitrate and phosphate), dissolved O_2, Apparent Oxygen Utilization (AOU), depth and iodide concentrations (Supplementary Fig. S1) were utilized in the PCA. Radium data were not included in the PCA, as the number of available data points for $^{224}Ra_{ex}/^{223}Ra$ was much lower than for the other parameters. Surface waters shallower than 50 m were excluded from the PCA to remove the influence of ~~local processes in surface waters, such as~~ localized atmospheric deposition and photochemical processes, which in particular influence Mn and iodide distributions. The PCA generated three principal components (PC) with eigenvalues larger than 1, with PC1 explaining 53.6% and PC2 25.5% of the total variance in the dataset (together 79.1%). Inclusion of PC3 in the analysis explained only 6.8% more of the variance.

The first PC group is formed by dCd, dCu, dNi and dPb (Fig. 4), which are associated with depth, AOU, nitrate and phosphate. This indicates that the distribution of Cd, Cu, Ni, and potentially Pb, are controlled by organic matter remineralization processes. This is in agreement with strong Pearson correlations R >0.9 for the relationships of dCd and dNi with depth, nitrate and silicic acid (Supplementary Material, Table S1). Weaker correlations with major nutrients were observed for dPb (R >0.6) and dCu (R >0.4), potentially due to additional remineralization or removal mechanisms for these elements (e.g. prior atmospheric inputs and water mass transport, Pb; sediments, Cu and Pb, and scavenging). The second group of TMs is composed of dFe, dCo and dMn that are associated with elevated iodide and turbidity, and low dissolved O_2 (Fig. 4). Iodide (I^-) is the reduced form of iodine (I), which is typically present as iodate (IO_3^-) in oxygenated subsurface water. Both I forms are present as soluble anions in seawater. Due to a relatively high redox potential (pE ~10), iodine is one of the first redox-sensitive elements to undergo reduction under suboxic conditions and is therefore a useful indicator for active reductive processes (Rue et al., 1997). Despite their role as micronutrients, Fe, Mn and Co do not correlate with nutrients indicating that processes other than remineralization controlled their distributions.

The anti-correlation with O_2 (also shown in Fig. ~~S1~~S2) and correlation with iodide support the notion that Fe, Co and Mn distributions were strongly influenced by water column O_2 concentrations, presumably through: (i) enhanced benthic metal fluxes from anoxic sediments, and (ii) decreased oxidation rates in the overlying water column under O_2-depleted conditions. This is also supported by

elevated benthic Fe(II) fluxes observed at the seafloor within the shallow OMZ, with benthic fluxes of 15–27 µmol m^{-2} d^{-1} (Schroller-Lomnitz et al., 2018).

Variability in the redox-sensitive metals, Fe, Mn and Co, were not fully explained by either O_2 or iodide concentrations; Pearson correlations with O_2 were -0.55, -0.61 and -0.58, respectively (Supplementary Material, Table S1). As shown before, other factors such as, for example, water mass mixing and age, the amount and type of particles present, and remineralization all likely impact their dissolved concentrations. Consequently, such a complex chain of factors and processes means that one variable alone is unlikely to explain the behaviour of Fe, Mn, and Co.

3.4 Influence of the different sources of Fe, Mn and Co

The main sources of TMs in our study region are sedimentary release and atmospheric dust deposition (e.g. Rijkenberg et al., 2012). Also release of TMs via organic matter remineralization may have an important influence on the distribution of TMs. In the following, we discuss the relative influence of remineralization, atmospheric dust deposition and sedimentary release on the supply of Fe, Co and Mn to surface waters.

3.4.1 Remineralization

To quantify the influence of remineralization for dFe, we employed dFe to carbon (dFe/C) ratios (carbon was calculated using AOU, with an AOU/carbon ratio of 1.6; Martin et al., 1989). Surface data, where O_2 was over-saturated (due to biological O_2 production), were excluded. Dissolved Fe/C ratios for the entire transect varied between 15 and 74 µmol mol^{-1}. These results agree with those for shelf-influenced waters with dFe/C ratios of 13.3–40.6 µmol mol^{-1} further south at 12°N (Milne et al., 2017). Reported ratios for the North Atlantic, further away from the shelf were lower and ranged between 4 and 12.4 µmol mol^{-1} (Fitzsimmons et al., 2013; Milne et al., 2017; Rijkenberg et al., 2014). To estimate the amount of dFe being derived by remineralization, we assume a dFe/C ratio of 4–12 µmol mol^{-1} from organic matter remineralization, similar to the observed dFe/C ratios in the open ocean close to our study area without a strong shelf influence. These offshore ratios may still be influenced by an atmospheric source of dFe, which would result in an overestimation of dFe/C ratios from remineralization and thereby an overestimation of the fraction of remineralized dFe. Apart from additional inputs, the dFe/C ratios are influenced by the respective Fe/C stoichiometry in the sinking organic matter and removal of dFe by scavenging. Furthermore, it is not clear if the offshore ratios can be transferred to a location close to the coast, as the balance between remineralization and scavenging processes might be different due to differences in phytoplankton productivity and particle load. Hence, this approach only provides a broad estimate of the relative influence of remineralization on the distribution of dFe in the study area.

We obtain a range between 5 ± 3% and 54 ± 27% for dFe being derived from remineralization processes with lowest values observed on the shelf at 34 m depth at station 4 (5 ± 3%) and highest values estimated beyond the shelf break at Stn 9 at 213 m depth (54 ± 27%) and Stn 2 at 450 m depth (52 ± 26%). However, no clear increase in the contribution of remineralized dFe to total dFe with depth or distance to the coast was observed. For example at depths between 35 and 200 m, our estimates of dFe from remineralization ranged between 10 ± 5% and 51 ± 25% with high values of up to 41 ± 20% at 50 m depth at station 7 close to the coast, whereas relatively low values of 19 ± 9% were observed at 89 m at station 2. These results indicate that, locally, remineralization can be an important control on dFe concentrations, but that the contribution varies largely with additional important controls, often dominating over remineralization.

Similar analysis for dCo/C ratios revealed an increased importance of an additional source close to the shelf. Observed dCo/C ratios ranged between 0.81 and 2.2 µmol mol^{-1}. The larger ratios were observed close to the coast and decreased further offshore. Overall, the observed ratios were somewhat higher than reported cellular ratios of phytoplankton in the North Atlantic of 0.5–1.4 µmol mol^{-1} (Twining et al., 2015). However, relatively constant dCo/C ratios beyond the shelf break (dCo/C: 0.82–1.09 µmol mol^{-1}, stations 2, 5 and 9) that are similar to cellular ratios of phytoplankton suggest a large influence of remineralization on dCo beyond the shelf break, whereas enhanced ratios close to the coast suggest an additional benthic source. Due to the lack of comparable data of offshore dCo/C ratios and the multiple processes influencing this ratio (varying phytoplankton nutrient stoichiometry and scavenging), we did not use these values to estimate the remineralized dCo fraction.

The distribution of Mn was not predominantly determined by biological uptake and remineralization processes in our study region. In contrast, dMn/C ratios were largely influenced by photoreduction in the surface (Sunda and Huntsman, 1994), removal via biotic oxidation and formation of Mn oxides at depth (Tebo et al., 2004). Therefore, we did not assess remineralization processes for Mn using dMn/C ratios.

3.4.2 Atmospheric deposition

Aluminum is present as a relatively constant fraction of ~8.15 wt% in the continental crust (Rudnick and Gao, 2006), is supplied to open ocean surface waters mainly by atmospheric deposition (Orians and Bruland, 1986) and is not considered ~~not~~ to be taken up by phytoplankton (apart from a small amount being incorporated into siliceous diatom frustules; Gehlen et al., 2002). Therefore, dAl in the surface mixed layer is used as a tracer for atmospheric deposition to the surface ocean (Measures and Brown, 1996; Measures and Vink, 2000). The atmospheric input in the study region is mainly influenced by North African/Saharan mineral dust with only a small contribution of anthropogenic sources which differ greatly in TM composition and solubilities from mineral dust (Baker et al., 2013; Patey et al., 2015; Shelley et al., 2015). Close to continental shelves~~, in addition to atmospheric input~~,

Al can also be supplied by sediment resuspension in addition to atmospheric input (Menzel Barraqueta et al., 2018; Middag et al., 2012; Moran and Moore, 1991). Enhanced aerosol optical depth above our study region (Supplementary Fig. S3&4) indicates high dust loading at the time of our cruise.

Our dAl concentrations in surface water ranged between 30 and 49 nmol L^{-1} and LpAl between 3.4 and 18.2 nmol L^{-1}. Dissolved Al concentrations decreased with depth (Fig. 8), indicating that Al was released by aeolian dust deposition to surface waters and removed through scavenging at depth (Orians and Bruland, 1985). ~~Trace metal (Fe, Co, and Mn) to Al ratios were utilized to investigate the influence of atmospheric dust deposition. We present molar ratios for dissolved (dTM/dAl), total dissolvable (TDTM/TDAl) and leachable particulate (LpTM/LpAl) concentrations. In the surface mixed layer, dFe/dAl molar ratios ranged between 0.019 and 0.114, TDFe/TDAl between 0.236 and 0.826 and LpFe/LpAl between 1.04 and 9.50.~~

~~Literature particulate Fe/Al ratios from aerosol samples collected in the remote North Atlantic between 8.7°N and 23°N were in the range of 0.31 ± 0.06 (Buck et al., 2010; Patey et al., 2015) and 0.37 ± 0.02 in the North East Atlantic ~18°N under the Saharan dust plume (Shelley et al., 2015). In contrast, upper crustal material ratios are lower ranging from 0.19 to 0.23 suggesting a slight Fe enrichment of aeolian mineral dust particles (McLennan, 2001; Rudnick and Gao, 2006; Wedepohl, 1995). Lower Fe than Al solubilities from aerosol leach experiments in ultra-high purity water (UHP) and 25% acetic acid (HAc) and seawater have been reported (Baker et al., 2006; Buck et al., 2010; Shelley et al., 2018), but soluble Fe/Al ratios from these experiments varied dependant on the leach medium (UHP: 0.21 ± 0.04, 25% HAc: 0.25 ± 0.04, seawater: 0.051 ± 0.009; Shelley et al., 2018). This indicates that dFe/dAl and LpFe/LpAl ratios in seawater from atmospheric deposition are likely to be lower than particulate ratios of digested aerosol samples in the study region.~~

~~Our dFe/dAl ratios at the upper end (dFe/dAl: 0.114) are larger than aerosol leaches in seawater indicating a potential additional input of dFe, whereas our lower dFe/dAl ratios than reported ratios in aerosol leaches suggest removal of dFe by biological uptake or scavenging. Our LpFe/LpAl are all larger than reported ratios in aerosol leaches and total aerosol ratios, which shows that there is an additional source of LpFe or transfer of sediment derived dFe onto the particulate phase by biological uptake or sorption to particles. Total dissolvable ratios comprise both dissolved and leachable particulate phases, thereby being independent of the phase transfer from dissolved to particulate phase (via biological uptake or sorption). The lower end of total dissolvable ratios (TDFe/TDAl: 0.236) were close to the total ratios in aerosol samples, suggesting that atmospheric deposition represented an important source of Fe and Al to the surface ocean. At the upper end, ratios were much larger (TDFe/TDAl: 0.826) than aerosol ratios and indicate an additional benthic source of Fe.~~

~~These interpretations only apply, however, if residence times of dissolved and particulate Fe and Al phases supplied via atmospheric deposition are similar. This is difficult to assess, as estimated~~

~~residence times for both elements are dependent on input and removal rates and vary largely between locations. Overall, our Fe/Al ratios suggest that atmospheric deposition is an important source of Fe to surface waters with an additional contribution of benthic inputs. However, uncertainties in solubilities and residence times cause a high uncertainty in the interpretation of the role of atmospheric deposition.~~

~~Observed dCo/dAl ratios in the upper 50 m were 0.001–0.004, TDCo/TDAl ratios were slightly higher at 0.003–0.005 and LpCo/LpAl ratios were 0.006–0.020. Cobalt is present in the upper continental crust in a much smaller molar fraction than Fe (Co/Al: 0.000071–0.000097; McLennan, 2001; Rudnick and Gao, 2006; Wedepohl, 1995). However, ratios in aerosol samples under the North African dust plume were slightly higher (Co/Al: 0.00016 ± 0.00002; Shelley et al., 2015) than crustal ratios and solubility of Co from these aerosol samples was much higher than Al solubility resulting in soluble Co/Al of 0.0021 ± 0.0009 in UHP (Shelley et al., 2018). The soluble ratios also varied largely depending on the leach medium and might therefore also vary from the actual aerosol solubility in seawater at our study site. Our ratios of all fractions were larger than total aerosol ratios and mostly higher than soluble ratios from aerosol leaches. This indicates that an additional benthic source of Co likely contributed to the Co present in surface waters.~~

~~Dissolved Mn/dAl ratios in the upper 50 m ranged between 0.082 and 0.347, and TDMn/TDAl between 0.083 and 0.256. The ratios are much larger than upper crustal ratios (Mn/Al: 0.0032–0.0037; McLennan, 2001; Rudnick and Gao, 2006; Wedepohl, 1995) but similar to the soluble ratios of Mn/Al from aerosols in UHP (Mn/Al: 0.24 ± 0.09; Shelley et al., 2018) indicating that a large amount of Mn may be derived from atmospheric deposition. However, these ratios are heavily overprinted by the long residence time of Mn in surface waters due to photoreduction. Therefore, it is not possible to reliably estimate the contribution of atmospheric Mn deposition based on the Al data.~~

Dissolved atmospheric deposition fluxes can vary largely depending on the aerosol solubility, which is dependent on aerosol source, atmospheric aerosol processing during transport and dissolution in surface waters (Jickells, 1999). Here, ~~A~~atmospheric dFe fluxes were calculated using the dAl inventory in the surface mixed layer, a residence time of dAl of 0.65 ± 0.45 years as reported for the Canary Current System (Dammshäuser et al., 2011), and a ratio of 0.31 for dust derived dissolved Fe/Al (Buck et al., 2010). This approach is independent of the fractional solubility of Al, as we do not account for total atmospheric deposition fluxes, and only use the already dissolved fraction of Al. However, this approach is dependent on the ratio of Fe/Al from dissolution of aerosols. This ratio, however, is not clearly defined and can vary between different dust sources and deposition pathways, such as wet or dry deposition (e.g. Shelley et al., 2018). In our study region, dry deposition is the dominant deposition pathway, as it is located north of the Intertropical Convergence Zone and precipitation is minimal < 0.001 g/cm^{-3} (NASA). Here, we utilized a ratio observed for total aerosol samples in the remote North Atlantic from a Saharan dust source (Buck et al. 2010). Soluble ratios under the Saharan dust plume were however lower for all leach media (Fe/Al: 0.051–0.25; Shelley et

al. 2018), indicating that the ratio of 0.31 utilized here, might result in an overestimation of the dFe flux estimates. This approach also assumes that dAl is only supplied to the surface ocean via atmospheric deposition. Vertical fluxes of Al from sediment resuspension are unlikely to ~~largely~~ contribute significantly to concentrations of dAl in surface waters here as dAl concentrations ~~were decreasing~~ decreased with depth~~.~~, indicating removal of dAl via scavenging.

Mean atmospheric dFe fluxes of the individual stations were 0.63–1.4~~3~~ µmol m^{-2} d^{-1} (Fig. 5, Supplementary Table S2), values similar to reported fluxes close to our study region of 2.12 µmol m^{-2} d^{-1} further north between 22.5–25°N and 26.5–27.5°W (Rijkenberg et al., 2012) and 0.120 µmol m^{-2} d^{-1} around 20°N close to the African coast (Ussher et al., 2013). The uncertainty in the residence time of dAl, however, creates a large uncertainty in calculated fluxes resulting in a lowest flux of 0.37 µmol m^{-2} d^{-1} when using the largest estimated residence time of 1.1 years and a highest flux of 4.65 µmol m^{-2} d^{-1} when using the shortest estimated residence time of 0.2 years. In fact, a residence time of 3 months has been shown to give similar results for total Al atmospheric deposition fluxes as modeling studies (Menzel Barraquetta et al., 2019). Low residence times of a few months have also been suggested for Al and Fe in areas with a large dust deposition including our study region (e.g. Croot et al. 2004, Dammshäuser et al., 2011). Therefore, we suggest that the atmospheric dFe flux is more likely to be closer to the upper range of our flux estimates. However, the atmospheric deposition fluxes using a short residence time may be larger than the annual average since the dust load is highest between June and August in our study area (Supplementary Fig. S4).

3.4.3 Vertical trace element fluxes to surface waters

The vertical diffusive and advective fluxes ~~(diffusive and advective)~~ of dFe from shallow O_2 depleted waters to surface waters with enhanced chlorophyll *a* fluorescence ~~the top of the shallow O_2 depleted waters (between 23 and 89 m depending on station) into surface waters~~ were determined to assess the potential Fe contribution to phytoplankton growth from suboxic waters (Fig. 5). A detailed summary of ~~calculated~~ the individual dFe flux~~es~~ estimates, ~~the contribution of diffusive and advective term~~ and their uncertainties ~~for dFe for all stations~~ is given in Supplementary ~~Information~~ Table S2.

Vertical dFe fluxes increased by two orders of magnitude from 70 km offshore to the shallow shelf region. ~~Closest to~~On the shelf (bottom depth: 50 m), an elevated mean dFe flux~~es were~~ of 13.5 µmol m^{-2} d^{-1} was estimated. The contribution from vertical advection (upwelling) here was an order of magnitude larger than the diffusive flux. Despite the large number, our estimate agrees with a previous study (Milne et al., 2017) who estimated a vertical dFe flux of 16 µmol m^{-2} d^{-1} on the shelf at 12°N. Average estimates from the upper continental slope and the lower shelf region (stations 3, 7 and 8, bottom depth: 90–300 m) were between 1 µmol m^{-2} d^{-1} and 2.5 µmol m^{-2} d^{-1}. Here, the vertical diffusive fluxes dominated and were about a factor of three larger than vertical advective fluxes. The elevated diffusive fluxes at the upper continental slope and lower shelf region are due to enhanced

diapycnal mixing that originates from tide – topography interactions (Schafstall et al., 2010). At the repeated station (3) at a water depth of 170 m depth, vertical dFe Flux estimates were 2.3 µmol m^{-2} d^{-1} and 1.4 µmol m^{-2} d^{-1}, respectively. The differences in the two estimates are due to differences in the strength of turbulent mixing during the two station occupations. For the offshore stations 2 and 9 (bottom depth > 500 m), mean dFe fluxes were 0.08–0.16 µmol m^{-2} d^{-1}. ~~Further offshore, vertical dFe fluxes decreased to 0.16 µmol m^{-2} d^{-1} (station 2, bottom depth: 1136 m, 77 km offshore) (Fig. 5).~~ However, one offshore station ~~at~~ (station 5) exhibited elevated ~~higher~~ dFe fluxes ~~were observed (dFe: of~~ 1.3 µmol m^{-2} d^{-1}.~~) than at stations 9 (closer to the shelf) and 2 (further offshore). At station 5,~~ Here, diapycnal mixing ~~eddy diffusivity~~ was determined from only 5 microstructure profiles that exhibited elevated turbulence levels~~and was unusual high at this station~~. It is thus very likely that the observations captured ~~Therefore, the enhanced vertical fluxes are likely caused by~~ a rare elevated mixing event during station occupation and the associated elevated vertical fluxes ~~and~~ do not represent a longer-term average. ~~Between repeat stations 3A and 3B, mean fluxes decreased from 2.3 (Stn 3A) to 1.35 µmol m^{-2} d^{-1} (Stn 3B), which was partly caused by a difference in the vertical concentration gradient of dFe and partly by a change in diffusivity.~~

~~On the shelf (station 4, bottom depth: 45 m), dFe fluxes were dominated by vertical advective rather than diffusive fluxes due to the strong upwelling velocity on the shelf (Table S2). At the continental slope stations (stations 3, 7 and 8, bottom depth: 90–400 m), fluxes were dominated by high diffusive fluxes, which were around 3 times larger than the advective flux term. Further offshore (stations 2 and 9, bottom depth: >400 m) the contribution of advective and diffusive fluxes were similarly low except for station 5 with particularly strong vertical mixing. Similar vertical dFe (16 µmol m^{-2} d^{-1}) to the upper water column were reported on the shelf at 12°N (Milne et al., 2017).~~ Although, in the study region atmospheric fluxes of dFe were enhanced relative to global averages (Mahowald et al., 2009) with mean fluxes of 0.63–1.43 µmol m^{-2} d^{-1}, our vertical ~~dissolved~~ Fe fluxes from the shallow O_2 depleted waters of 0.95–13.5 µmol m^{-2} d^{-1} exceeded atmospheric fluxes at all stations apart from station 2 (0.16 µmol m^{-2} d^{-1}) furthest offshore and potentially station 9 (0.08 µmol m^{-2} d^{-1}), where no atmospheric fluxes were determined. The weaker influence of atmospheric deposition in this region close to the coast is in accordance with previous studies that demonstrated sediments to be the major contributor to the Fe inventory in the coastal region of the eastern tropical Atlantic, whereas the importance of atmospheric inputs increases further offshore (Milne et al., 2017). ~~Our vertical advective fluxes are likely lower than the annual average and also lower than usually during the relaxation period as upwelling favourable winds were particularly low in June 2014.~~It should be noted that there are considerable uncertainties in the flux estimates presented above. While uncertainties in the diffusive flux originate predominately from the elevated variability of turbulence (see Schafstall et al., 2010 for details), uncertainties in the vertical advective flux originate from unaccounted for contributions from e.g. the spatial structure of the wind, particularly in the offshore direction, its temporal variability (e.g. Capet et al., 2004; Desbiolles et al. 2014, 2016; Ndoye et al., 2014), and

uncertainties in the satellite wind product near the coast (e.g. Verhoef et al, 2012). Furthermore, the distribution of vertical velocities with depth is assumed to be linear here.

Dissolved Co fluxes ranged between 2 and 113 nmol m^{-2} d^{-1}. These values are lower than reported upwelling fluxes of dCo of 250 nmol m^{-2} d^{-1} for this region (Noble et al., 2017), but are larger than atmospheric deposition fluxes of 1.7 nmol m^{-2} d^{-1} (Shelley et al., 2015). Fluxes of dMn are downwards from surface waters to O_2 depleted waters due to higher concentrations in surface waters.

3.5 Removal mechanisms and particle interactions

Particles in the water column can either comprise a source or a sink of dissolved TMs. In the top 50 m of the water column a large part of the LpTMs may be part of living biological cells (e.g. phytoplankton) or organic detritus, and can enter the dissolved TM pool by remineralization (Bruland and Lohan, 2006). Additionally, LpTMs may be part of lithogenic phases from Saharan dust and sediment particles, or authigenic phases. Authigenic phases are formed in-situ by TM adsorption onto particle surfaces or by the formation of amorphous TM oxides and hydroxides (e.g. FeO(OH) in the mineral structure of goethite) (Sherrell and Boyle, 1992), processes referred to as scavenging. The extent of scavenging processes is largely influenced by the amount and type of particles present (Balistrieri et al., 1981; Honeyman et al., 1988).

Iron was mainly present in the size fraction >0.2 µm with TDFe concentrations being 0.44–44.5 times higher than dFe (<0.2 µm) (Fig. 6a). To investigate the influence of particle load on the distribution between dissolved and particulate phases, the fraction of Lp (Lp/TD) TMs and Lp concentrations are plotted against turbidity for Fe, Co and Mn (Fig. 6b, c). A low fraction of LpFe of around 60% was observed at lowest turbidity. As turbidity increases from 0.1 to 0.2 NTU, the LpFe fraction increased to >90%. This suggests that the fraction of LpFe is tightly coupled to the particle load. Iron adsorption onto particles has been demonstrated to be reversible with a constant exchange between dissolved and particulate fractions (Abadie et al., 2017; Fitzsimmons et al., 2017; John and Adkins, 2012; Labatut et al., 2014). Furthermore, offshore transport of acid-labile Fe particles formed by scavenging (oxidation/adsorption) of dissolved Fe originating from a ~~reductive dissolution processes from continental shelf~~benthic source~~s~~ was observed in the North Pacific (Lam and Bishop, 2008) and may contribute to the bioavailable Fe pool. Therefore an important fraction of Fe may be transported offshore adsorbed to particles and can enter the dissolved pool by cycling between dissolved and particulate phases.

~~Manganese and Co mainly occurred in the dissolved form.~~ The LpCo fraction ranged between 0 and 75%, and the fraction and concentration of LpCo, showed linear increases with turbidity, indicating an influence of particle load on Co size fractionation, similar to Fe. In contrast to Fe and Co, the fraction of LpMn varied between 3 and 40%, and did not show a correlation with turbidity, whereas LpMn concentrations showed an increase with turbidity. This indicates that an increased presence of particles

coincided with enhanced LpMn levels, but that the particle load did not substantially influence the distribution between dMn and LpMn phases and ~~that~~ particles therefore did not contribute to the dMn fraction. This suggests that particles did not play a major role in transport of dMn, which agrees with a study on hydrothermal vent plumes, where the distribution of the dMn plume was decoupled from the distribution of the particulate Mn plume (Fitzsimmons et al., 2017).

The increase in LpFe concentrations with increasing turbidity was weaker in the surface waters compared to water depths below 50 m (Fig. 6c). This suggests a large additional LpFe source at depth with either a higher Fe content of particles or the presence of different sizes of particles causing different responses in turbidity measurements. The large additional LpFe source at depth~~s~~ is likely associated with benthic dFe inputs, with a subsequent transfer to the particulate phase by ~~adsorption or oxidation with subsequent formation of Fe(oxihydr)oxides~~scavenging. Enhanced turbidity at depth may also indicate sediment resuspension, which would result in the release of TM-containing particles from sediments and enhanced release of dTMs from sediment pore water. The effect of sediment resuspension is discussed in more detail below (section 3.6.2).

In contrast to Fe, the increase in LpCo and LpMn concentrations with turbidity was similar in surface waters and below and suggests less variability in the composition of the particulate Co and Mn phase throughout the water column with a potentially weaker influence of sediment release on the distribution of particulate Mn and Co. A weaker influence of sediment release might be influenced by a weaker release of Co and Mn from sediments in the dissolved form and slower oxidation rates compared to Fe, in particular for Co (Noble et al., 2012), resulting in a slower conversion into the particulate phase. Such an interpretation based on turbidity data alone, however, is very hypothetical and would require further investigation of particulate TM species composition in this area.

3.6 Temporal variability in redox-sensitive trace metals

Large temporal changes in O_2, turbidity and redox-sensitive TMs were observed within a short time scale of a few days at two repeat stations, station 3A/3B and station 8A/8B (Fig. 7 and Fig. S5).

Station 3 and 8 were sampled twice with a period of nine days between both deployments for station 3 (Fig. 7a) and two days for station 8 (Fig. 7b). At station 3, O_2 concentrations in the upper 50 m were very similar between both deployments, whereas below 50 m O_2 increased from 30 µmol kg^{-1} during the first deployment to 50 µmol kg^{-1} nine days later. At the same time, turbidity below 50 m had decreased from 0.35 to below 0.2, and dFe concentrations from a maximum of 10 nmol L^{-1} to 5 nmol L^{-1} nine days later. In addition, dMn and dCo concentrations decreased from 5 to 3 nmol L^{-1} and 0.14 to 0.12 nmol L^{-1}, respectively. Particularly large changes were also observed for LpTM concentrations with a decrease from 147–322 nmol L^{-1} to 31–51 nmol L^{-1} for LpFe, from 0.066–0.114 nmol L^{-1} to 0.015–0.031 nmol L^{-1} for LpCo and from 1.24–2.64 to 0.16–0.54 for LpMn. In contrast, no changes in water mass properties (T/S) occurred below 50 m (Fig. 7a).

Similar changes in O_2 and turbidity were observed at station 8. During the first deployment a local minimum in O_2 below 30 µmol kg^{-1} was present between 105 m and 120 m water depths which coincided with a maximum in turbidity of 0.4 (Fig. 7b). In contrast O_2 concentrations and turbidity during the second deployment were relatively constant (50–60 µmol kg^{-1} O_2 and turbidity 0.2) below 50 m. At the depth of the local O_2 minimum and turbidity maximum, concentrations of dFe, dMn and dCo were elevated during the first deployment with concentrations of 9.4 ± 2.1 nmol dFe L^{-1}, 3.7 ± 0.6 nmol dMn L^{-1} and 0.145 ± 0.033 nmol dCo L^{-1} in comparison to 4.6 ± 1.0 nmol dFe L^{-1}, 2.6 ± 0.5 nmol dMn L^{-1}, and 0.122 ± 0.028 nmol dCo L^{-1} at similar depth during the second deployment.

3.6.1 Remineralization

We compared the results of the redox-sensitive TMs to other nutrient-like TMs and PO_4. For both repeat stations only small changes in dCd (Stn 3A: 0.107–0.231 nmol L^{-1}; Stn 3B: 0.135–0.150 nmol L^{-1}) and PO_4 (Stn 3A: 1.59–1.85 µmol L^{-1}; Stn 3B: 1.55–1.71 µmol L^{-1}) concentrations were observed below 50 m (Fig. 8), suggesting that only a small fraction of dFe under lower O_2 conditions was supplied by more intense remineralization of biogenic particles in the water column.

A weak influence of remineralization processes on the variability in dFe concentrations was confirmed by substantially higher dFe/C ratios at lower O_2 concentrations (40–72 µmol mol^{-1} at Stn 3A compared to 33–41 µmol mol^{-1} at Stn 3B, both below 50 m water depth). Assuming a dFe/C ratio of around 12 (see section 3.4.1) from remineralization, only about 0.25 nmol L^{-1} of the difference in dFe concentrations between repeated deployments can be explained by the difference in remineralization, suggesting that most of the difference in dFe between deployments was caused by changes in source inputs, such as enhanced sediment release during lower bottom water O_2 concentrations, or slower removal by oxidation under lower O_2 conditions.

In contrast, dCo/C ratios were similar between repeat deployments within the OMZ (0.90–1.04 at Stn 3A and 0.92–1.06 µmol mol^{-1} at Stn 3B). Thus, ~~changes in~~ remineralization could be a reason for the changes in observed dCo concentrations during repeated deployments~~, indicating that the sensitivity of dCo sediment input or change in oxidation rates is low at an O_2 shift from 30 to 50 µmol kg^{-1}~~. This is in accordance with previously observed correlation of dCo with PO_4^{3-} in addition to O_2 (Baars and Croot, 2015; Saito et al., 2017). However, we observed a very low Pearson correlation of dCo with PO_4 of only 0.15 compared to oxygen (-0.58) (Supplementary Table S1) below 50 m water depth, suggesting a stronger influence of oxygen than remineralization on the overall distribution of dCo for our study area.

Similar to Fe, higher dMn/C ratios were observed at lower O_2 concentrations (3.4–5.5 µmol mol^{-1} at Stn 3A compared to 2.1–2.9 µmol mol^{-1} at Stn 3B). These results indicate that ~~other~~ processes other than remineralization are also important for the change in dMn concentrations. An additional factor compared to Fe, might involve changes in intensity of photoreduction which may be influenced by

differences in surface turbidity observed at station 3 (lower dMn/C and higher surface turbidity during second deployment). This, however, cannot explain the changes in dMn/C at station 8, where a higher surface turbidity coincided with a higher dMn/C ratio at the local minimum in O_2.

3.6.2 Atmospheric dust deposition and sediment resuspension

Within the OMZ at station 3 and 8, dAl concentrations ranged between 10 and 15 nmol L^{-1}, and LpAl concentration between 1.2 and 11.1 nmol L^{-1} and no substantial changes were observed between deployments (Fig. 8). As lithogenic material has a high Al content, no substantial changes in Al concentrations signify that lithogenic inputs did not differ ~~much~~ greatly between the deployments. Consequently neither increased atmospheric input, nor sediment resuspension are likely to explain the differences in turbidity and redox-sensitive TM concentrations. Hence, changes in turbidity may mainly have been caused by biogenic particles, such as resuspended organic matter (Thomsen et al., ~~2018~~2019). This finding can be confirmed by substantial changes in TM/Al ratios observed during the deployments (Table 2 and Fig. ~~S2~~S6). The Fe/Al ratios in the solid phase of underlying sediments during the cruise were 0.23–0.30 (Schroller-Lomnitz et al., 2018) with Mn/Al ratios of 0.0015–0.0020 (Schroller-Lomnitz, pers. com.). Slight increases in LpAl towards the sediment indicate some influence of sediment resuspension on the TM distribution. Overall much higher TM/Al ratios compared to ratios in the sediments and aerosol samples from this region (Fe/Al: 0.37 ± 0.02, Co/Al: 0.00016 ± 0.00002, Mn/Al: 0.0061 ± 0.0002; Shelley et al., 2015), suggest a large additional source of Fe, Co and Mn in the OMZ close to the shelf. This again points towards a large influence of benthic release of Fe, Co and Mn from sediment pore waters and subsequent partial adsorption to particle surfaces.

3.6.3 Other possible causes for TM variability

From the comparison above, we can conclude that the variations in Fe concentrations during repeated deployments were not caused by increased remineralization or changes in lithogenic inputs from atmospheric deposition or sediment resuspension. The large changes in the Lp fractions must therefore be of biogenic or authigenic origin. If all LpCo would be present in biogenic particles of suspended phytoplankton cells, at our observed maximum of 0.114 nmol L^{-1} LpCo at station 3A we would expect around 4.6 nmol L^{-1} LpFe in sinking phytoplankton, using an average Fe/Co ratio in phytoplankton of 40 (Moore et al., 2013) (observed ratios close to our study area were 20–40; Twining et al., 2015). However, LpFe concentrations were 322 nmol L^{-1} and thereby 70 times larger than our estimate in biogenic particles (4.6 nmol L^{-1}), revealing that the majority of LpFe must be authigenically formed. Altogether our results suggest that changes in particle load as indicated by changes in turbidity do not comprise a major source of dFe, moreover a sink of previously dissolved Fe. Therefore, higher dissolved and Lp concentrations during the first deployment with lower O_2 concentrations must be caused by a stronger benthic source of dissolved Fe.

It is not possible to extract from our data whether the stronger benthic source under low O_2 conditions is directly driven by lower O_2 concentrations in surface sediments and in the water column resulting in higher benthic Fe fluxes and slower oxidation rates in the water column, or by a longer residence time of the water mass on the shelf. However, increased benthic fluxes are in accordance with previous findings from ex-situ sediment incubation experiments, where Fe fluxes increased with decreasing O_2 concentrations (Homoky et al., 2012). Therefore, we hypothesize that with a reduction of bottom water O_2 concentrations from 50 to 30 µmol kg^{-1}, drastically more Fe is effectively released from the sediments by diminished oxidation rates at the sediment-water interface, and that a large fraction gets directly adsorbed onto particles. Therefore, particles do not compose a major source of Fe here, but may play an important role in Fe offshore transport.

Due to much lower changes in concentrations of dissolved and LpCo, and the additional effect of photoreduction and strong scavenging for Mn, we were unable to resolve the main mechanisms for changes in Co and Mn concentrations with changes in O_2 and turbidity. Nevertheless, due to their similar redox-sensitive behavior and distribution in OMZs, it is likely that they are also affected by reduced O_2 conditions. The magnitude of response however, is much lower.

4. CONCLUSION

Sediments are an important source of Fe, Co and Mn to OMZ waters in the Mauritanian shelf region. Remineralization and atmospheric deposition appear less important than benthic sources for dFe, with vertical fluxes exceeding atmospheric fluxes but gaining importance with distance from shelf. However, deposition of atmospheric dust is a source of Fe to sediments in our study region and consequently indirectly contributes to benthic released TMs. We showed that changes in O_2 concentrations from 30 to 50 µmol kg^{-1} had a substantial influence on dissolved and LpFe concentrations and to a lesser extent on Co and Mn concentrations by decreasing the sediment source strength. The presence of a large part of sediment-derived Fe in the leachable particulate phase highlights the importance of offshore particle transport on the Fe inventory, including the dissolved form by reversible scavenging. To our knowledge, this is the first field study that demonstrated strong short-term variability in redox-sensitive TMs over a few days to be directly linked to changes in O_2. These findings demonstrate that projected long-term changes in oceanic O_2 concentrations will impact biogeochemical cycles and have important implications for global TM distributions and their process parameterisations in biogeochemical models. Current models do not account for small changes in O_2 on TM distributions and benthic TM fluxes. Determining the processes involved and quantifying the effect of O_2 will be crucial for the implementation into current modeling approaches. Not all processes could be resolved in this study, including the influence of the residence time of the water masses on the shelf compared to the direct influence of O_2, and it is unclear whether the changes observed on a small scale are readily transferable to a global scale. Therefore, we suggest further investigations on short-term variability of O_2 and particle load in the Mauritanian and other dynamic OMZs including

water column TM measurement in combination with benthic TM fluxes and more detailed analysis of amount and types/composition of present particles.

Data availability. The CTD sensor and nutrient bottle data are freely available at https://doi.pangaea.de/10.1594/PANGAEA.860480 and https://doi.pangaea.de/10.1594/PANGAEA.885109 respectively. According to the SFB754 data policy (https://www.sfb754.de/de/data, all remaining data (trace metal data set) associated with this manuscript will be published at PANGEA (www.pangea.de, search projects:sfb754) upon publication of this manuscript.

Author contributions. IR analyzed the trace metal concentrations and drafted the manuscript. EPA and MG designed the project and CS carried out the trace metal sampling at sea. J-LMB oversaw, and BW carried out, the aluminium sample analysis. MD carried out the microstructure measurements at sea, oversaw the calculation of the vertical flux estimates and contributed to the writing of the manuscript. JL carried out the processing of microstructure data and calculation of the eddy diffusivity. JS, BG and PR carried out the radium isotope analysis and their interpretation. IR and MG oversaw, and Fabian Wolf carried out, the iodide analysis. All co-authors commented on the manuscript.

Competing interests. The authors declare that they have no conflict of interest.

Acknowledgements. The authors would like to thank the captain and the crew from RV Meteor and chief scientist Dr. Stefan Sommer from the M107 cruise. This work was funded by the Deutsche Forschungsgemeinschaft as part of Sonderforschungsbereich (SFB) 754: 'Climate-Biogeochemistry Interactions in the Tropical Ocean'. Fabian Wolf is thanked for carrying out the analysis of iodide and Peter Streu for help with the general lab work. The International Atomic Energy Agency is grateful to the Government of the Principality of Monaco for the support provided to its Environment Laboratories. Analyses and visualizations of aerosol optical depth (Supplementary Material) were produced with the Giovanni online data system, developed and maintained by the NASA GES DISC.

REFERENCES

Abadie, C., Lacan, F., Radic, A., Pradoux, C., and Poitrasson, F.: Iron isotopes reveal distinct dissolved iron sources and pathways in the intermediate versus deep Southern Ocean, P Natl Acad Sci USA, 114, 858-863, https://doi.org/10.1073/pnas.1603107114, 2017.

Achterberg, E. P., Steigenberger, S., Marsay, C. M., LeMoigne, F. A. C., Painter, S. C., Baker, A. R., Connelly, D. P., Moore, C. M., Tagliabue, A., and Tanhua, T.: Iron Biogeochemistry in the High Latitude North Atlantic Ocean, Sci Rep, 8, https://doi.org/10.1038/s41598-018-19472-1, 2018.

Baars, O., and Croot, P. L.: Dissolved cobalt speciation and reactivity in the eastern tropical North Atlantic, Mar. Chem., 173, 310-319, https://doi.org/10.1016/j.marchem.2014.10.006, 2015.

~~Baker, A. R., Jickells, T. D., Witt, M., and Linge, K. L.: Trends in the solubility of iron, aluminium, manganese and phosphorus in aerosol collected over the Atlantic Ocean, Mar Chem, 98, 43-58, https://doi.org/10.1016/j.marchem.2005.06.004, 2006.~~

Baker, A. R., Adams, C., Bell, T. G., Jickells, T. D., and Ganzeveld, L.: Estimation of atmospheric nutrient inputs to the Atlantic Ocean from 50°N to 50°S based on large-scale field sampling: Iron and other dust-associated elements, Global Biogeochem Cy, 27, 755-767, https://doi.org/10.1002/gbc.20062, 2013.

Balistrieri, L., Brewer, P. G., and Murray, J. W.: Scavenging residence times of trace metals and surface chemistry of sinking particles in the deep ocean, Deep Sea Res Part A. Oceanogr Res Pap, 28(2), 101-121, https://doi.org/10.1016/0198-0149(81)90085-6, 1981.

Barton, E. D.: The Poleward Undercurrent On The Eastern Boundary Of The Subtropical North Atlantic. In: Poleward Flows Along Eastern Ocean Boundaries, Neshyba, S. J., Mooers, C. N. K., Smith, R. L., and Barber, R. T. (Eds.), Springer-Verlag, New York, https://doi.org/10.1029/CE034p0082, 1989.

Barton, E. D., Aristegui, J., Tett, P., Canton, M., Garcia-Braun, J., Hernandez-Leon, S., Nykjaer, L., Almeida, C., Almunia, J., Ballesteros, S., Basterretxea, G., Escanez, J., Garcia-Weill, L., Hernandez-Guerra, A., Lopez-Laatzen, F., Molina, R., Montero, M. F., Navarro-Perez, E., Rodriguez, J. M., van Lenning, K., Velez, H., and Wild, K.: The transition zone of the Canary Current upwelling region, Prog Oceanogr, 41, 455-504, https://doi.org/ 10.1016/S0079-6611(98)00023-8, 1998.

Beck, A. J., Tsukamoto, Y., Tovar-Sanchez, A., Huerta-Diaz, M., Bokuniewicz, H. J., and Sanudo-Wilhelmy, S. A.: Importance of geochemical transformations in determining submarine groundwater discharge-derived trace metal and nutrient fluxes, Appl Geochem, 22, 477-490, https://doi.org/ 10.1016/j.apgeochem.2006.10.005, 2007.

Biller, D. V. and Bruland, K. W.: Sources and distributions of Mn, Fe, Co, Ni, Cu, Zn, and Cd relative to macronutrients along the central California coast during the spring and summer upwelling season, Mar Chem, 155, 50-70, https://doi.org/ 10.1016/j.marchem.2013.06.003, 2013.

Boyd, P. W.: Biogeochemistry - Iron findings, Nature, 446, 989-991, https://doi.org/ 10.1038/446989a, 2007.

Boyle, E. A., Lee, J.-M., Echegoyen, Y., Noble, A., Moos, S., Carrasco, G., Zhao, N., Kayser, R., Zhang, J., and Gamo, T.: Anthropogenic lead emissions in the ocean: The evolving global experiment, Oceanography, 27, 69-75, https://doi.org/10.5670/oceanog.2014.10, 2014.

Brandt, P., Bange, H. W., Banyte, D., Dengler, M., Didwischus, S. H., Fischer, T., Greatbatch, R. J., Hahn, J., Kanzow, T., Karstensen, J., Krortzinger, A., Krahmann, G., Schmidtko, S., Stramma, L., Tanhua, T., and Visbeck, M.: On the role of circulation and mixing in the ventilation of

oxygen minimum zones with a focus on the eastern tropical North Atlantic, Biogeosciences, 12, 489-512, https://doi.org/10.5194/bg-12-489-2015, 2015.

Bridgestock, L., van de Flierdt, T. V., Rehkamper, M., Paul, M., Middag, R., Milne, A., Lohan, M. C., Baker, A. R., Chance, R., Khondoker, R., Strekopytov, S., Humphreys-Williams, E., Achterberg, E. P., Rijkenberg, M. J. A., Gerringa, L. J. A., and de Baar, H. J. W.: Return of naturally sourced Pb to Atlantic surface waters, Nat Commun, 7, 12921, https://doi.org/10.1038/ncomms12921, 2016.

Browning, T. J., Achterberg, E. P., Rapp, I., Engel, A., Bertrand, E. M., Tagliabue, A., and Moore, C. M.: Nutrient co-limitation at the boundary of an oceanic gyre, Nature, 551, 242-246, https://doi.org/10.1038/nature24063, 2017.

Bruland, K. W. and Lohan, M. C.: Controls of Trace Metals in Seawater. In: The Oceans and Marine Geochemistry, Elderfield, H. (Ed.), Treatise on Geochemistry, 6, Elsevier, Oxford, 2006.

Buck, C. S., Landing, W. M., Resing, J. A., and Measures, C. I.: The solubility and deposition of aerosol Fe and other trace elements in the North Atlantic Ocean: Observations from the A16N CLIVAR/CO2 repeat hydrography section, Mar Chem, 120, 57-70, https://doi.org/10.1016/j.marchem.2008.08.003, 2010.

Burdige, D. J.: The biogeochemistry of manganese and iron reduction in marine sediments, Earth-Sci Rev, 35, 249-284, https://doi.org/10.1016/0012-8252(93)90040-E, 1993.

Capet, X. J., Marchesiello, P., and McWilliams, J. C.: Upwelling response to coastal wind profiles, Geophys Res Lett, 31, L13311, https://doi.org/10.1029/2004GL020123, 2004.

Chaillou, G., Anschutz, P., Lavaux, G., Schafer, J., and Blanc, G.: The distribution of Mo, U, and Cd in relation to major redox species in muddy sediments of the Bay of Biscay, Mar Chem, 80, 41-59, https://doi.org/10.1016/S0304-4203(02)00097-X, 2002.

Charette, M. A., Morris, P. J., Henderson, P. B., and Moore, W. S.: Radium isotope distributions during the US GEOTRACES North Atlantic cruises, Mar Chem, 177, 184-195, https://doi.org/10.1016/j.marchem.2015.01.001, 2015.

Conway, T. M. and John, S. G.: Quantification of dissolved iron sources to the North Atlantic Ocean, Nature, 511, 212-215, https://doi.org/10.1038/nature13482, 2014.

Croot, P. L., Streu, P., and Baker, A. R.: Short residence time for iron in surface seawater impacted by atmospheric dry deposition from Saharan dust events, Geophys Res Lett, 31(23), https://doi.org/10.1029/2004GL020153, 2004.

Cyr, F., Bourgault, D., Galbraith, P. S., and Gosselin, M.: Turbulent nitrate fluxes in the Lower St. Lawrence Estuary, Canada, J Geophys Res-Oceans, 120, 2308-2330, https://doi.org/10.1002/2014jc010272, 2015.

Dale, A.W., Sommer, S., Ryabenko, E., Noffke, A., Bohlen, L., Wallmann, K., Stolpovsky, K., Greinert, J. and Pfannkuche, O.: Benthic nitrogen fluxes and fractionation of nitrate in the

Mauritanian oxygen minimum zone (Eastern Tropical North Atlantic), Geochim Cosmochim Acta, 134 (0), 234–256, https://doi.org/10.1016/j.gca.2014.02.026, 2014.

Dammshäuser, A., Wagener, T., and Croot, P. L.: Surface water dissolved aluminum and titanium: Tracers for specific time scales of dust deposition to the Atlantic?, Geophys Res Lett, 38, L24601, https://doi.org/10.1029/2011gl049847, 2011.

Desbiolles, F., Blanke, B., and Bentamy, A.: Short-term upwelling events at the western African coast related to synoptic atmospheric structures as derived from satellite observations, J Geophys Res-Oceans, 119, 461-483, https://doi.org/10.1002/2013JC009278, 2014.

Desbiolles, F., Blanke, B., Bentamy, A., and Roy, C.: Response of the Southern Benguela upwelling system to fine-scale modifications of the coastal wind, J Mar Syst, 156, 46-55, https://doi.org/10.1016/j.jmarsys.2015.12.002, 2016.

Elrod, V. A., Berelson, W. M., Coale, K. H., and Johnson, K. S.: The flux of iron from continental shelf sediments: A missing source for global budgets, Geophys Res Lett, 31, L12307, https://doi.org/10.1029/2004gl020216, 2004.

Eriksen, C. C.: Observations of internal wave reflection off sloping bottoms, J Geophys Res-Oceans, 87, 525-538, https://doi.org/10.1029/JC087iC01p00525, 1982.

Fairall, C.W., Bradley, E.F., Hare, J.E., Grachev, A.A., and Edson, J.B.: Bulk Parameterization of Air–Sea Fluxes: Updates and Verification for the COARE Algorithm, J Climate, 16, 571–591, https://doi.org/10.1175/1520-0442(2003)016<0571:BPOASF>2.0.CO;2, 2003.

Fitzsimmons, J. N., Zhang, R. F., and Boyle, E. A.: Dissolved iron in the tropical North Atlantic Ocean, Mar Chem, 154, 87-99, https://doi.org/10.1016/j.marchem.2013.05.009, 2013.

Fitzsimmons, J. N., John, S. G., Marsay, C. M., Hoffman, C. L., Nicholas, S. L., Toner, B. M., German, C. R., and Sherrell, R. M.: Iron persistence in a distal hydrothermal plume supported by dissolved-particulate exchange, Nat Geosci, 10, 195-201, https://doi.org/10.1038/Ngeo2900, 2017.

Froelich, P. N., Klinkhammer, G. P., Bender, M. L., Luedtke, N. A., Heath, G. R., Cullen, D., Dauphin, P., Hammond, D., Hartman, B., and Maynard, V.: Early oxidation of organic matter in pelagic sediments of the Eastern Equatorial Atlantic: suboxic diagenesis, Geochim Cosmochim Ac, 43, 1075-1090, https://doi.org/10.1016/0016-7037(79)90095-4, 1979.

Garcia-Solsona, E., Garcia-Orellana, J., Masqué, P., and Dulaiova, H.: Uncertainties associated with ^{223}Ra and ^{224}Ra measurements in water via a Delayed Coincidence Counter (RaDeCC), Mar Chem, 109, 198-219, https://doi.org/10.1016/j.marchem.2007.11.006, 2008.

Gehlen, M., Beck, L., Calas, G., Flank, A. M., Van Bennekom, A. J., and Van Beusekom, J. E. E.: Unraveling the atomic structure of biogenic silica: Evidence of the structural association of Al and Si in diatom frustules, Geochim Cosmochim Ac, 66, 1601-1609, https://doi.org/10.1016/S0016-7037(01)00877-8, 2002.

Gill, A.: Atmosphere-Ocean Dynamics, Academic Press, California, 1982.

Grasshoff, K., Ehrhardt, M., and Kremling, K.: Methods of Seawater Analysis, Verlag Chemie, Weinheim, 1983.

Green, M. A., Aller, R. C., Cochran, J. K., Lee, C., and Aller, J. Y.: Bioturbation in shelf/slope sediments off Cape Hatteras, North Carolina: the use of ^{234}Th, Chl-*a*, and Br^- to evaluate rates of particle and solute transport, Deep-Sea Res Pt II, 49, 4627-4644, https://doi.org/10.1016/S0967-0645(02)00132-7, 2002.

Hahn, J., Brandt, P., Schmidtko, S., and Krahmann, G.: Decadal oxygen change in the eastern tropical North Atlantic, Ocean Sci, 13, 551-576, https://doi.org/10.5194/os-13-551-2017, 2017.

Hansen, H. P.: Determination of oxygen, Methods of Seawater Analysis, Third Edition, 2007. 75-89, 2007.

Hartmann, M., Müller, P.J., Suess, E., and van der Weijden, C.H.: Chemistry of Late Quaternary sediments and their interstitial waters of sediment cores from the North-West African continental margin, in Supplement to: Hartmann, M et al. (1976): Chemistry of Late Quaternary sediments and their interstitial waters from the northwest African continental margin. Meteor Forschungsergebnisse, Deutsche Forschungsgemeinschaft, Reihe C Geologie und Geophysik, Gebrüder Bornträger, Berlin, Stuttgart, C24, 1-67, edited, PANGAEA, 1976.

Hatta, M., Measures, C. I., Wu, J. F., Roshan, S., Fitzsimmons, J. N., Sedwick, P., and Morton, P.: An overview of dissolved Fe and Mn distributions during the 2010-2011 US GEOTRACES north Atlantic cruises: GEOTRACES GA03, Deep-Sea Res Pt II, 116, 117-129, https://doi.org/10.1016/j.dsr2.2014.07.005, 2015.

Hayes, S. P., Chang, P., and McPhaden, M. J.: Variability of the sea surface temperature in the eastern equatorial Pacific during 1986–1988, J Geophys Res, 96, 10553-10566, https://doi.org/10.1029/91JC00942, 1991.

Hawco, N. J., Ohnemus, D. C., Resing, J. A., Twining, B. S., and Saito, M. A.: A dissolved cobalt plume in the oxygen minimum zone of the eastern tropical South Pacific, Biogeosciences, 13, 5697-5717, https://doi.org/10.5194/bg-13-5697-2016, 2016.

Heggie, D. T.: Copper in Surface Waters of the Bering Sea, Geochim Cosmochim Ac, 46, 1301-1306, https://doi.org/10.1016/0016-7037(82)90014-X, 1982.

Helly, J. J. and Levin, L. A.: Global distribution of naturally occurring marine hypoxia on continental margins, Deep-Sea Res Pt I, 51, 1159-1168, https://doi.org/ 10.1016/j.dsr.2004.03.009, 2004.

Henderson, P., Morris, P., Moore, W., and Charette, M.: Methodological advances for measuring low-level radium isotopes in seawater, J Radioanal Nucl Ch, 296, 357-362, https://doi.org/10.1007/s10967-012-2047-9, 2013.

Homoky, W. B., Severmann, S., McManus, J., Berelson, W. M., Riedel, T. E., Statham, P. J., and Mills, R. A.: Dissolved oxygen and suspended particles regulate the benthic flux of iron from continental margins, Mar Chem, 134, 59-70, https://doi.org/10.1016/j.marchem.2012.03.003, 2012.

Homoky, W. B., Weber, T., Berelson, W. M., Conway, T. M., Henderson, G. M., van Hulten, M., Jeandel, C., Severmann, S., and Tagliabue, A.: Quantifying trace element and isotope fluxes at the ocean-sediment boundary: a review, Philos T R Soc A, 374, 20160246, https://doi.org/10.1098/rsta.2016.0246, 2016.

Honeyman, B. D., Balistrieri, L. S., and Murray, J. W.: Oceanic trace metal scavenging: the importance of particle concentration. Deep Sea Res Part A. Oceanogr Res Pap, 35(2), 227-246, https://doi.org/10.1016/0198-0149(88)90038-6, 1988.

Hurst, M. P., Aguilar-Islas, A. M., and Bruland, K. W.: Iron in the southeastern Bering Sea: Elevated leachable particulate Fe in shelf bottom waters as an important source for surface waters, Cont Shelf Res, 30, 467-480, https://doi.org/10.1016/j.csr.2010.01.001, 2010.

Hydes, D. J. and Liss, P. S.: Fluorimetric method for determination of low concentrations of dissolved aluminum in natural waters, Analyst, 101, 922-931, https://doi.org/10.1039/an9760100922, 1976.

Jickells, T. D.: The inputs of dust derived elements to the Sargasso Sea; a synthesis, Mar Chem, 68(1-2), 5-14, https://doi.org/10.1016/S0304-4203(99)00061-4, 1999.

John, S. G. and Adkins, J.: The vertical distribution of iron stable isotopes in the North Atlantic near Bermuda, Global Biogeochem Cy, 26, GB2034, https://doi.org/10.1029/2011gb004043, 2012.

Johnson, K. S., Stout, P. M., Berelson, W. M., and Sakamotoarnold, C. M.: Cobalt and copper distributions in the waters of Santa-Monica Basin, California, Nature, 332, 527-530, https://doi.org/10.1038/332527a0, 1988.

Kagaya, S., Maeba, E., Inoue, Y., Kamichatani, W., Kajiwara, T., Yanai, H., Saito, M., and Tohda, K.: A solid phase extraction using a chelate resin immobilizing carboxymethylated pentaethylenehexamine for separation and preconcentration of trace elements in water samples, Talanta, 79, 146-152, https://doi.org/10.1016/j.talanta.2009.03.016, 2009.

Karstensen, J., Stramma, L., and Visbeck, M.: Oxygen minimum zones in the eastern tropical Atlantic and Pacific oceans, Prog Oceanogr, 77, 331-350, https://doi.org/10.1016/j.pocean.2007.05.009, 2008.

Klenz, T., Dengler, M., and Brandt, P.: Seasonal variability of the Mauritanian Undercurrent and Hydrography at 18°N, J Geophys Res: Oceans, ~~in press~~123, 8122-8137, https://doi.org/10.1029/2018JC014264, 2018.

Kock, A., Schafstall, J., Dengler, M., Brandt, P., and Bange, H. W.: Sea-to-air and diapycnal nitrous oxide fluxes in the eastern tropical North Atlantic Ocean, Biogeosciences, 9, 957-964, https://doi.org/10.5194/bg-9-957-2012, 2012.

Köllner, M., Visbeck, M., Tanhua, T., and Fischer, T.: Diapycnal diffusivity in the core and oxycline of the tropical North Atlantic oxygen minimum zone, J Marine Syst, 160, 54-63, https://doi.org/10.1016/j.jmarsys.2016.03.012, 2016.

Kounta, L., Capet, X., Jouanno, J., Kolodziejczyk, N., Sow, B., and Gaye, A. T.: A model perspective on the dynamics of the shadow zone of the eastern tropical North Atlantic – Part 1: the poleward slope currents along West Africa, Ocean Sci, 14, 971-997, https://doi.org/10.5194/os-14-971-2018, 2018.

Labatut, M., Lacan, F., Pradoux, C., Chmeleff, J., Radic, A., Murray, J. W., Poitrasson, F., Johansen, A. M., and Thil, F.: Iron sources and dissolved-particulate interactions in the seawater of the Western Equatorial Pacific, iron isotope perspectives, Global Biogeochem Cy, 28, 1044-1065, https://doi.org/10.1002/2014gb004928, 2014.

Lam, P. J. and Bishop, J. K. B.: The continental margin is a key source of iron to the HNLC North Pacific Ocean, Geophys Res Lett, 35, L07608, https://doi.org/10.1029/2008gl033294, 2008.

Lam, P. J., Ohnemus, D. C., and Marcus, M. A.: The speciation of marine particulate iron adjacent to active and passive continental margins, Geochim Cosmochim Ac, 80, 108-124, https://doi.org/10.1016/j.gca.2011.11.044, 2012.

Lathuilière, C., Echevin, V., and Lévy, M.: Seasonal and intraseasonal surface chlorophyll-a variability along the northwest African coast, J Geophys Res, 113, C05007, https://doi.org/10.1029/2007JC004433, 2008.

Liu, X. W. and Millero, F. J.: The solubility of iron in seawater, Mar Chem, 77, 43-54, https://doi.org/10.1016/S0304-4203(01)00074-3, 2002.

Lohan, M. C. and Bruland, K. W.: Elevated Fe(II) and dissolved Fe in hypoxic shelf waters off Oregon and Washington: An enhanced source of iron to coastal upwelling regimes, Environ Sci Technol, 42, 6462-6468, https://doi.org/10.1021/es800144j, 2008.

Luther, G. W., Swartz, C. B., and Ullman, W. J.: Direct determination of iodide in seawater by Cathodic Stripping Square-Wave Voltammetry, Anal Chem, 60, 1721-1724, https://doi.org/10.1021/ac00168a017, 1988.

Mahowald, N. M., Engelstaedter, S., Luo, C., Sealy, A., Artaxo, P., Benitez-Nelson, C., Bonnet, S., Chen, Y., Chuang, P. Y., Cohen, D. D., Dulac, F., Herut, B., Johansen, A. M., Kubilay, N., Losno, R., Maenhaut, W., Paytan, A., Prospero, J. A., Shank, L. M., and Siefert, R. L.: Atmospheric Iron Deposition: Global Distribution, Variability, and Human Perturbations, Annu Rev Mar Sci, 1, 245-278, https://doi.org/10.1146/annurev.marine.010908.163727, 2009.

Martin, J. H., Gordon, R. M., Fitzwater, S., and Broenkow, W. W.: Vertex - Phytoplankton Iron Studies in the Gulf of Alaska, Deep-Sea Res, 36, 649-680, https://doi.org/10.1016/0198-0149(89)90144-1, 1989.

Mawji, E. and Schlitzer, R. and Dodas, E. M. and Abadie, C. and Abouchami, W. and Anderson, R. F. and Baars, O. and Bakker, K. and Baskaran, M. and Bates, N. R. and Bluhm, K. and Bowie, A. and Bown, J. and Boye, M. and Boyle, E. A. and Branellec, P. and Bruland, K. W. and Brzezinski, M. A. and Bucciarelli, E. and Buesseler, K. and Butler, E. and Cai, P. H. and Cardinal, D. and Casciotti, K. and Chaves, J. and Cheng, H. and Chever, F. and Church, T. M.

and Colman, A. S. and Conway, T. M. and Croot, P. L. and Cutter, G. A. and de Baar, H. J. W. and de Souza, G. F. and Dehairs, F. and Deng, F. F. and Dieu, H. T. and Dulaquais, G. and Echegoyen-Sanz, Y. and Edwards, R. L. and Fahrbach, E. and Fitzsimmons, J. and Fleisher, M. and Frank, M. and Friedrich, J. and Fripiat, F. and Galer, S. J. G. and Gamo, T. and Solsona, E. G. and Gerringa, L. J. A. and Godoy, J. M. and Gonzalez, S. and Grossteffan, E. and Hatta, M. and Hayes, C. T. and Heller, M. I. and Henderson, G. and Huang, K. F. and Jeandel, C. and Jenkins, W. J. and John, S. and Kenna, T. C. and Klunder, M. and Kretschmer, S. and Kumamoto, Y. and Laan, P. and Labatut, M. and Lacan, F. and Lam, P. J. and Lannuzel, D. and le Moigne, F. and Lechtenfeld, O. J. and Lohan, M. C. and Lu, Y. B. and Masque, P. and McClain, C. R. and Measures, C. and Middag, R. and Moffett, J. and Navidad, A. and Nishioka, J. and Noble, A. and Obata, H. and Ohnemus, D. C. and Owens, S. and Planchon, F. and Pradoux, C. and Puigcorbe, V. and Quay, P. and Radic, A. and Rehkamper, M. and Remenyi, T. and Rijkenberg, M. J. A. and Rintoul, S. and Robinson, L. F. and Roeske, T. and Rosenberg, M. and van der Loeff, M. R. and Ryabenko, E. and Saito, M. A. and Roshan, S. and Salt, L. and Sarthou, G. and Schauer, U. and Scott, P. and Sedwick, P. N. and Sha, L. J. and Shiller, A. M. and Sigman, D. M. and Smethie, W. and Smith, G. J. and Sohrin, Y. and Speich, S. and Stichel, T. and Stutsman, J. and Swift, J. H. and Tagliabue, A. and Thomas, A. and Tsunogai, U. and Twining, B. S. and van Aken, H. M. and van Heuven, S. and van Ooijen, J. and van Weerlee, E. and Venchiarutti, C. and Voelker, A. H. L. and Wake, B. and Warner, M. J. and Woodward, E. M. S. and Wu, J. F. and Wyatt, N. and Yoshikawa, H. and Zheng, X. Y. and Xue, Z. C. and Zieringer, M. and Zimmer, L. A.: The GEOTRACES Intermediate Data Product 2014, Mar Chem, 177, 1-8, https://doi.org/10.1016/j.marchem.2015.04.005, 2015.

~~McLennan, S. M.: Relationships between the trace element composition of sedimentary rocks and upper continental crust, Geochem Geophy Geosy, 2, 1021, https://doi.org/10.1029/2000GC000109, 2001.~~

Measures, C. I. and Brown, E. T.: Estimating dust input to the Atlantic Ocean using surface water aluminium concentrations. In: The impact of desert dust across the Mediterranean, Guerzoni, S. and Chester, R. (Eds.), Environmental Science and Technology Library, Springer, Dordrecht, 1996.

Measures, C. I. and Vink, S.: On the use of dissolved aluminum in surface waters to estimate dust deposition to the ocean, Global Biogeochem Cy, 14, 317-327, https://doi.org/10.1029/1999gb001188, 2000.

Menzel Barraqueta, J.-L., Schlosser, C., Planquette, H., Gourain, A., Cheize, M., Boutorh, J., Shelley, R., Pereira, L. C., Gledhill, M., Hopwood, M. J., Lacan, F., Lherminier, P., Sarthou, G., and Achterberg, E. P.: Aluminium in the North Atlantic Ocean and the Labrador Sea

(GEOTRACES GA01 section): roles of continental inputs and biogenic particle removal, Biogeosciences, 15, 5271-5286, https://doi.org/10.5194/bg-15-5271-2018, 2018.

Menzel Barraqueta, J.-L., Klar, J. K., Gledhill, M., Schlosser, C., Shelley, R., Planquette, H. F., Wenzel, B., Sarthou, G., and Achterberg, E. P.: Atmospheric deposition fluxes over the Atlantic Ocean: a GEOTRACES case study, Biogeosciences, 16, 1525-1542, https://doi.org/10.5194/bg-16-1525-2019, 2019.

Middag, R., de Baar, H. J. W., Laan, P., and Huhn, O.: The effects of continental margins and water mass circulation on the distribution of dissolved aluminum and manganese in Drake Passage, J Geophys Res-Oceans, 117, C01019, https://doi.org/10.1029/2011jc007434, 2012.

Milne, A., Schlosser, C., Wake, B. D., Achterberg, E. P., Chance, R., Baker, A. R., Forryan, A., and Lohan, M. C.: Particulate phases are key in controlling dissolved iron concentrations in the (sub)tropical North Atlantic, Geophys Res Lett, 44, 2377-2387, https://doi.org/10.1002/2016gl072314, 2017.

Mittelstaedt, E.: The upwelling area off Northwest Africa—A description of phenomena related to coastal upwelling, Prog Oceanogr, 12, 307-331, https://doi.org/10.1016/0079-6611(83)90012-5, 1983.

Mittelstaedt, E.: The ocean boundary along the northwest African coast: Circulation and oceanographic properties at the sea-surface, Prog Oceanogr, 26, 307-355, https://doi.org/10.1016/0079-6611(91)90011-A, 1991.

Moffett, J. W.: The Relationship between cerium and manganese oxidation in the marine environment, Limnol Oceanogr, 39, 1309-1318, https://doi.org/10.4319/lo.1994.39.6.1309, 1994.

Moffett, J. W. and Ho, J.: Oxidation of cobalt and manganese in seawater via a common microbially catalyzed pathway, Geochim Cosmochim Ac, 60, 3415-3424, https://doi.org/10.1016/0016-7037(96)00176-7, 1996.

Moffett, J. W. and Zika, R. G.: Reaction kinetics of hydrogen peroxide with copper and iron in seawater, Environ Sci Technol, 21, 804-810, https://doi.org/10.1021/es00162a012, 1987.

Moffett, J. W., Vedamati, J., Goepfert, T. J., Pratihary, A., Gauns, M., and Naqvi, S. W. A.: Biogeochemistry of iron in the Arabian Sea, Limnol Oceanogr, 60, 1671-1688, https://doi.org/10.1002/lno.10132, 2015.

Moore, C. M., Mills, M. M., Achterberg, E. P., Geider, R. J., LaRoche, J., Lucas, M. I., McDonagh, E. L., Pan, X., Poulton, A. J., Rijkenberg, M. J. A., Suggett, D. J., Ussher, S. J., and Woodward, E. M. S.: Large-scale distribution of Atlantic nitrogen fixation controlled by iron availability, Nat Geosci, 2, 867-871, https://doi.org/10.1038/ngeo667, 2009.

Moore, C. M., Mills, M. M., Arrigo, K. R., Berman-Frank, I., Bopp, L., Boyd, P. W., Galbraith, E. D., Geider, R. J., Guieu, C., Jaccard, S. L., Jickells, T. D., La Roche, J., Lenton, T. M., Mahowald, N. M., Maranon, E., Marinov, I., Moore, J. K., Nakatsuka, T., Oschlies, A., Saito, M. A.,

Thingstad, T. F., Tsuda, A., and Ulloa, O.: Processes and patterns of oceanic nutrient limitation, Nat Geosci, 6, 701-710, https://doi.org/10.1038/Ngeo1765, 2013.

Moore, W. S.: ^{228}Ra in the South-Atlantic Bight, J Geophys Res-Oceans, 92, 5177-5190, https://doi.org/10.1029/JC092iC05p05177, 1987.

Moore, W. S.: Ages of continental shelf waters determined from ^{223}Ra and ^{224}Ra, J Geophys Res-Oceans, 105, 22117-22122, https://doi.org/10.1029/1999jc000289, 2000.

Moore, W. S.: Seasonal distribution and flux of radium isotopes on the southeastern U.S. continental shelf, J Geophys Res, 112, C10013, https://doi.org/10.1029/2007JC004199, 2007.

Moore, W. S. and Arnold, R.: Measurement of ^{223}Ra and ^{224}Ra in coastal waters using a delayed coincidence counter, J Geophys Res, 101, 1321-1329, https://doi.org/10.1029/95jc03139, 1996.

Moore, W. S. and Cai, P.: Calibration of RaDeCC systems for ^{223}Ra measurements, Mar Chem, 156, 130-137, https://doi.org/10.1016/j.marchem.2013.03.002, 2013.

Moran, S. B. and Moore, R. M.: The potential source of dissolved aluminum from resuspended sediments to the North Atlantic Deep Water, Geochim Cosmochim Ac, 55, 2745-2751, https://doi.org/10.1016/0016-7037(91)90441-7, 1991.

Morel, F. M. M. and Price, N. M.: The biogeochemical cycles of trace metals in the oceans, Science, 300, 944-947, https://doi.org/10.1126/science.1083545, 2003.

Naykki, T., Virtanen, A., Kaukonen, L., Magnusson, B., Vaisanen, T., and Leito, I.: Application of the Nordtest method for "real-time" uncertainty estimation of on-line field measurement, Environ Monit Assess, 187, 360, https://doi.org/10.1007/s10661-015-4856-0, 2015.

Ndoye, S., Capet, X., Estrade, P., Sow, B., Dagorne, D., Lazar, A., Gaye, A., and Brehmer, P.: SST patterns and dynamics of the southern Senegal-Gambia upwelling center, J Geophys Res Oceans, 119, 8315-8335, https://doi.org/10.1002/2014JC010242, 2014.

Noble, A. E., Lamborg, C. H., Ohnemus, D. C., Lam, P. J., Goepfert, T. J., Measures, C. I., Frame, C. H., Casciotti, K. L., DiTullio, G. R., Jennings, J., and Saito, M. A.: Basin-scale inputs of cobalt, iron, and manganese from the Benguela-Angola front to the South Atlantic Ocean, Limnol Oceanogr, 57, 989-1010, https://doi.org/10.4319/lo.2012.57.4.0989, 2012.

Noble, A. E., Echegoyen-Sanz, Y., Boyle, E. A., Ohnemus, D. C., Lam, P. J., Kayser, R., Reuer, M., Wu, J. F., and Smethie, W.: Dynamic variability of dissolved Pb and Pb isotope composition from the US North Atlantic GEOTRACES transect, Deep-Sea Res Pt II, 116, 208-225, https://doi.org/10.1016/j.dsr2.2014.11.011, 2015.

Noble, A. E., Ohnemus, D. C., Hawco, N. J., Lam, P. J., and Saito, M. A.: Coastal sources, sinks and strong organic complexation of dissolved cobalt within the US North Atlantic GEOTRACES transect GA03, Biogeosciences, 14, 2715-2739, https://doi.org/10.5194/bg-14-2715-2017, 2017.

Noffke, A., Hensen, C., Sommer, S., Scholz, F., Bohlen, L., Mosch, T., Graco, M., and Wallmann, K.: Benthic iron and phosphorus fluxes across the Peruvian oxygen minimum zone, Limnol Oceanogr, 57, 851-867, https://doi.org/10.4319/lo.2012.57.3.0851, 2012.

Nriagu, J. O. and Pacyna, J. M.: Quantitative assessment of worldwide contamination of air, water and soils by trace metals, Nature, 333, 134-139, https://doi.org/10.1038/333134a0, 1988.

Nychka, D., Furrer, R., Paige, J., and Sain, S.: fields: Tools for Spatial Data, R package version 8.3-6, https://CRAN.R-project.org/package=fields, 2016.

Oksanen, J., Blanchet, F. G., Friendly, M., Kindt, R., Legendre, P., McGlinn, D., Minchin, P., B. O'Hara, R., Simpson, G., Solymos, P., Stevens, H., Szöcs, E., and Wagner, H.: vegan: Community Ecology Package. Ordination methods, diversity analysis and other functions for community and vegetation ecologists, version 2.4-4, https://CRAN.R-project.org/package=vegan, 2017.

Oldham, V. E., Jones, M. R., Tebo, B. M., and Luther, G. W.: Oxidative and reductive processes contributing to manganese cycling at oxic-anoxic interfaces, Mar Chem, 195, 122-128, https://doi.org/10.1016/j.marchem.2017.06.002, 2017.

Orians, K. J. and Bruland, K. W.: Dissolved aluminum in the Central North Pacific, Nature, 316, 427-429, https://doi.org/10.1038/316427a0, 1985.

Orians, K. J. and Bruland, K. W.: The biogeochemistry of aluminum in the Pacific Ocean, Earth Planet Sc Lett, 78, 397-410, https://doi.org/10.1016/0012-821x(86)90006-3, 1986.

Osborn, T. R.: Estimates of the local rate of vertical diffusion from dissipation measurements, J Phys Oceanogr, 10, 83-89, https://doi.org/ 10.1175/1520-0485(1980)010<0083:Eotlro>2.0.Co;2, 1980.

Parker, D. L., Morita, T., Mozafarzadeh, M. L., Verity, R., McCarthy, J. K., and Tebo, B. M.: Inter-relationships of MnO_2 precipitation, siderophore-Mn(III) complex formation, siderophore degradation, and iron limitation in Mn(II)-oxidizing bacterial cultures, Geochim Cosmochim Ac, 71, 5672-5683, https://doi.org/10.1016/j.gca.2007.03.042, 2007.

Patey, M. D., Achterberg, E. P., Rijkenberg, M. J., and Pearce, R.: Aerosol time-series measurements over the tropical Northeast Atlantic Ocean: Dust sources, elemental composition and mineralogy, Mar Chem, 174, 103-119, https://doi.org/10.1016/j.marchem.2015.06.004, 2015.

Peña-Izquierdo, J., van Sebille, E., Pelegri, J. L., Sprintall, J., Mason, E., Llanillo, P. J., and Machin, F.: Water mass pathways to the North Atlantic oxygen minimum zone, J Geophys Res-Oceans, 120, 3350-3372, https://doi.org/10.1002/2014jc010557, 2015.

Rama and Moore, W. S.: Using the radium quartet for evaluating groundwater input and water exchange in salt marshes, Geochim Cosmochim Ac, 60, 4645-4652, https://doi.org/10.1016/S0016-7037(96)00289-X, 1996.

Rapp, I., Schlosser, C., Rusiecka, D., Gledhill, M., and Achterberg, E. P.: Automated preconcentration of Fe, Zn, Cu, Ni, Cd, Pb, Co, and Mn in seawater with analysis using high-resolution sector

field inductively-coupled plasma mass spectrometry, Anal Chim Acta, 976, 1-13, https://doi.org/10.1016/j.aca.2017.05.008, 2017.

Rhein, M., Dengler, M., Sültenfuß, J., Hummels, R., Hüttl-Kabus, S., and Bourles, B.: Upwelling and associated heat flux in the equatorial Atlantic inferred from helium isotope disequilibrium, J Geophys Res, 115, C08021, https://doi.org/10.1029/2009JC005772, 2010.

Ricciardulli, L. and Wentz, F. J.: Remote Sensing Systems ASCAT C-2015 Daily Ocean Vector Winds on 0.25 deg grid, Version 02.1. Santa Rosa, CA: Remote Sensing Systems. Available at www.remss.com/missions/ascat, 2016.

Rijkenberg, M. J. A., Steigenberger, S., Powell, C. F., van Haren, H., Patey, M. D., Baker, A. R., and Achterberg, E. P.: Fluxes and distribution of dissolved iron in the eastern (sub-) tropical North Atlantic Ocean, Global Biogeochem Cy, 26, GB3004, https://doi.org/10.1029/2011gb004264, 2012.

Rijkenberg, M. J. A., Middag, R., Laan, P., Gerringa, L. J. A., van Aken, H. M., Schoemann, V., de Jong, J. T. M., and de Baar, H. J. W.: The distribution of dissolved iron in the West Atlantic Ocean, Plos One, 9, e101323, https://doi.org/10.1371/journal.pone.0101323, 2014.

Rudnick, R. L. and Gao, S.: Composition of the continental crust. In: Treatise on geochemistry, Holland, H. D. and Turekian, K. K. (Eds.), Pergamon, Oxford, UK, 2006.

Rue, E. L., Smith, G. J., Cutter, G. A., and Bruland, K. W.: The response of trace element redox couples to suboxic conditions in the water column, Deep-Sea Res Pt I, 44, 113-134, https://doi.org/10.1016/S0967-0637(96)00088-X, 1997.

Rusiecka, D., Gledhill, M., Milne, A., Achterberg, E. P., Annett, A. L., Atkinson, S., Birchill, A., Karstensen, J., Lohan, M., Mariez, C., Middag, R., Rolison, J. M., Tanhua, T., Ussher, S., and Connelly, D.: Anthropogenic signatures of lead in the Northeast Atlantic, Geophys Res Lett, 45, 2734-2743, https://doi.org/10.1002/2017gl076825, 2018.

Saito, M. A., Goepfert, T. J., and Ritt, J. T.: Some thoughts on the concept of colimitation: Three definitions and the importance of bioavailability, Limnol Oceanogr, 53, 276-290, https://doi.org/10.4319/lo.2008.53.1.0276, 2008.

Saito, M. A., Noble, A. E., Hawco, N., Twining, B. S., Ohnemus, D. C., John, S. G., Lam, P., Conway, T. M., Johnson, R., Moran, D., and McIlvin, M.: The acceleration of dissolved cobalt's ecological stoichiometry due to biological uptake, remineralization, and scavenging in the Atlantic Ocean, Biogeosciences, 14, 4637-4662, https://doi.org/10.5194/bg-14-4637-2017, 2017.

Schafstall, J., Dengler, M., Brandt, P., and Bange, H.: Tidal-induced mixing and diapycnal nutrient fluxes in the Mauritanian upwelling region, J Geophys Res-Oceans, 115, C10014, https://doi.org/10.1029/2009jc005940, 2010.

Schlitzer, R. and Anderson, R. F. and Dodas, E. M. and Lohan, M. and Geibert, W. and Tagliabue, A. and Bowie, A. and Jeandel, C. and Maldonado, M. T. and Landing, W. M. and Cockwell, D.

and Abadie, C. and Abouchami, W. and Achterberg, E. P. and Agather, A. and Aguliar-Islas, A. and van Aken, H. M. and Andersen, M. and Archer, C. and Auro, M. and de Baar, H. J. and Baars, O. and Baker, A. R. and Bakker, K. and Basak, C. and Baskaran, M. and Bates, N. R. and Bauch, D. and van Beek, P. and Behrens, M. K. and Black, E. and Bluhm, K. and Bopp, L. and Bouman, H. and Bowman, K. and Bown, J. and Boyd, P. and Boye, M. and Boyle, E. A. and Branellec, P. and Bridgestock, L. and Brissebrat, G. and Browning, T. and Bruland, K. W. and Brumsack, H.-J. and Brzezinski, M. and Buck, C. S. and Buck, K. N. and Buesseler, K. and Bull, A. and Butler, E. and Cai, P. and Mor, P. C. and Cardinal, D. and Carlson, C. and Carrasco, G. and Casacuberta, N. and Casciotti, K. L. and Castrillejo, M. and Chamizo, E. and Chance, R. and Charette, M. A. and Chaves, J. E. and Cheng, H. and Chever, F. and Christl, M. and Church, T. M. and Closset, I. and Colman, A. and Conway, T. M. and Cossa, D. and Croot, P. and Cullen, J. T. and Cutter, G. A. and Daniels, C. and Dehairs, F. and Deng, F. and Dieu, H. T. and Duggan, B. and Dulaquais, G. and Dumousseaud, C. and Echegoyen-Sanz, Y. and Edwards, R. L. and Ellwood, M. and Fahrbach, E. and Fitzsimmons, J. N. and Russell Flegal, A. and Fleisher, M. Q. and van de Flierdt, T. and Frank, M. and Friedrich, J. and Fripiat, F. and Fröllje, H. and Galer, S. J. G. and Gamo, T. and Ganeshram, R. S. and Garcia-Orellana, J. and Garcia-Solsona, E. and Gault-Ringold, M. and George, E. and Gerringa, L. J. A. and Gilbert, M. and Godoy, J. M. and Goldstein, S. L. and Gonzalez, S. R. and Grissom, K. and Hammerschmidt, C. and Hartman, A. and Hassler, C. S. and Hathorne, E. C. and Hatta, M. and Hawco, N. and Hayes, C. T. and Heimbürger, L.-E. and Helgoe, J. and Heller, M. and Henderson, G. M. and Henderson, P. B. and van Heuven, S. and Ho, P. and Horner, T. J. and Hsieh, Y.-T. and Huang, K.-F. and Humphreys, M. P. and Isshiki, K. and Jacquot, J. E. and Janssen, D. J. and Jenkins, W. J. and John, S. and Jones, E. M. and Jones, J. L. and Kadko, D. C. and Kayser, R. and Kenna, T. C. and Khondoker, R. and Kim, T. and Kipp, L. and Klar, J. K. and Klunder, M. and Kretschmer, S. and Kumamoto, Y. and Laan, P. and Labatut, M. and Lacan, F. and Lam, P. J. and Lambelet, M. and Lamborg, C. H. and Le Moigne, F. A. C. and Le Roy, E. and Lechtenfeld, O. J. and Lee, J.-M. and Lherminier, P. and Little, S. and López-Lora, M. and Lu, Y. and Masque, P. and Mawji, E. and McClain, C. R. and Measures, C. and Mehic, S. and Barraqueta, J.-L. M. and van der Merwe, P. and Middag, R. and Mieruch, S. and Milne, A. and Minami, T. and Moffett, J. W. and Moncoiffe, G. and Moore, W. S. and Morris, P. J. and Morton, P. L. and Nakaguchi, Y. and Nakayama, N. and Niedermiller, J. and Nishioka, J. and Nishiuchi, A. and Noble, A. and Obata, H. and Ober, S. and Ohnemus, D. C. and van Ooijen, J. and O'Sullivan, J. and Owens, S. and Pahnke, K. and Paul, M. and Pavia, F. and Pena, L. D. and Peters, B. and Planchon, F. and Planquette, H. and Pradoux, C. and Puigcorbé, V. and Quay, P. and Queroue, F. and Radic, A. and Rauschenberg, S. and Rehkämper, M. and Rember, R. and Remenyi, T. and Resing, J. A. and Rickli, J. and Rigaud, S. and Rijkenberg, M. J. A. and Rintoul, S. and Robinson, L. F. and Roca-Martí, M. and

Rodellas, V. and Roeske, T. and Rolison, J. M. and Rosenberg, M. and Roshan, S. and Rutgers van der Loeff, M. M. and Ryabenko, E. and Saito, M. A. and Salt, L. A. and Sanial, V. and Sarthou, G. and Schallenberg, C. and Schauer, U. and Scher, H. and Schlosser, C. and Schnetger, B. and Scott, P. and Sedwick, P. N. and Semiletov, I. and Shelley, R. and Sherrell, R. M. and Shiller, A. M. and Sigman, D. M. and Singh, S. K. and Slagter, H. A. and Slater, E. and Smethie, W. M. and Snaith, H. and Sohrin, Y. and Sohst, B. and Sonke, J. E. and Speich, S. and Steinfeldt, R. and Stewart, G. and Stichel, T. and Stirling, C. H. and Stutsman, J. and Swarr, G. J. and Swift, J. H. and Thomas, A. and Thorne, K. and Till, C. P. and Till, R. and Townsend, A. T. and Townsend, E. and Tuerena, R. and Twining, B. S. and Vance, D. and Velazquez, S. and Venchiarutti, C. and Villa-Alfageme, M. and Vivancos, S. M. and Voelker, A. H. L. and Wake, B. and Warner, M. J. and Watson, R. and van Weerlee, E. and Alexandra Weigand, M. and Weinstein, Y. and Weiss, D. and Wisotzki, A. and Woodward, E. M. S. and Wu, J. and Wu, Y. and Wuttig, K. and Wyatt, N. and Xiang, Y. and Xie, R. C. and Xue, Z. and Yoshikawa, H. and Zhang, J. and Zhang, P. and Zhao, Y. and Zheng, L. and Zheng, X.-Y. and Zieringer, M. and Zimmer, L. A. and Ziveri, P. and Zunino, P. and Zurbrick, C.: The GEOTRACES Intermediate Data Product 2017, Chem Geol, 493, 210-223, https://doi.org/10.1016/j.chemgeo.2018.05.040, 2018.

Schlosser, C., Streu, P., Frank, M., Lavik, G., Croot, P. L., Dengler, M., and Achterberg, E. P.: H_2S events in the Peruvian oxygen minimum zone facilitate enhanced dissolved Fe concentrations, Sci Rep, 8, https://doi.org/10.1038/s41598-018-30580-w, 2018.

Schmidtko, S., Stramma, L., and Visbeck, M.: Decline in global oceanic oxygen content during the past five decades, Nature, 542, 335-339, https://doi.org/10.1038/nature21399, 2017.

Scholten, J. C., Pham, M. K., Blinova, O., Charette, M. A., Dulaiova, H., and Eriksson, M.: Preparation of Mn-fiber standards for the efficiency calibration of the delayed coincidence counting system (RaDeCC), Mar Chem, 121, 206-214, https://doi.org/10.1016/j.marchem.2010.04.009, 2010.

Scholz, F., Loscher, C. R., Fiskal, A., Sommer, S., Hensen, C., Lomnitz, U., Wuttig, K., Gottlicher, J., Kossel, E., Steininger, R., and Canfield, D. E.: Nitrate-dependent iron oxidation limits iron transport in anoxic ocean regions, Earth Planet Sc Lett, 454, 272-281, https://doi.org/10.1016/j.epsl.2016.09.025, 2016.

Schroller-Lomnitz, U., Hensen, C., Dale, A. W., Scholz, F., Clemens, D., Sommer, S., Noffke, A., and Wallmann, K.: Dissolved benthic phosphate, iron and carbon fluxes in the Mauritanian upwelling system and implications for ongoing deoxygenation, Deep-Sea Res Pt I, ~~in review~~143, 70-84, https://doi.org/10.1016/j.dsr.2018.11.008, ~~2018~~2019.

Severmann, S., McManus, J., Berelson, W. M., and Hammond, D. E.: The continental shelf benthic iron flux and its isotope composition, Geochim Cosmochim Ac, 74, 3984-4004, https://doi.org/10.1016/j.gca.2010.04.022, 2010.

Shelley, R. U., Morton, P. L., and Landing, W. M.: Elemental ratios and enrichment factors in aerosols from the US-GEOTRACES North Atlantic transects, Deep-Sea Res Pt II, 116, 262-272, https://doi.org/10.1016/j.dsr2.2014.12.005, 2015.

Shelley, R. U., Landing, W. M., Ussher, S. J., Planquette, H., and Sarthou, G.: Regional trends in the fractional solubility of Fe and other metals from North Atlantic aerosols (GEOTRACES cruises GA01 and GA03) following a two-stage leach, Biogeosciences, 15, 2271-2288, https://doi.org/10.5194/bg-15-2271-2018, 2018.

Sherrell, R. M. and Boyle, E. A.: The trace metal composition of suspended particles in the oceanic water column near Bermuda, Earth Planet Sc Lett, 111, 155-174, https://doi.org/10.1016/0012-821x(92)90176-V, 1992.

Soataert, K., Petzoldt, T., and Meysman, F.: marelac: Tools for Aquatic Sciences, Version 2.1.6, https://CRAN.R-project.org/package=marelac, ~~2016.~~ 2016.

Sommer, S., Dengler, M., and Treude, T.: Benthic element cycling, fluxes and transport of solutes across the benthic boundary layer in the Mauritanian oxygen minimum zone, (SFB754) – Cruise No. M107 – May 30 – July 03, 2014 – Fortaleza (Brazil) – Las Palmas (Spain), METEOR-Berichte, M107, DFG-Senatskommission für Ozeanographie, https://doi.org/10.2312/cr_m107, 2015.

Steinfeldt, R., Sultenfuss, J., Dengler, M., Fischer, T., and Rhein, M.: Coastal upwelling off Peru and Mauritania inferred from helium isotope disequilibrium, Biogeosciences, 12, 7519-7533, https://doi.org/10.5194/bg-12-7519-2015, 2015.

Stramma, L., Brandt, P., Schafstall, J., Schott, F., Fischer, J., and Kortzinger, A.: Oxygen minimum zone in the North Atlantic south and east of the Cape Verde Islands, J Geophys Res-Oceans, 113, C04014, https://doi.org/10.1029/2007jc004369, 2008a.

Stramma, L., Johnson, G. C., Sprintall, J., and Mohrholz, V.: Expanding oxygen-minimum zones in the tropical oceans, Science, 320, 655-658, https://doi.org/10.1126/science.1153847, 2008b.

Stumm, W. and Morgan, J. J.: Aquatic Chemistry: Chemical Equilibria and Rates in Natural Waters, John Wiley & Sons, New York, 1995.

Sunda, W. G. and Huntsman, S. A.: Effect of sunlight on redox cycles of manganese in the Southwestern Sargasso Sea, Deep-Sea Res, 35, 1297-1317, https://doi.org/10.1016/0198-0149(88)90084-2, 1988.

Sunda, W. G. and Huntsman, S. A.: Photoreduction of manganese oxides in seawater, Mar Chem, 46, 133-152, https://doi.org/10.1016/0304-4203(94)90051-5, 1994.

Tanhua, T., and Liu, M.: Upwelling velocity and ventilation in the Mauritanian upwelling system estimated by CFC-12 and SF6 observations, J Mar Sys, 151, 57-70, https://doi.org/10.1016/j.jmarsys.2015.07.002, 2015.

Tebo, B. M. and Emerson, S.: Microbial manganese(II) oxidation in the marine environment: a quantitative study, Biogeochemistry, 2, 149-161, https://doi.org/10.1007/Bf02180192, 1986.

Tebo, B. M., Bargar, J. R., Clement, B. G., Dick, G. J., Murray, K. J., Parker, D., Verity, R., and Webb, S. M.: Biogenic manganese oxides: Properties and mechanisms of formation, Annu Rev Earth Pl Sc, 32, 287-328, https://doi.org/10.1146/annurev.earth.32.101802.120213, 2004.

Thomsen, S., Karstensen, J., Kiko, R., Krahmann, G., Dengler, M., and Engel, A.: Remote and local drivers of oxygen and nitrate variability in the shallow oxygen minimum zone off Mauritania in June 2014, Biogeosciences, 16, 9791 ~~29~~998, https://doi.org/10.5194/bg-16-979-2019~~https://doi.org/10.5194/bg-2018-252~~, ~~2018~~2019.

Tomczak, M.: An analysis of mixing in the frontal zone of South and North Atlantic Central Water off North-West Africa, Prog Oceanogr, 10, 173-192, https://doi.org/10.1016/0079-6611(81)90011-2, 1981.

Tweddle, J. F., Sharples, J., Palmer, M. R., Davidson K., and McNeill, S.: Enhanced nutrient fluxes at the shelf sea seasonal thermoclinecaused by stratified flow over a bank, Prog Oceanogr, 117, 37-47, https://doi.org/10.1016/j.pocean.2013.06.018, 2013.

Twining, B. S., Rauschenberg, S., Morton, P. L., and Vogt, S.: Metal contents of phytoplankton and labile particulate material in the North Atlantic Ocean, Prog Oceanogr, 137, 261-283, https://doi.org/10.1016/j.pocean.2015.07.001, 2015.

Ussher, S. J., Achterberg, E. P., Powell, C., Baker, A. R., Jickells, T. D., Torres, R., and Worsfold, P. J.: Impact of atmospheric deposition on the contrasting iron biogeochemistry of the North and South Atlantic Ocean, Global Biogeochem Cy, 27, 1096-1107, https://doi.org/10.1002/gbc.20056, 2013.

Verhoef, A., Portabella, M., and Stoffelen, A.: High resolution ASCAT scatterometer winds near the coast, IEEE, Trans Geosci Remote Sens, 50, 2481-248, https://doi.org/10.1109/TGRS.2011.2175001, 2012.

Véron, A., Patterson, C., and Flegal, A.: Use of stable lead isotopes to characterize the sources of anthropogenic lead in North Atlantic surface waters, Geochim Cosmochim Ac, 58, 3199-3206, https://doi.org/10.1016/0016-7037(94)90047-7, 1994.

von Langen, P. J., Johnson, K. S., Coale, K. H., and Elrod, V. A.: Oxidation kinetics of manganese(II) in seawater at nanomolar concentrations, Geochim Cosmochim Ac, 61, 4945-4954, https://doi.org/10.1016/S0016-7037(97)00355-4, 1997.

~~Wedepohl, K. H.: The composition of the continental crust, Geochim Cosmochim Ac, 59, 1217-1232, https://doi.org/10.1016/0016-7037(95)00038-2, 1995.~~

Weiss, R. F.: The solubility of nitrogen, oxygen and argon in water and seawater, Deep Sea Res and Oceanographic Abstracts, 17, 721-735, https://doi.org/10.1016/0011-7471(70)90037-9, 1970.

Winkler, L. W.: Bestimmung des im Wasser gelösten Sauerstoffs, Ber Dtsch Chem Ges, 21, 2843-2855, https://doi.org/10.1002/cber.188802102122, ~~1988~~1888.

Wu, J. F. and Luther, G. W.: Size-fractionated iron concentrations in the water column of the western North Atlantic Ocean, Limnol Oceanogr, 39, 1119-1129, https://doi.org/10.4319/lo.1994.39.5.1119, 1994.

Wuttig, K., Heller, M. I., and Croot, P. L.: Pathways of Superoxide (O_2^-) Decay in the Eastern Tropical North Atlantic, Environ Sci Technol, 47(18), 10249-10256, https://doi.org/10.1021/es401658t, 2013.

Wyrtki, K.: The oxygen minima in relation to ocean circulation, Deep-Sea Res, 9, 11-23, https://doi.org/10.1016/0011-7471(62)90243-7, 1962.

Yücel, M., Beaton, A. D., Dengler, M., Mowlem, M. C., Sohl, F., and Sommer, S.: Nitrate and Nitrite Variability at the Seafloor of an Oxygen Minimum Zone Revealed by a Novel Microfluidic In-Situ Chemical Sensor, PLoS ONE 10(7), e0132785, https://doi.org/10.1371/journal.pone.0132785, 2015.

Zenk, W., Klein, B., and Schroder, M.: Cape-Verde Frontal Zone, Deep-Sea Res, 38, S505-S530, https://doi.org/10.1016/S0198-0149(12)80022-7, 1991.

Table 1. Analyzed reference seawater, procedural blanks and detection limits (three times the standard deviation of the blank). Mean values and standard deviation for Cd, Pb, Fe, Ni, Cu, Mn and Co and available consensus values (± 1 standard deviation), n = number of measurements.

	SAFe S (nmol L^{-1}) n=11	SAFe S consensus value (nmol L^{-1})	SAFe D2 (nmol L^{-1}) n=7	SAFe D2 consensus value (nmol L^{-1})	Blank (pmol L^{-1})	Detection limit (pmol L^{-1})
Cd	0.003 ± 0.002	0.001	1.089 ± 0.043	1.011 ± 0.024	2.2 ± 0.3	0.8
Pb	0.050 ± 0.003	0.049 ± 0.002	0.028 ± 0.001	0.029 ± 0.002	0.4 ± 0.2	0.6
Fe	0.091 ± 0.009	0.095 ± 0.008	1.029 ± 0.038	0.956 ± 0.024	68 ± 10	29
Ni	2.415 ± 0.086	2.34 ± 0.09	9.625 ± 0.175	8.85 ± 0.26	112 ± 20	59
Cu	0.514 ± 0.037	0.53 ± 0.05	2.176 ± 0.152	2.34 ± 0.15	14 ± 3	9.3
Co	0.005 ± 0.001	0.005 ± 0.001	0.048 ± 0.003	0.047 ± 0.003	2.7 ± 0.8	2.5
Mn	0.814 ± 0.033	0.810 ± 0.062	0.437 ± 0.029	0.36 ± 0.05	14 ± 6	17

Table 1. TM/Al ratios of different fractions for the repeated deployments at station 3 within the OMZ below 50 m water depth.

Parameter	Stn 3A	Stn 3B
dFe/dAl	0.38–0.79	0.35–0.37
TDFe/TDAl	4.00–13.42	1.83–2.81
LpFe/LpAl	10.00–29.50	3.64–8.59
dCo/dAl	0.009–0.011	0.009–0.011
TDCo/TDAl	0.009–0.010	0.006–0.008
LpCo/LpAl	0.007–0.011	0.001–0.005
dMn/dAl	0.26–0.45	0.19–0.21
TDMn/TDAl	0.26–0.32	0.12–0.17
LpMn/LpAl	0.14–0.28	0.02–0.09

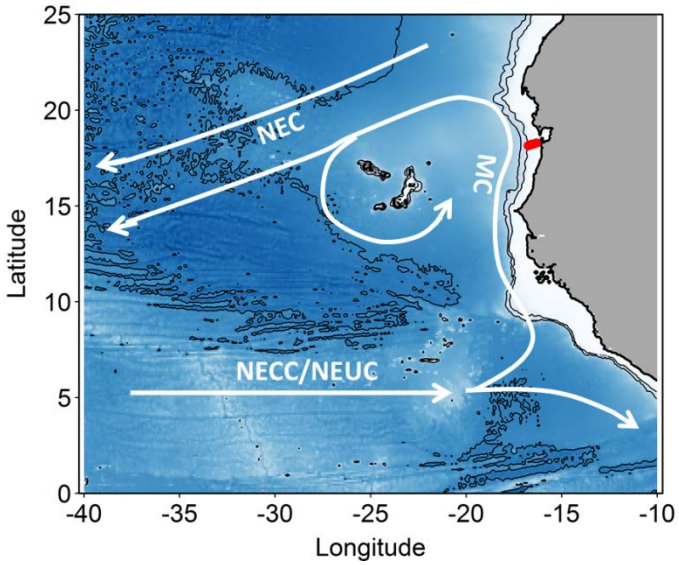

Figure 1. Map of the study area. Stations along the transect during M107 (June 2014) are displayed in red circles and major currents in white lines (adapted from Brandt et al. 2015). MC = Mauritania Current; NEC = North Equatorial Current; NECC = North Equatorial Countercurrent; NEUC = North Equatorial Undercurrent.

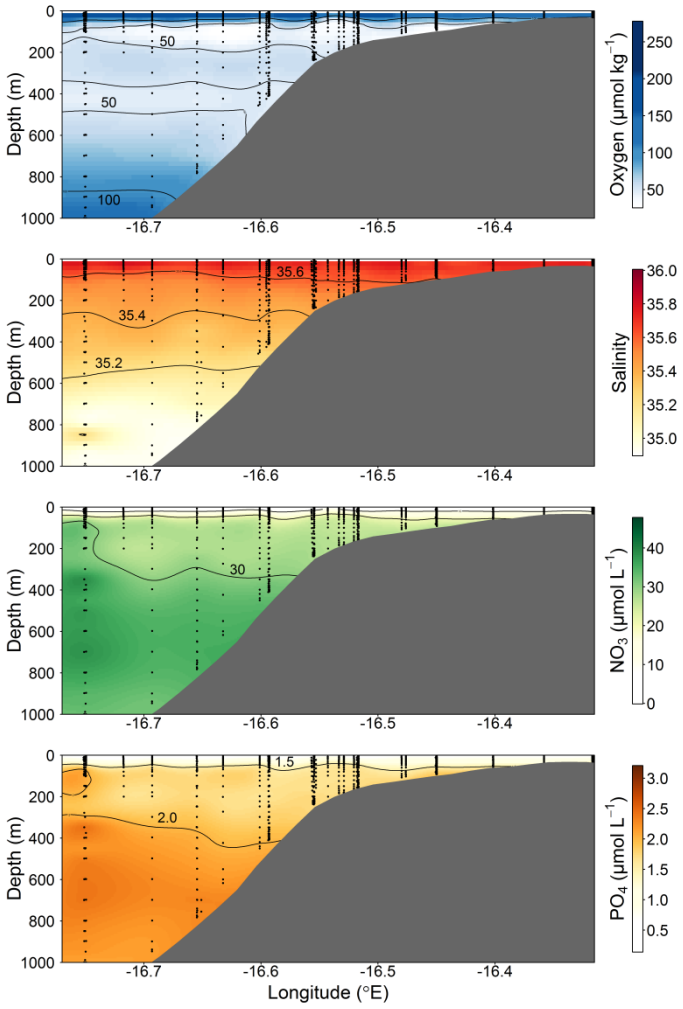

Figure 2. Section plots of oxygen (µmol kg^{-1}), salinity (PSU), NO_3 (µmol L^{-1}) and PO_4 (µmol L^{-1}) along the transect off the Mauritanian coast in June 2014.

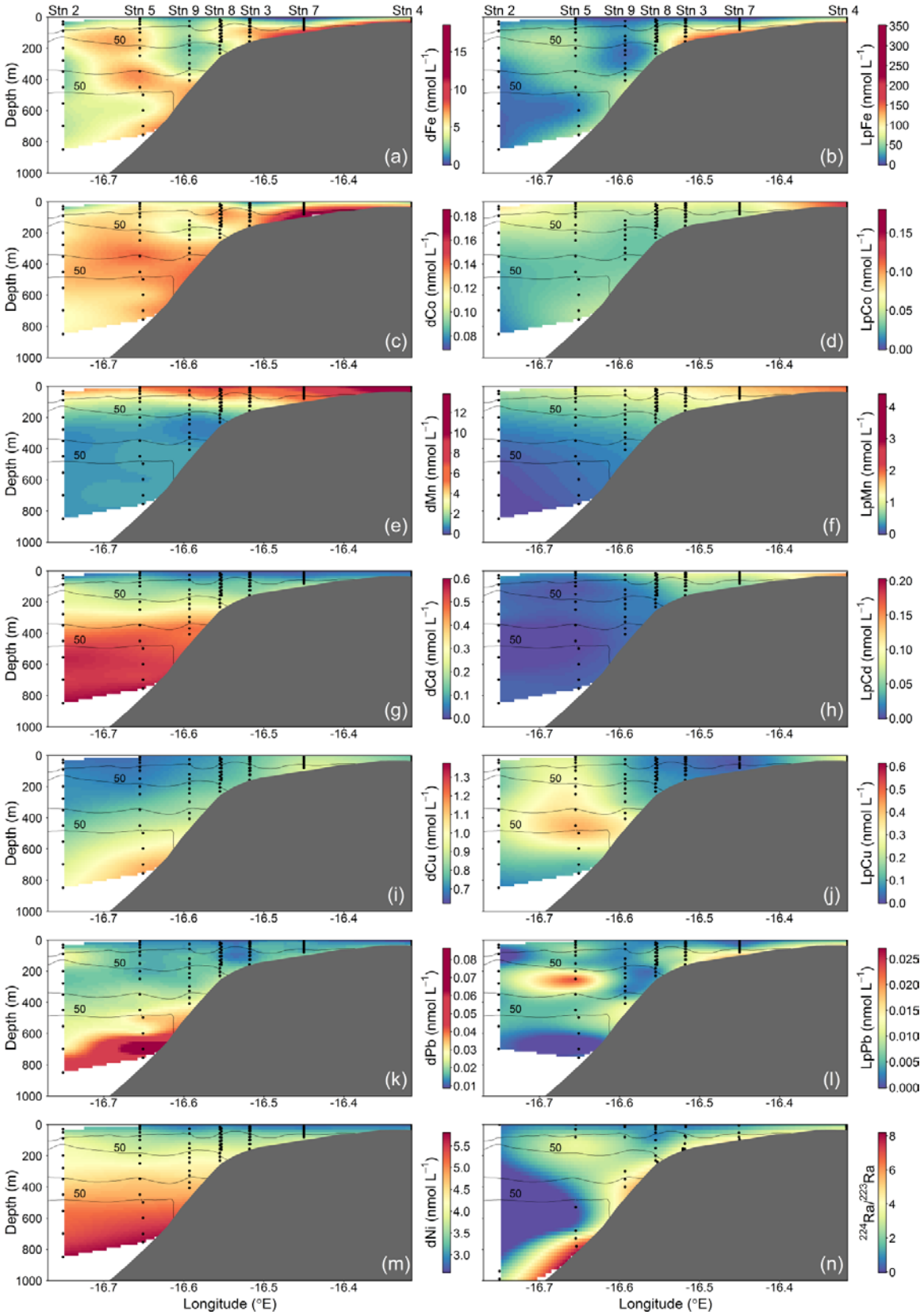

Figure 3. Spatial distributions of dissolved (d) and leachable particulate (Lp) trace metals and $^{224}Ra/^{223}Ra$ across the Mauritanian shelf at 18°20'N in June 2014. Each sample location is indicated as black dot and oxygen contours at 50 µmol kg^{-1} enclosing the upper and lower OMZ are displayed as black contour lines.

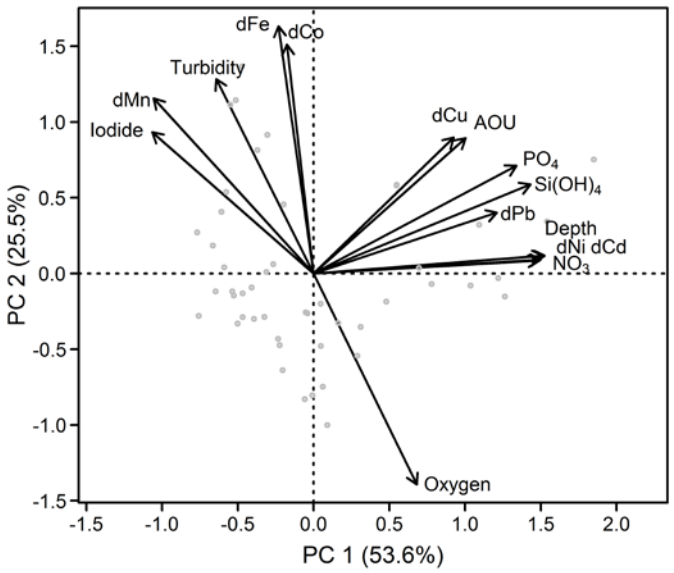

Figure 4. Principal component analysis of the Mauritanian shelf data set. Principal component loadings for each variable are indicated by black vectors. Component scores of each sample are indicated as grey circles. Loadings/scores have been scaled symmetrically by square root of the eigenvalue.

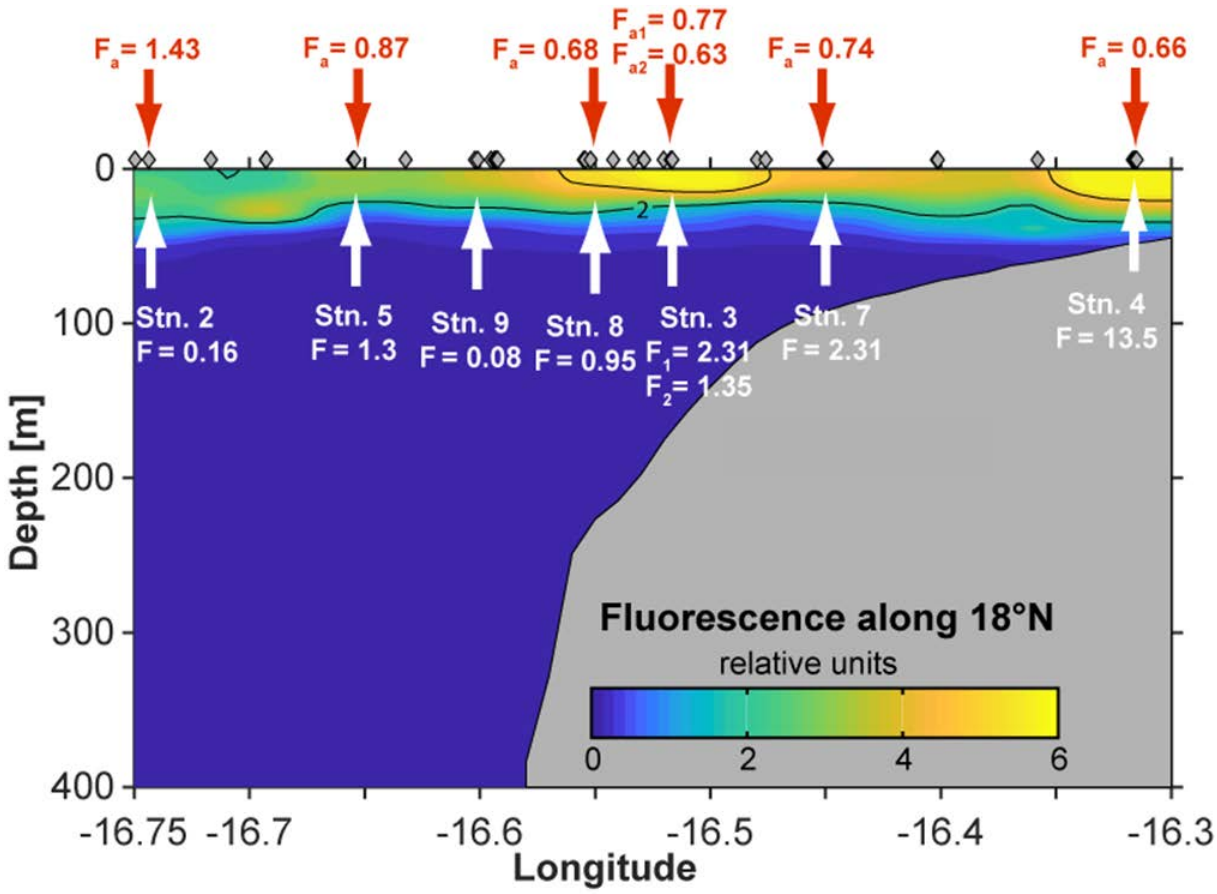

Figure 5. Atmospheric dFe fluxes (F_a; red) and vertical dFe fluxes (F; ~~orange~~white) in µmol m^{-2} d^{-1} along the transect at 18°20'N in June 2014.

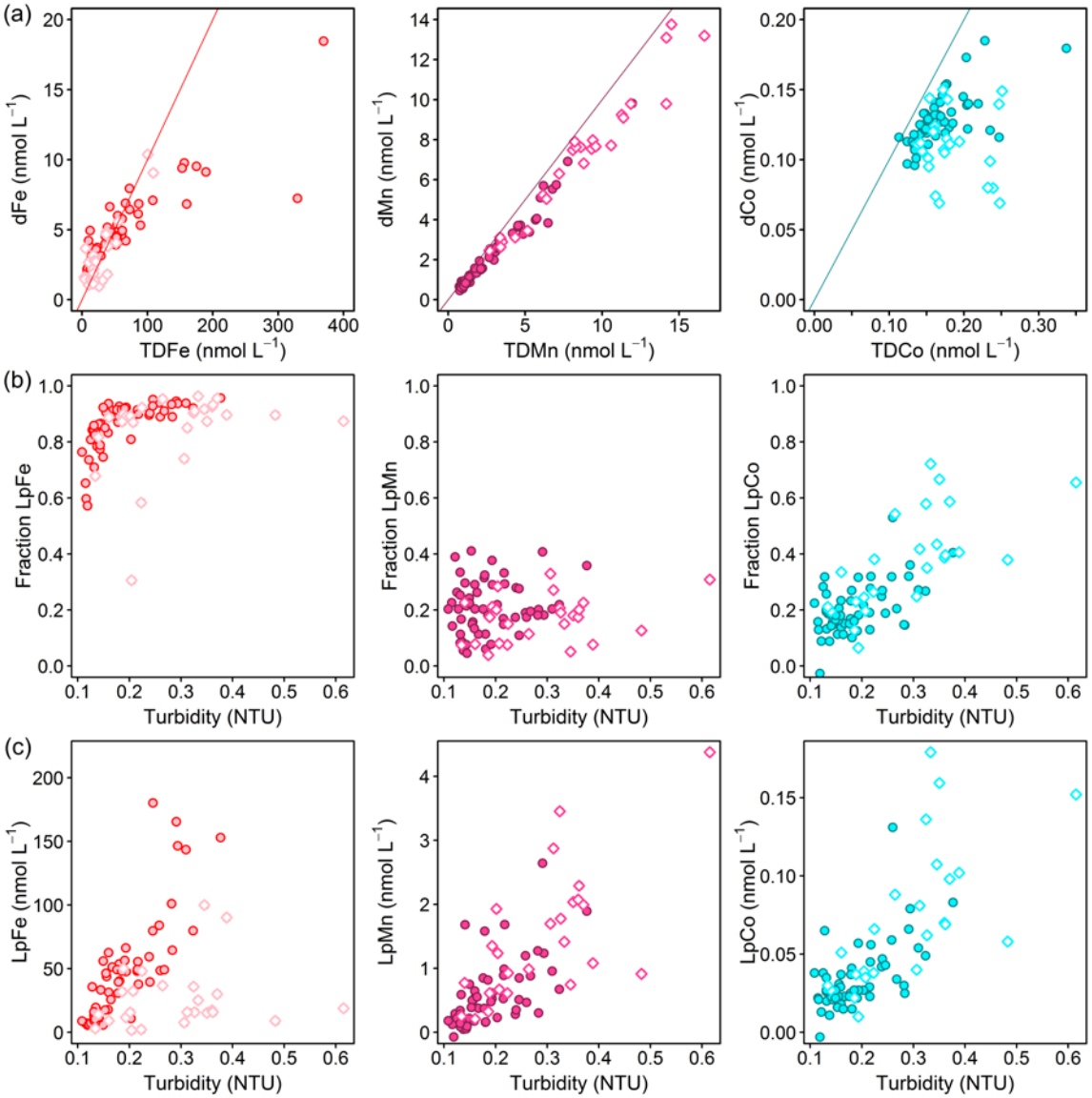

Figure 6. (a) Dissolved against total dissolvable trace metal concentrations for Fe (left; red line: TDFe = 10*dFe), Mn (middle; purple line: TDMn = dMn) and Co (right; turquoise line: TDCo = dCo). (b) Fraction of leachable particulate trace metals (Lp/TD) against turbidity and (c) Leachable particulate concentrations against turbidity for Fe (left), Mn (middle) and Co (right). Filled circles display all data points below 50 m depth, open ~~circles~~ diamonds at depths shallower than 50 m.

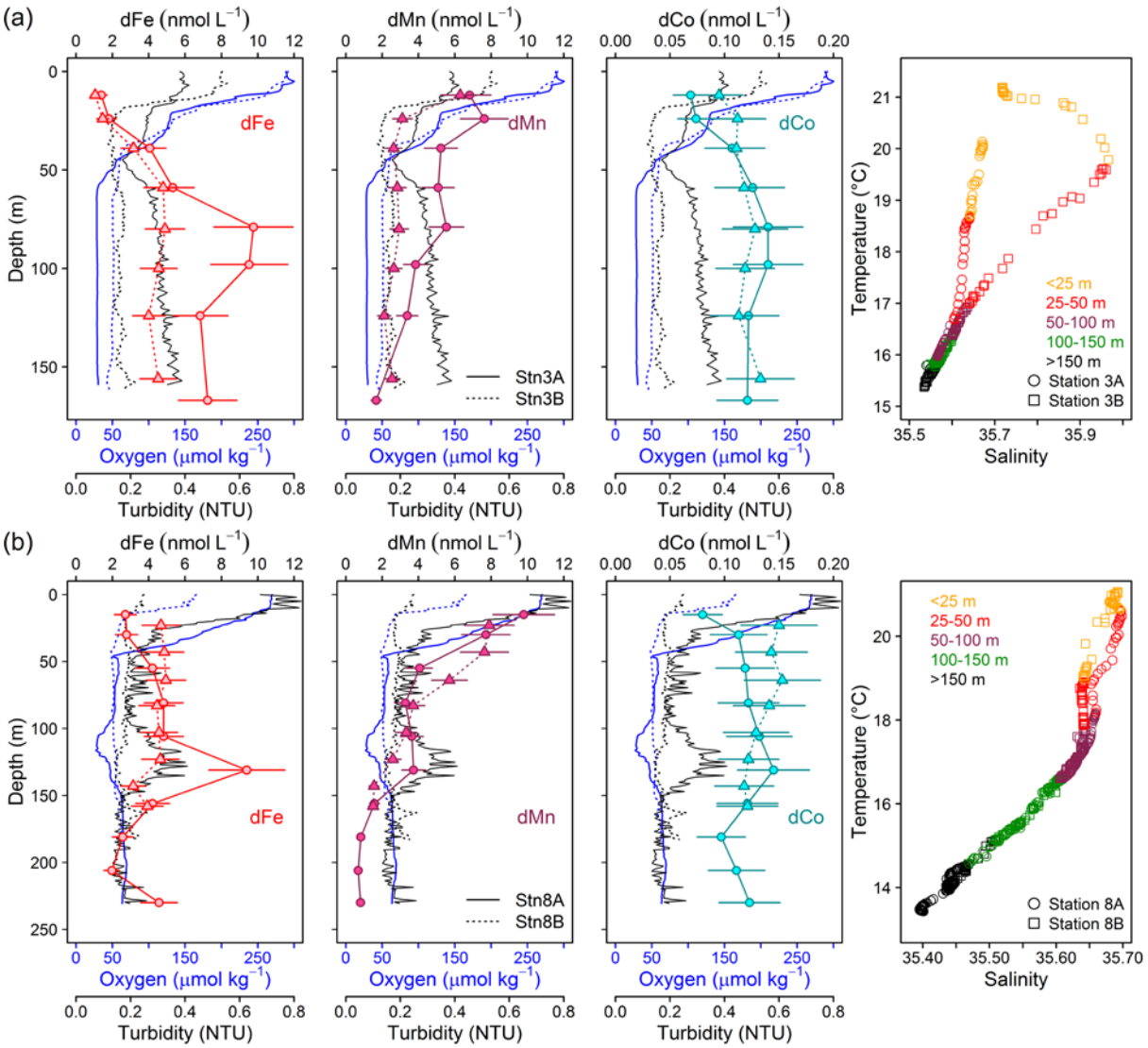

Figure 7. Repeat stations: oxygen concentration, turbidity and dissolved trace metals (Fe, Mn and Co) and temperature vs salinity plots. First deployment displayed as solid line and circles and second deployment displayed as dashed line and triangles. (a) Station 3 (18.23°N, 16.52°W, 170 m water depth, 9 days between deployments). (b) Station 8 (18.22°N, 16.55°N, 189–238 m water depth, 2 days between deployments).

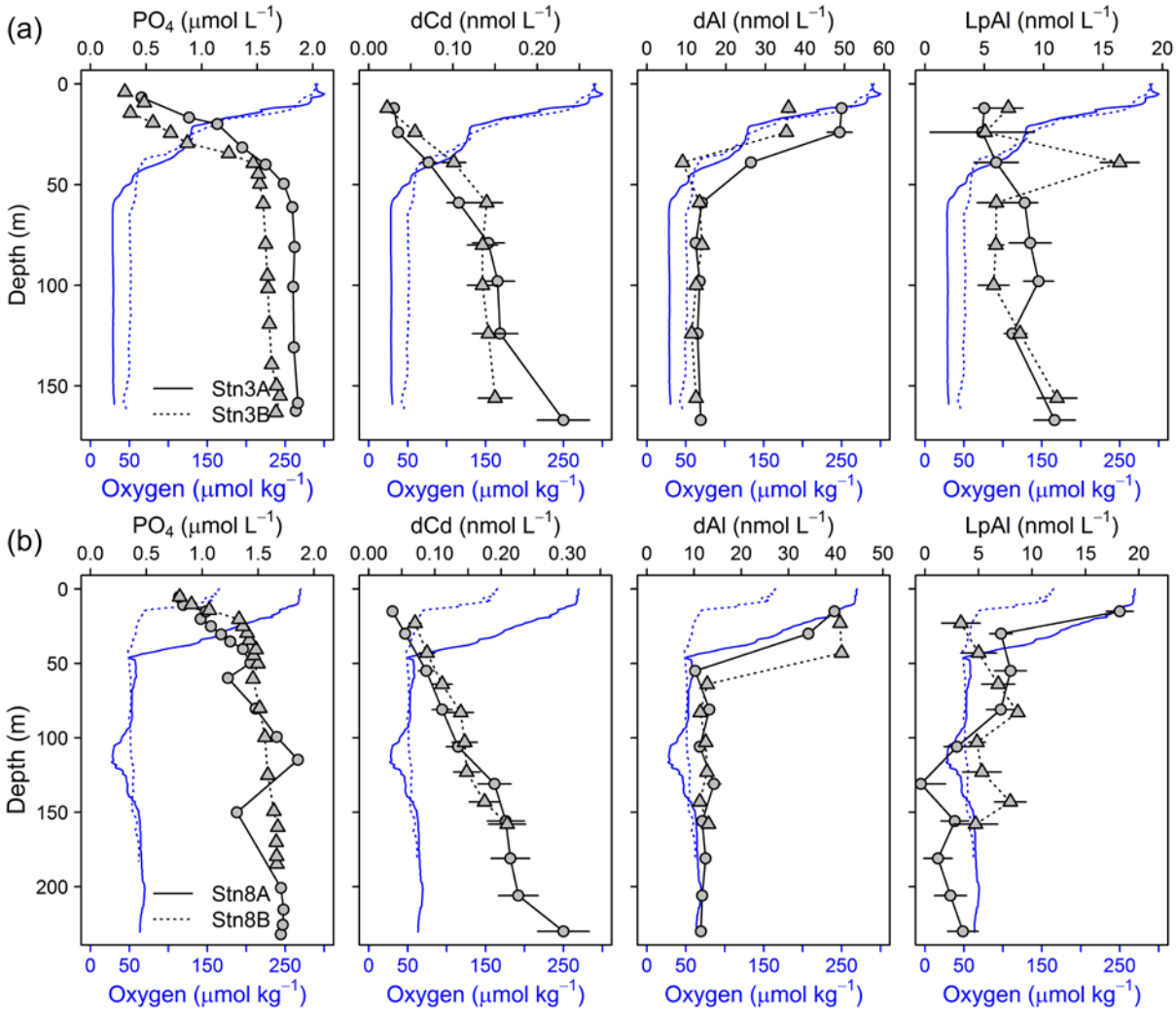

Figure 8. Depth profiles of dCd, PO_4, dAl and LpAl of repeat stations. First deployment displayed as solid black line and circles and second deployment displayed as dashed black line and triangles. Oxygen concentrations are indicated as blue solid line for the first deployment and dashed blue line for the second deployment. (a) Station 3 (18.23°N, 16.52°W, 170 m water depth, 9 days between deployments and (b) Station 8 (18.22°N, 16.55°N, 189–238 m water depth, 2 days between deployments).